ETH
Eidgenössische Technische Hochschule Zürich
Swiss Federal Institute of Technology Zurich

Institute for
Dynamic Systems and Control
IDSC
Institut für Dynamische Systeme
und Regelungstechnik

Max Planck Institute for
Intelligent Systems

Julian Nubert

Learning-based Approximate Model Predictive Control with Guarantees

Joining Neural Networks with Recent Robust MPC

Master Thesis

Intelligent Control Systems Group
Max Planck Institute for Intelligent Systems

Institute for Dynamic Systems and Control
Swiss Federal Institute of Technology (ETH) Zurich

Supervision

Johannes Köhler
Dr. Vincent Berenz
Prof. Dr. Raffaello D'Andrea
Dr. Sebastian Trimpe

31.08.2019
Updated Version: 04.03.2020

Abstract

In this work, we present a model predictive control (MPC) method for applications in complex constrained physical systems. We base our work on a novel robust model predictive control (RMPC) scheme guaranteeing constraint satisfaction and recursive feasibility under disturbances. The used scheme keeps the computational complexity comparable to the nominal case. We adopt this approach and extend it by practical useful additions, such as robust dynamic set point tracking and the handling of nonlinear constraints in the output function. We are able to demonstrate this method's practical significance by controlling a complex robotic system (MPI Apollo robot). Furthermore we tackle the inherent computational complexity of the optimization problem by approximating the RMPC controller with neural network (NN) regression. By only using the NN, we are able to control the robot in a much more dynamic way due to a computational speed-up of several magnitudes. Finally, we also analyze the quality of the approximation by providing closed loop statistical guarantees for the NN controller, also taking into account additional experimentally validated non-idealities of our model. Most of the code, including the TensorFlow NN inference, is fully written in C++ and available on the Max Planck Autonomous Motion Department Gitlab server.

Preface

This literary work was created as a result of the work on my (i.e. Julian Nubert's) Master Thesis. Besides doing some of the work at the University of Stuttgart, the prime part of the work was performed at the Max Planck Institute for Intelligent Systems. This work is the written part of my Master Thesis for my Master's degree studies in Robotics, Systems & Control at ETH Zürich, under the official supervision of Prof. Dr. Raffaello D'Andrea. My supervisors at the Max Planck Institute for Intelligent Systems are Dr. Sebastian Trimpe and Dr. Vincent Berenz and my supervisor at the University of Stuttgart is Johannes Köhler.

The core idea of this work, i.e. approximating a robust model predictive controller with a supervised learning technique and to be in a position to give statistical guarantees, originally results from a joint idea of my two supervisors Dr. Sebastian Trimpe and Johannes Köhler. This idea was first elaborated in a previous work done by Michael Hertneck [19], which was supervised by Dr. Sebastian Trimpe and Johannes Köhler.

This thesis can be understood as a continuation of this previous work focusing on further extensions, newly used approaches, more advanced frameworks and the application to a real world robotic use case. It was performed in the time interval lasting from January 2019 till August 2019.

I would like to thank the Max Planck Institute for Intelligent Systems, enabling me to do work on such a great project including real world robot experiments for my Master Thesis. Also big thanks go to Prof. Dr. Raffaello D'Andrea who is the tutor of my Master's degree and the ETH supervisor of this thesis, making it possible for me to work on it externally. Furthermore, I would like to thank the Intelligent Control Systems Group, which welcomed me in a unique positive way. Conversations with the members of the group, interns and other master students were extremely helpful in tackling involved challenges. Special thanks go to my supervisor, Dr. Vincent Berenz who supported me along the way regarding implementation and framework questions. Another big thank goes to Johannes Köhler who helped me, even remotely during the first three months, in understanding, implementing and extending the robust model predictive control theory and was available whenever help was needed. Last but not least, I would like to thank Dr. Sebastian Trimpe who hired me for this project, supported me during the 8 months by any account, was always available and also offered off-topic help and advice.

Thanks to all of you! Yours sincerely, Julian.

Contents

Nomenclature

Symbols

$t \in \mathbb{R}$	Time	[s]
$T \in \mathbb{R}$	Sampling Time of Controller	[s]
$x \in \mathcal{X} \subset \mathbb{R}^n$	System State Vector	
$u \in \mathcal{U} \subset \mathbb{R}^m$	Input Vector	
$y = h(x, u)$	System Output Vector	
Θ	Angle	[rad]
$\dot{\Theta}$	Angular Velocity	$[{}^{rad}/_{s}]$
$\ddot{\Theta}$	Angular Acceleration	$[{}^{rad}/_{s^2}]$

Notation

$x(k\|t)$	Predicted discrete time system state at time step k starting at time t for $k \in \mathbb{N}$
$x(\tau\|t)$	Predicted continuous time system state in sampling interval, for $\tau \in [0, h)$
$\|x\|_Q^2$	Quadratic matrix norm given as $x^T Q x$
A, B	Matrices of linear System Dynamics

Acronyms and Abbreviations

AMPC	Approximate Model Predictive Control
CSTR	Chemical Stirred-Tank Reactor
CT	Continuous-Time
DH	Denavit-Hartenberg
DT	Discrete-Time
ETH	Eidgenössische Technische Hochschule
GPS	Guided Policy Search
LQR	Linear Quadratic Regulator
MPC	Model Predictive Control
MPI	Max-Planck-Institute
NN	Neural Network
RMPC	Robust Model Predictive Control
SL	Simulation Laboratory (robot control framework)

Chapter 1

Introduction

Applications of modern electrical, mechanical or electro mechanical systems would not be possible without the use of feedback control. Classical control schemes such as *P*-, *PI*-, *PD*- or *PID* control have performed reliably for a long time and are nowadays de facto still industrial standard. However, due to increasing complexity of the systems and rising demands in terms of performance, such modest approaches are often not longer expedient. In the last decades, optimal and robust control techniques such as Linear Quadratic Regulator (LQR)- [27], H_2- and H_∞- [76] control became more and more prominent. Especially for multivariate systems, these approaches guarantee stability and achieve good results for many applications, offering properties such as optimal performance for a given problem set (LQR) or acting robustly with respect to defined disturbances and uncertainties (H_2, H_∞).

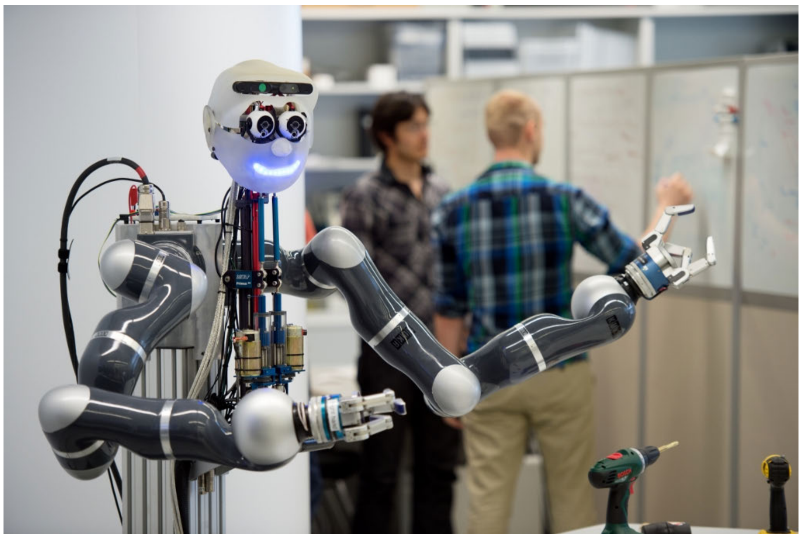

Figure 1.1: Apollo robot at the MPI in Tübingen equipped with two KUKA LBR4 robotic arms. Max Planck Institute for Intelligent Systems©.

Nevertheless, none of these approaches is able to properly handle additional restrictions such as state and input constraints. Extensions and ways of handling nonlinearities are possible but still challenging in many situations. In contrast to this, Model Predictive Control (MPC) techniques allow one to consider state and input constraints in the formulation and therefore to steer the system in the optimal way, potentially even by consciously applying inputs lying at the constraint boundaries. Even handling nonlinear output constraints is possible, as we demonstrate within this work. MPC allows for finding the optimal solution along a predicted trajectory, given some constraints and a predefined objective. Furthermore, MPC is relatively easily extendable to general nonlinear dynamics.

However, standard MPC design only works well if the given model reflects reality to a certain degree. Even basic requirements, such as stability, can only be guaranteed for the nominal, often non-realistic case. To be in a position to deal with uncertain real world scenarios and hence, to guarantee safe operation, several robust MPC (RMPC) schemes have been developed in the past years. With those, it is possible to take disturbances and uncertainties into account and to guarantee stability and recursive feasibility under certain (predefined) disturbances. However, a general drawback of MPC or RMPC approaches is its computational complexity, since a mathematical optimization problem needs to be solved in every time step. Therefore, MPC controllers have first been applied to control of systems with larger time constants such as chemical reactors [71].

1.1 Problem Formulation

Examples for challenges and requirements in modern control design can, e.g., be found in two recent research areas; automated driving and human-robot-collaboration. It is obvious that both examples are complex, highly safety critical, relatively uncertain and constrained. In fact, they are representative for a full class of modern control problems. Besides the mentioned challenges, many of them are highly nonlinear and in addition high-dimensional.

The overarching goal of this thesis is the deployment of a novel control approach for a complex, real-world robotic system, more precisely the end-effector control of an humanoid-like robot called Apollo (Fig. 1.1). Apollo is equipped with two KUKA LBR4+ robotic arms and located at the MPI for Intelligent Systems in Tübingen. We try to obtain

1. state of the art performance,
2. while ensuring safety,
3. as well as the ability to deploy our approach in fast acting or computationally constrained systems.

Guaranteeing safety in this area requires the avoidance of real world obstacles, in particular in a robust manner. Furthermore, providing a time efficient solution finding would even facilitate utilization in other, even more resource-critical areas such as flight-control for quadrotors. Apollo has hard constraints in its state- and input space. Moreover, we require to take obstacles in the task space into account. This motivates the following chosen approach.

1.2 Approach

The presented approach is developed with the requirements given in the last section in mind. For reaching state of the art performance within our use case, we aim to perform MPC-based end-effector control. To guarantee safety, we build upon a novel robust MPC (RMPC) scheme by Koehler et al. [36]. This approach guarantees stability, robust constraint satisfaction as well as recursive feasibility under bounded disturbances. The biggest advantages of this approach are moderately introduced conservatism and a computational complexity comparable to the nominal case. To tackle the time critical demands, we choose to get an explicit representation of the RMPC by approximating it with supervised learning, neural networks (NN) in our case. We denote the resulting controller as approximate model predictive controller (AMPC).

Our RMPC scheme is related to works by Limon et al. [41, 46, 42]. For this purpose, we expand [36] by introducing additional features that are needed in order to be used for our application on the robotic system. These include the extension to dynamic robust (output) set-point tracking, online-determination of a suitable terminal set and the robust handling of nonlinear output constraints. The inherent computational complexity of the optimization problem is tackled with a recent learning-based approach, based on the idea in [19]. The idea of using sampled solutions of the optimization problem and creating an explicit MPC controller is not new and was done before (see Chapter 2). However, in comparison to most existing solutions, we are able to provide statistical guarantees regarding stability, even though machine learning techniques are used. This is done by taking approximation errors into account during the design procedure of the RMPC controller and therfore, to enable the controller to compensate for them. We consider disturbances in the form of imprecisions of the NN and model uncertainties of the real world system. We improve the given approach in [19] by introducing a new and less conservative validation criterion, using more advanced learning techniques and by improving the sampling of the data points. In particular, for the high dimensional robot control the sampling acts as the bottleneck of the whole pipeline.

Strong focus also lies on the development of a suitable software framework. During this project, we developed a reliable and fast working software framework, fully implemented in C++. It is used to sample the controller, train the networks, do the validation and to actually control the robot. An overview of the just mentioned components can be seen in Figure 1.2. The RMPC is used to

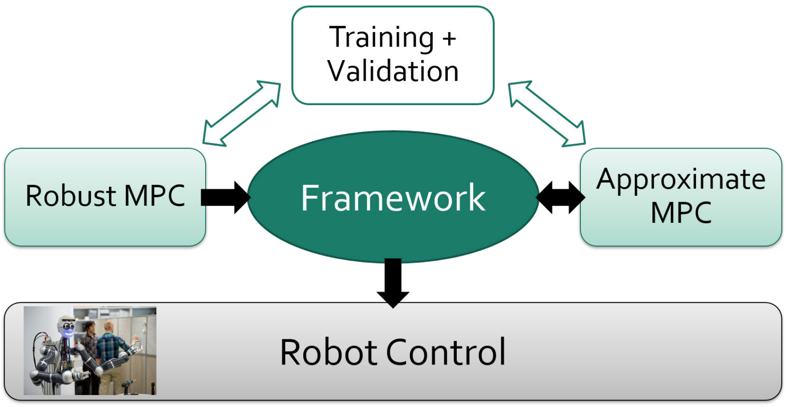

Figure 1.2: Overview of the main components of this work. We use a novel RMPC design [36] to guarantee safe behavior, including stability and recursive constraint satisfaction. Furthermore, we use this controller to train an AMPC. Vice versa, the RMPC is used afterwards to validate the resulting AMPC. The development of the framework was a central part of this work, among others to be able to use the RMPC as well as the AMPC to control Apollo robot.

train the NN and hence, to obtain the resulting AMPC. Vice versa, it also validates the AMPC in order to provide statistical guarantees. The framework is able to utilize the RMPC as well as the AMPC for the actual robot control. Furthermore, it is also used to sample the controller randomly or trajectory-wise and to train the network. From the very beginning we put emphasis on using fast and powerful tools regarding numerics, optimization and ML.

1.3 Contributions

As introduced in the last section, we worked on all areas which are depicted in Figure 1.2. None of the topics remained unaffected compared to previous work and we can present improvements in each of the areas. This thesis makes contributions to the two broader areas of robust MPC (RMPC) and approximate MPC (AMPC). Furthermore, a real-time safe software framework is developed to deploy both approaches on the robot. Finally, we were able to demonstrate both the extended RMPC scheme as well as this AMPC controller on a complex real world system for the first time, pointing out the significance for the robotics community. In the following, we make this more specific.

In this work, we extend a RMPC scheme based on [36] in order to make it suitable for the described motion control task of a robotic system. We provide all derivations and needed computations within this work. The main extensions compared to the work in [36] are the following:

- We perform output set point tracking, i.e. the reference x_t in the state space is unknown; only the reference output of the system y_t is given, i.e. the reference of the robot in the task space. To overcome this, an artificial set point x_s is included in the formulation according to [43].

- We are able to track dynamic set points, i.e. the artificial set point x_s is not known in advance and changes during operation. This requires the design and computation of proper terminal ingredients. We propose a formulation of suitable terminal ingredients for which the size of the terminal set is optimized in an online fashion.

- We deploy a quasi continuous-time pre-stabilization to make the system more good-natured and allow for a more dynamic behavior.

The design contains additional features and considerations which are needed for many real world use cases but often ignored in theoretical analysis. Regarding the theory for these special use cases, we got inspired by works of Koehler et al. [32, 35].

As a separate contribution, we present a revised formulation of the AMPC controller in [19]. In particular, we increased practical significance by

- introducing a new and less conservative validation criterion for the AMPC controller.

Besides the fact that this new formulation enables us to be less conservative, in contrast to [19], it also allows us to take additional disturbances such as model uncertainties or measurement noise into account. We also present alternative techniques and approaches for the data sampling and NN training used within our AMPC approach. This includes mainly the following:

- We present more efficient sampling techniques such as recursive sampling and trajectory-wise sampling. We can also demonstrate its advantages compared to the obvious (uniform or random) approaches.

- We deploy additional supervised classification to eliminate the need for a high sampling density in all areas of the state space.

For a higher dimensional problem we try to overcome the curse of dimensionality and achieve decent results despite a small sampling density. In this case we combine random sampling - allowing the network to get an estimate of all areas - with trajectory-wise sampling, leading to higher precision in regions of higher interest. The introduced improvements enable us to reach a speed up by a factor of up to 50 in terms of sampling the data for the simulation example investigated in [19], while achieving similar performance.

As another important part of this work, we demonstrate the direct control of the position of the end effector of an industrial robot in a complex real world robot experiment, using the presented RMPC as well as the AMPC. Hence

- we show the practicability of the approaches in [36] and [19], by demonstrating it for a complex real world system for the very first time.

No additional packages or algorithms for path planning, inverse kinematics etc. are needed. This approach is flexible and allows for easy integration of additional constraints.

For reaching those goals and really underlining its practical significance, we developed a software framework, notably including C++ code integrated in a real-time environment. It involves extensive optimization and neural network inference, self written sampling procedures, parallelization and simulations. Furthermore, we present MATLAB code for doing the RMPC offline calculations and for performing the uncertainty quantification. Finally, we also developed Python code for the training of the NNs, ready to be used in a condor cluster environment.

Parts of this Thesis have been accepted for publication in the IEEE Robotics and Automation Letters (RA-L) journal and for presentation at the International Conference on Robotics and Automation (ICRA) [52].

1.4 Overview

As seen in the last section, this Master Thesis consists of multiple bigger parts. In Chapter 2, we present related work and delimitate it to what we have done. In Chapter 3, we introduce the concepts for MPC and RMPC design that are needed to understand our used concepts and their motivation. In Chapter 4, we then go into detail regarding the used RMPC scheme and explain the needed modifications we propose in order to obtain the required functionality while still guaranteeing stability and recursive feasibility. Chapter 5 then introduces the formulation of our AMPC approach and explains the modified criterion we use for the validation.

With Chapter 6 - introducing the used frameworks and toolboxes - we get started with the more practical parts of this work. We set up the whole pipeline once for a simpler simulation example. We choose a chemical stirred tank reactor (CSTR) which is also used in [19]. We show the needed steps and results in Chapter 7. Providing the theory, doing the computations and implementing the software is the biggest and most challenging part of this thesis. Regarding this, we go into detail in Chapter 9, after having introduced the robotic system we are using in Chapter 8.

We conclude the thesis in Chapter 10. We discuss our results, summarize our findings and show potential areas for future work.

Additionally, we provide a user manual which can be found in Appendix A of this thesis, containing more practical components, e.g. how to install the frameworks and how to make use of them. Also a detailed description of how to use our developed code is provided.

Last but not least, in Appendix B we present an extrapolation over the potential of this thesis for tackling climate change. Even though connections are not directly obvious, it is exciting to think about these potential use cases and areas of impact.

Chapter 2

Related Work

In this chapter we will mainly describe related work with respect to two aspects: other approaches to do fast explicit (and potentially approximate) MPC and other techniques to do robot end-effector control with relations to ours. Work we have used to design our approach (i.e. mainly for the RMPC design) as well as further extensions for potential future work are described directly in the related chapters.

2.1 Explicit MPC Representation

In [44], Lovelett et al. tackle the computational complexity of solving the MPC formulations at every time step. They make use of data mining and manifold learning to make predictions of the MPC control policy for complicated function mapping from the system state. Particularly, they design a similarity measure to learn an intrinsic parameterization of the MPC controller using a diffusion maps algorithm (i.e. a nonlinear dimensionality reduction). In contrast to a fully learned formulation as in our case, they use this function approximation to first project the points from the state space to this intrinsic space. Then, in a next step another function approximation is used to map it from this space to the state policy space. The mapping from the intrinsic space to the control policy is usually also done by using polynomial regression or artificial neural networks. The first part, the manifold learning, is amenable to alternative parameterizations (instead of diffusion maps). They also demonstrate the approach by showing a simulation example of the continuously stirred-tank reactor (CSTR) as we do in Section 7.

In [10], Chen et al. present an approach for approximating explicit MPC by using constrained neural networks. The corresponding optimal MPC control law for constrained LQR problems is piecewise affine on polytopes but becomes computationally intractable for high dimensional systems. As a solution, the authors propose a modified reinforcement learning policy gradient making use of knowledge about the system model. Noticeable is that guarantees can be given with respect to the feasibility of the control inputs generated by the network, by deploying *Dykstra's* algorithm for projecting the output of the NN. The latter could also be an interesting extension to our work. A strong drawback of this approach is that this projection is done to an offline computed control invariant set, which is inherently limited to low dimensional linear systems. They evaluate the performance of the described approach on numerical examples including a 2D double integrator and a 4D linear system.

Lucia et al. propose in [45] a deep learning-based approach to robust nonlinear model predictive control. This approach's idea of approximating generated policies with deep networks is similar to the one of [19] and ours. However, in contrast to [19] or us, they use multi-stage NMPC for generating data. One of their main results is that they were able to show that deep networks perform significantly better in learning the policy compared to shallow networks. However, a big downside here is that the underlying multi-stage NMPC only provides an approximation for continuous-valued uncertainty and disturbance. Furthermore, no guarantees on the resulting NN can be given, in contrast to [10] and [19] or us.

Another recent work is given in [74], where the authors present a framework for approximating the explicit MPC law for linear parameter-varying systems. In particular, additional to the control policy they also learn a *certificate policy* to estimate the sub-optimality during execution time. Both policies are learned from data while providing a randomized strategy guaranteeing the quality of the learned policy. This allows the authors to bound the probability of a solution for being infeasible or sub-optimal. The algorithm doesn't require the solution of an optimization problem online and can therefore be applied on resource-constrained systems, similar to us. They are able to achieve a performance speedup of up to two magnitudes with small performance degradation on a vehicle dynamics control problem in simulation.

In [8], the authors present an approximation of a nonlinear model predictive controller back in 2008. Set membership function approximation methodologies are used by applying the nearest point approach. Furthermore, a finite number of solutions of the nonlinear MPC controller is computed offline. The functions deployed for the approximation fulfill input constraints and are computation-wise time independent w.r.t. the control horizon. However, this approach is not easily scalable to higher dimensions and increases in computational complexity and memory demands with increasing number of samples.

Another interesting work is given in [28]. In this work, the authors analyze the ability of deep neural networks to approximate MPC control laws from a theoretical perspective. They provide theoretical bounds on the minimum number of hidden layers and neurons per layer that a network should have to exactly represent a given policy. Finally, they also present an approximate explicit MPC scheme. On the one hand, they deal with the approximation error similar to [10] by doing feasibility recovery based on control invariant sets which can be challenging in practice. On the other hand, they present an a-posteriori statistical verification technique to compute safe sets, based on trajectories. The safe set is obtained by either representing it as an ellipsoidal with a convex optimization for finding the maximum-sized hypercube enclosing this ellipsoidal, or by using support vector machines (SVM) with a suitable SVM learning problem. The ellipsoidal set is a more conservative solution while the SVM allows a trade-off between the size of the safe set and the proneness towards misclassification. Finally, they validate those safe sets, since their computation is based on a finite number of data points. In contrast to [19] and similar to us, Karg et al. don't try to find statistical guarantees on the closed-loop behavior but instead on the closed-loop performance of the approximate solution. For the sake of this statistical verification, the authors also use Hoeffding's inequality, similar to us.

In contrast to the previously mentioned works, in [24] the authors are not proposing another approach for approximating MPC controllers but instead, they present a hybrid system approach (*Verisig*) to verifying safety properties of closed-loop systems using neural networks as controllers. In contrast to other work in this field, *Verisig* is also able to verify properties of the closed-loop system for sigmoid-based networks. By exploiting the fact that sigmoid functions are a solution of quadratic differential equations they find a way of transforming the neural network to an equivalent hybrid system. They can decide for reachability for networks with one hidden layer or for general networks with Schanuel's conjecture. In the end, the authors evaluate *Versisig* on a neural network used to approximate an MPC. However, this approach is only applicable to linear hybrid systems and finite number of possible actions (e.g. bang-bang control of control-affine systems following a piece-wise linear plan).

2.2 Control of Redundant Robot Manipulators

In the following we will explain how control of redundant robot manipulators is usually done.

In a tutorial [60] from 1990, Siciliano et al. explained the state of the art motion control techniques at that time. They formulated the kinematic control problem as finding a joint space trajectory $q(t)$ s.t. $f(q(t)) = x(t)$, with $x(t)$ being the trajectory in the task space. The direct kinematic mapping can be written as $x = f(q)$ and therefore $\dot{x} = J(q)\dot{q}$. As usually redundant robots are used, the inverse kinematics problem admits an infinite number of solutions. The authors suggest to exploit this redundancy to meet additional constraints and describe that most approaches at that time tried to invert the mapping from joint space to task space. One way is for example to use the Moore-Penrose pseudoinverse of the Jacobian matrix to obtain $\dot{q} = J^{\dagger}(q)\dot{x}$. This approach generates the minimum norm joint velocities. However, this approach doesn't avoid kinematic singularities in any practical sense. As a result other (non-singular) inversion variants of the Jacobian have been proposed. Siciliano et al. mention, that one of the big drawbacks of this class of approaches is that a solution of the type $\dot{q} = K(q)\dot{x}$ as we have just described is inherently open-loop, since this equation is integrated over time to generate the desired joint path $q(t)$. This results in unavoidable drifts in the task space due to integration on the computer in DT. To overcome this, an additional error term can be introduced to the task space vector $\dot{x}$ which captures the deviation to the desired trajectory in the task space. This would then look as following: $\dot{x} = \dot{x}_d + \Lambda \cdot e$. In this tutorial, further approaches such as gradient projection, task space augmentation and the finding of inverse kinematic functions are described. The solution of the latter is always given for simple non-redundant geometries and allows for online implementation. However, all of the mentioned approaches assume a trajectory $x(t)$ given beforehand, which is not given in our case (see Chapter 8).

A more recent and more complete collection of methods and approaches is given in the book [61]. In Chapter 4 of the book, methods for trajectory planning are described. In Chapter 8, the authors devoted a separate chapter to motion control. In this chapter they explain two classes of methods: joint space control as well as operational space control. For both of the formulations calculation of inverse kinematics is needed. For joint space control this is done before the feedback loop, i.e. the control is done in an open loop fashion, for the latter formulation the inverse kinematics are embedded in the feedback control loop. In contrast, our approach only requires forward kinematics and thus, we don't need to design multiple decoupled components as involved in other robot control approaches.

As a next step, we will mention works which address robot control more recently and with more advanced techniques.

In 2006, Bertram et al. [5] describe an integrated approach for path planning of redundant manipulators. They propose a way of unifying the calculation of the goal configuration with the search of a suitable path. They adopt workspace heuristic functions implicitly defining goal regions of the configuration space and guide an extension of rapidly-exploring Random Trees (RRT) used for searching these regions. The approach is demonstrated in simulation for a humanoid grasping task.

In [65], Vahrenkamp et al. present an approach for efficient motion planning for a dual-arm manipulator. They investigate solving of the inverse kinematics problem and motion planning by combining a gradient-descent approach in the robots pre-computed reachability space with random sampling of free parameters. Additionally they propose two RRT-based motion planning algorithms that interleave the search for an inverse kinematic solution with the search of a collision-free trajectory. They demonstrate this approach in simulation and on the humanoid robot ARMAR-III.

Bargsten et al. propose a full framework for control of the KUKA LBR4+ robot from performing system identification to model-based control [3]. For the control task, they are solving a trajectory tracking problem by using a computed torque controller (a.k.a. inverse dynamics controller). They choose a feedback for linearizing the dynamics of the system, i.e. they are performing exact feedback linearization to the system. This is also highly relevant, since it allows to transform the robot dynamics to the kinematic formulation we investigate in this work. They tested it on the real world system but only for sampling rates up to 100 Hz, since Python was used for the implementation. However, they still achieved decent tracking results.

In the next step, we will look into MPC approaches used for robot control.

In [13], the authors look at a real-time feasible implementation of a model predictive path-following control for the KUKA LBR4+ robot. They investigate constrained output path-following with and without reference speed assignments. Similar to our work, they are also trying to track a geometric reference in the output space. They also consider the system with input and state constraints and make use of a CT sampled-data nonlinear MPC scheme which they denote as model predictive path-following control. In contrast to us, they base the control on an augmented system description not only containing the original states but also a path parameter Θ. In their work they treat contact forces as disturbances and solve the optimization problem by using the ACADO real-time iteration scheme. They demonstrate their approach in practical results. For the optimization they consider a quadratic cost trying to minimize the error, the deviation to Θ as well as to $\dot{\Theta}_{ref}$. For the whole computation they assume the geometric reference in the output space to be given by $\mathcal{P} = \{y \in \mathbb{R}^{n_u} \mid \Theta \in \mathbb{R} \mapsto y = p(\Theta)\}$ with parameterization $p(\Theta)$. In our work, we are not constraining ourselves to such a parameterization and can principally track every (even non-reachable) 3D output reference.

In [2], the authors also describe a MPC path following and trajectory tracking approach, however not specifically for the KUKA LBR4 robotic arm. Arbo et al. propose a model predictive path following approach which allows robotic manipulators to stop at obstructions. Similar to us, they assume the robot to have known forward kinematics. In contrast to us, they deploy a constrained path-timing variable s moving from 0 to s_f and for their approach the path needs to be given in the task space beforehand. They define two cost functions for the two approaches (path following and trajectory tracking) and demonstrate their work. They compare it to model predictive trajectory tracking in a simulation example for a two-link manipulator.

Chapter 3

Theoretical Background

In this section, we introduce the necessary theoretical background that this thesis builds upon. We start by describing standard MPC theory in Section 3.1. Then we will describe techniques for doing RMPC, including the core work from Köhler et al. [36], in Section 3.2. Finally, we will close this chapter with background theory in Machine Learning (ML).

3.1 MPC - Theory

MPC is a control scheme trying to repeatedly obtain the open-loop finite horizon optimal control. In contrast to standard optimal control such as LQR control, its formulation is easily expandable to nonlinear systems and it is also able to take several types of constraints, such as input and state constraints into account. In this chapter we we will show the formulation of the corresponding optimization problem. Additionally, we will provide the most important requirements for successfully designing a nominal MPC controller. In Sec. 3.1.2 we will introduce a special formulation to be in a position to perform (output) set point reference tracking, which will be used in the practical application (Chap. 8) of this thesis.

3.1.1 General MPC Formulation

For theory on MPC we refer to the standard work in [55]. We first make the following definition:

Definition 3.1. *Compact nonlinear constraint set:*
$\mathcal{Z} = \{(x,u) \in \mathbb{R}^{n+m} | g_j(x,u) \leq 0, \quad j = 1,...,p\} \subset \mathbb{R}^{n+m}$

Including the definition of this constraint set, the simplest standard MPC formulation can be seen in (3.1):

$$\begin{aligned}
V_N(x(t)) \quad &= \quad \min_{u(\cdot|t)} \sum_{k=0}^{N-1} l(x(k|t), u(k|t)) && (3.1a)\\
\text{subject to} \quad & x(0|t) = x(t), && (3.1b)\\
& x(k+1|t) = f(x(k|t), u(k|t)), && (3.1c)\\
& (x(k|t), u(k|t)) \in \mathcal{Z}, && (3.1d)\\
& k = 0, ..., N-1.
\end{aligned}$$

Here, $l(x(k|t), u(k|t))$ denotes the objective and $\mathcal{Z}$ defines the state and input constraints. Additionally, the state must evolve according to the given state dynamics. In practice, the objective is very often formulated as a sum of 2 quadratic norm terms:

$$l(x,u) = |x|_Q^2 + |u|_R^2. \tag{3.2}$$

Practically, systems are usually controlled using the receding horizon strategy [49]. This means that at every time step a complete optimization problem along a prediction horizon is solved and the optimal input $u^*(0|t)$ is applied to the system. Sometimes it is possible to obtain good results by using the simple formulation in (3.1). However, having stable and converging open-loop solutions does not necessarily imply stability for the resulting closed-loop system. Especially short prediction horizons can cause the loss of stability properties, i.e. the trajectories may not converge to the origin. Moreover, no recursive feasibility is guaranteed, i.e. the problem might not have a solution at all future time steps, due to non avoidable constraint violations. We pick up on the following common definition.

Definition 3.2. *The feasible set $\mathcal{X}_N$ is defined as the set of initial states x for which the MPC problem with horizon N is feasible.*

For the standard MPC formulation, the initial state at future time steps might not lie within the feasible set. This problem originates from the use of a short sight strategy; ideally we would solve the MPC problem with an infinite horizon which is practically intractable. For more information see [72].

Stability and Recursive Feasibility

We introduce three common definitions (see [72]).

Definition 3.3. *The MPC problem is called* recursively feasible*, if for all feasible initial states feasibility is guaranteed at every state along the closed-loop trajectory.*

Definition 3.4. *Lyapunov Stability: The equilibrium point at the origin of a system $x(k+1) = f(x(k), \kappa(x(k)))$ is said to be stable in $\mathcal{X}$, if for every $\epsilon > 0$ there exists a $\delta(\epsilon) > 0$ such that for every $x(0) \in \mathcal{X}$:*
$||x(0)|| \leq \delta(\epsilon) \Rightarrow ||x(k)|| < \epsilon \quad \forall k \in \mathbb{N}$.

Definition 3.5. *Invariant Set: A set $\mathcal{O}$ is called positively invariant for system $x(k+1) = f(x(k), \kappa(x(k)))$, if*
$x \in \mathcal{O} \Rightarrow f(x, \kappa(x)) \in \mathcal{O}, \quad \forall k \in \mathbb{N}$.

The main approach for ensuring stability and feasibility is to introduce terminal ingredients, i.e. a terminal cost and a terminal set. The MPC formulation then looks as follows:

$$\begin{aligned} V_N(x(t)) \quad &= \quad \min_{u(\cdot|t)} \sum_{k=0}^{N-1} l(x(k|t), u(k|t)) + V_f(x(N|t)) && (3.3a)\\ \text{subject to} \quad & x(0|t) = x(t), && (3.3b)\\ & x(k+1|t) = f(x(k|t), u(k|t)), && (3.3c)\\ & (x(k|t), u(k|t)) \in \mathcal{Z}, && (3.3d)\\ & x(N|t) \in \mathcal{X}_f, && (3.3e)\\ & k = 0, ..., N-1, \end{aligned}$$

Introducing terminal ingredients provides many desirable properties for the control scheme. However, it comes at the cost of a smaller region of attraction. Especially for non reachable set points this MPC formulation can become infeasible in situations when controllers without terminal ingredients still perform well. In the following we will always assume to have reachable set points or use the set point tracking formulation from Sec. 3.1.2. A first trivial solution for the terminal set is to use the following constraint:

$$\text{Equality Constraint: } x(N|t) \in \mathcal{X}_f = 0, \tag{3.4}$$

which guarantees recursive feasibility and stability under the assumption of $x(0|t)$ belonging to the feasible set. The terminal cost is zero, i.e. $V_f(x(N|t)) = 0$. However, it strongly reduces the region of attraction (feasible set). Therefore, the general goal is to use a more general set for $\mathcal{X}_f$

$$\text{Set Constraint: } x(N|t) \in \mathcal{X}_f, \tag{3.5}$$

that contains the set point (or without loss of generality the origin after transforming the coordinates $\tilde{x} = x - x_s$) in it's interior.

Assumption 3.1. *The stage cost is a positive definite function. The terminal set is positive invariant under the local control law $\kappa_f(x)$. All state and input constraints are satisfied in $\mathcal{X}_f$. The terminal cost $V_f(x)$ is a continuous Lyapunov function in the terminal set $\mathcal{X}_f$.*

Theorem 3.1. *Under Assumpt. 3.1 and the knowledge of $x(t)$ being part of the feasible set $\mathcal{X}_N$, recursive feasibility and stability are guaranteed.*

Proof. This can be shown and is a standard proof, e.g. see [72]. □

This argument holds for general nonlinear systems. However, this doesn't tell us how to find the terminal ingredients.

Linear Systems For linear systems the problem can be split up in two subproblems: until time step $N-1$ we allow constraints being active whereas for $k \geq N$ we require the constraints to be inactive. Then we can assume to apply the LQR control law from step N to ∞ and therefore get for the terminal cost the infinite horizon cost of the LQR controller

$$V_f(x(N|t)) = |x(N|t)|_P^2, \tag{3.6}$$

with P being the solution of the DT algebraic Riccati equation. To make the previous terminal cost valid, the terminal set $\mathcal{X}_f$ needs to be chosen such that constraint satisfaction can be guaranteed when applying the LQR control law $K_{LQR}x$.

Nonlinear Systems For nonlinear systems, Chen et al. [9] present a MPC scheme that guarantees asymptotic closed-loop stability and recursive feasibility, given the optimization problem at time $t = 0$ is feasible. For this purpose, a terminal region is introduced which is invariant for the nonlinear system, controlled by a local linear state feedback. The introduced terminal cost is quadratic and bounds the infinite horizon cost of the nonlinear system controlled by the same linear state feedback, starting from their terminal region. The size of the obtained terminal region hereby strongly depends on the nonlinearity of the system to be controlled; the stronger the nonlinearity, the smaller the terminal region will be. For details on how to find the terminal region and terminal cost for this approach please have a look at Sec. 4.4.

3.1.2 Set Point Tracking MPC

In many situations the goal of using a controller is to do output reference tracking, i.e. to track a given set point y_t with the actual output y of the corresponding plant. MPC controllers in their standard formulation (see (3.1) and (3.3)) can not be used for this task, particularly not if no inverse transformation from the output to the states is known along the prediction horizon, i.e.

$$x_s = g_x(y_s), \quad u_s = g_u(y_s) \tag{3.7}$$

are unknown. For this application Limon et al. developed a MPC formulation allowing for output reference tracking. It was introduced in [40] and gerneralized to nonlinear systems in [43]. The cost function in (3.8) was slightly adapted to our use case but is conceptually taken from [43]:

$$J_N(x, y_t; u(\cdot|t), y_s, x_s, u_s) = \sum_{k=0}^{N-1} l(x(k|t) - x_s, u(k|t) - u_s) + V_f(x(N|t) - x_s, y_s) + V_O(y_s - y_t). \tag{3.8}$$

Here, V_O needs to be positive definite. Next to the well known control inputs $u(\cdot|t)$, additional decision variables y_s, x_s and u_s are introduced. With this cost function we get the *set point tracking*

MPC control law according to [43]:

$$\begin{aligned}
V_N(x(t), y_t) = \quad & \min_{u(\cdot|t), x_s, u_s} \; J_N(x, y_t; u(\cdot|t)*, y_s, x_s, u_s) && (3.9a)\\
\text{subject to} \quad & x(0|t) = x(t), && (3.9b)\\
& x(k+1|t) = f(x(k|t), u(k|t)), && (3.9c)\\
& (x(k|t), u(k|t)) \in \mathcal{Z}, && (3.9d)\\
& x_s = f(x_s, u_s), \quad y_s = h(x_s, u_s), && (3.9e)\\
& (x(N|t), x_s) \in \mathcal{X}_f, && (3.9f)\\
& k = 0, ..., N-1,
\end{aligned}$$

Under convexity assumptions, this approach has several advantageous properties:

- It converges to the desired setpoint y_t, if admissible.
- The optimal setpoint is asymptotically stable for piece-wise constant references.
- For unreachable set points, the asymptotic stability of the optimal reachable set point is given.
- Constraint tightening of the RMPC approach can easily be applied.

We use this approach for our practical application on Apollo (Chap. 8). Further explanations on the implementation are provided along the way.

3.2 RMPC - Theory

In Section 3.1 we introduced several MPC formulations also including guarantees for stability and recursive feasibility. However, its design always relies on an exact model description which is never given in practice. As a result, it can happen that stability and recursive feasibility are lost when disturbances are introduced in simulation or the MPC is deployed on a real world (physical) system. RMPC tries to account for the deviation of the model by making it robust to disturbances.

3.2.1 Standard Tube-Based Robust Nonlinear MPC

One way of dealing with these disturbances for nonlinear systems is tube-based robust nonlinear MPC. Tube-based MPC can be seen as an implementable form of feedback MPC, which can ensure that the deviation of the actual state from the nominal state is smaller than that obtained with open-loop MPC [47].

For a linear system being controlled, the tube-based system control laws are given as

$$u_{system} = v_{nominal} + K(x - z_{nominal}), \tag{3.10}$$

with $v_{nominal}$ and $z_{nominal}$ being control and state of the conventional MPC determined on the nominal system. For its design for linear systems, providing robustness to bounded disturbances comes at the cost of a smaller domain of attraction, refer to [48, 11, 50, 41].

Mayne et al. [47] described in their work a popular tube-based MPC extension to nonlinear systems. In their approach, first a reference trajectory is determined by solving the nominal MPC problem with tightened constraints. Then in a second step, the trajectories of the disturbed system are forced to lie within a tube with the center being the previously computed nominal reference trajectory. In their description, only additive disturbances are covered, i.e.

$$x(k+1) = f(x, u) + w, \tag{3.11}$$

for $w \in \mathbb{W}$, with $\mathbb{W}$ being a compact, convex set containing the origin and f being twice continuously differentiable. The simple approach of using a linear feedback as in [48] is unlikely to work for nonlinear systems. Hence, Mayne et al. employ an conventional ancillary MPC controller additional to the nominal open-loop MPC trajectory to attract the actual state of the disturbed system towards the nominal one. Hence, they are introducing a second degree of freedom. Furthermore, constraint tightening is performed to get a robustly stabilizing feedback MPC controller.

For the ancillary controller, the cost function in (3.12) is used to attempt to steer each state encountered towards the nominal trajectory:

$$J_N(x(t), x_e; u^*) = V_f(x(N), x_e) + \sum_{k=0}^{N-1} l(x(k|t) - z^*(t+k, x_0, x_e), u(k|t) - v^*(t+k, x_0, x_e)). \quad (3.12)$$

In (3.12), z^* denotes the nominal reference trajectory and v^* the reference input sequence.

A big downside of this tube-based MPC approach is that offline tuning and validation are needed.

3.2.2 Min-Max MPC

Min-Max MPC is a well known technique to approach RMPC problems [54]. It tries to find the minimum cost with respect to the worst case disturbance, while still satisfying all of the constraints. The cost function can therefore be written as in the following:

$$\min_{u(\cdot|t)} \max_{w(\cdot|t)} J_N(x(\cdot|t), u(\cdot, t)). \quad (3.13)$$

It's especially useful as reference for other approaches. However, its high computational demand prohibits a practical application for most use cases.

3.2.3 Computationally Efficient RMPC [36]

For this thesis we decided to base our RMPC design on a newer work by Koehler et al., introducing a computationally efficient tube-inspired RMPC control scheme [36]. It can be interpreted as an approximate extension of [11] to nonlinear systems. The related work in [19] - this thesis conceptually builds upon in some topics - bases its RMPC design and formulation onto the work in [33]. Even though the results for the special case of additive disturbances are similar, the work in [36] covers more general types of disturbances and uncertainties and offers a less conservative formulation.

The whole work is based on the assumption of local incremental stabilizability. This is given in Assumption 3.2.

Assumption 3.2. *Local incremental stabilizability [36]: There exists a control law $\kappa(x, z, v)$, an incremental Lyapunov function $V_\delta(x, z, v)$ which is continuous in the first argument and satisfies $V_\delta(z, z, v) = 0$ for all $(z, v) \in \mathcal{Z}$, and parameters $c_{\delta,l}$, $c_{\delta,u}$, δ_{loc}, $k_{max} > 0$. $\rho \in (0, 1)$, such that the following properties hold for all $(x, z, v) \in \mathbb{R}^n \times \mathcal{Z}$ with $V_\delta \leq \delta$, and all $(x^+, z^+, v^+) \in \mathbb{R}^n \times \mathcal{Z}$ with $x^+ = f(x, \kappa(x, z, v))$, $z^+ = f(z, v)$:*

$$c_{\delta,l}||x - z||^2 \leq V_\delta(x, z, v) \leq c_{\delta,u}||x - z||^2, \quad (3.14a)$$

$$||\kappa(x, z, v) - v||^2 \leq \kappa_{max} V_\delta(x, z, v), \quad (3.14b)$$

$$V_\delta(x^+, z^+, v^+) \leq \rho^2 V_\delta(x, z, v). \quad (3.14c)$$

Problem Formulation

The work in [36] considers nonlinear perturbed (discrete time) systems of the form

$$x(t + 1) = f_w(x(t), u(t), d(t)), \quad d \in \mathbb{D} \subset \mathbb{R}^q. \quad (3.15)$$

This contains general nonlinear state and input dependent disturbances or uncertainty. Only a general assumption of the effect on the system compared to the nominal system is needed, as formulated in the following.

Assumption 3.3. *The perturbed system satisfies*

$$f_w(x, u, d) - f(x, u) \in \mathcal{W}(x, u), \tag{3.16}$$

with $\mathcal{W}(x, u)$ being compact. Correspondingly, there exists a scalar function $\hat{w}$ that satisfies $|d_w| \leq \hat{w}(x, u)$ for all $d_w \in \mathcal{W}(x, u)$.

Note that different norm definitions can be used for the constraint on d_w, e.g. the 2- or the ∞-norm. The state and input constraints are still denoted and given as defined in Def. 3.1. This RMPC scheme [36] addresses incrementally exponentially stabilizable nonlinear systems (see Assumpt. 3.2). It describes a MPC control formulation which ensures practical stability, recursive feasibility and guarantees constraint satisfaction under the general disturbance in (3.15) and Assumption 3.3.

Disturbance Description

The RMPC design could principally directly be conducted using the disturbance bound $\hat{w}$ from Assumption 3.3. However we would then always need to bound the disturbance using Lipschitz-like constants, introducing additional conservatism. Therefore, we directly consider the influence of the disturbance on the incremental Lyapunov function V_δ. To be in a proper position to do this, the following assumption is needed.

Assumption 3.4. *Consider $\hat{w}$, stabilizing feedback κ and V_δ. There exists a function w_δ, s.t. for any point $(x, z, v) \in \mathbb{R}^N \times \mathcal{Z}$ with $V_\delta(x, z, v) \leq c^2$, and any $c \in [0, \sqrt{\delta_{loc}}]$, we have*

$$\hat{w}(x, \kappa(x, z, v)) \leq w_\delta(z, v, c). \tag{3.17}$$

Furthermore, w_δ satisfies the monotonicity property: With constants $0 \leq c_2 \leq c_1 \leq \sqrt{\delta_{loc}}$ and $V_\delta(x, z, v) \leq (c_1 - c_2)^2$, we have

$$w_\delta(x, \kappa(x, z, v), c_2) \leq w_\delta(z, v, c_1). \tag{3.18}$$

Given this, it is possible to obtain the following proposition (see [36]).

Proposition 3.1. *Let Assumption 3.2, 3.3 and 3.4 hold. There exists $\tilde{w}_\delta$, s.t. for any $(x, z, v) \in \mathbb{R}^n \times \mathcal{Z}$, any $(z^+, v^+) \in \mathbb{R}^n \times \mathcal{Z}$ with $z^+ = f(z, v)$, and any disturbance $d_w \in \mathcal{W}(x, \kappa(x, z, v))$, we have*

$$V_\delta(z^+ + d_w, z^+, v^+) \leq \tilde{w}_\delta^2(z, v, c). \tag{3.19}$$

Furthermore, $\tilde{w}_\delta$ satisfies the same monotonicity property as in Assumption 3.4.

Proposition 3.1 can be shown for setting $\tilde{w}_\delta(z, v, c) = \sqrt{c_{\delta,u}} w_\delta(z, v, c)$.

General Paper Findings

The discussed paper [36] tackles this, by

1. presenting a constraint tightening for nonlinear robust MPC based on incremental stabilizability and
2. considering general nonlinear state and input dependent disturbances by including the predicted size of the tube as scalar variables in the MPC optimization scheme.

The tube size then determines the needed degree for the constraint tightening at a given time step.

General Nonlinear Disturbances For the general formulation, the disturbance descriptions in (3.15) and in Assumpt. 3.3 are taken to find a bound $\tilde{w}_\delta$ on how much the incremental Lyapunov function V_δ changes in the presence of the disturbance, as seen in Prop. 3.1:

$$V_\delta(z^+ + d_w, z^+, v^+) \leq \tilde{w}_\delta^2(z, v, c), \text{ for } V_\delta(x, z, v) \leq c^2 \text{ and } \forall d_w \in \mathcal{W}(x, \kappa(x, z, v)). \tag{3.20}$$

Additionally, a factor c_j is introduced which determines to which extent the effective constraints need to be tightened according to the used incremental Lyapunov function, in order to still satisfy the actual constraints under any possible disturbance.

Assumption 3.5. *$g_j(z, v)$ is the function defining the compact nonlinear constraint set in Equ. 3.1. We require that*

$$g_j(x, \kappa(x, z, v)) - g_j(z, v) \leq c_j \sqrt{V_\delta(x, z)}, \quad \forall (x, z, v) \in \mathbb{R}^N \times \mathcal{Z} \text{ with } V_\delta(x, z, v) \leq \delta \tag{3.21}$$

holds.

The paper [36] proposes the robust MPC scheme in (3.22)

$$\begin{aligned}
V_N(x(t)) \quad &= \quad \min_{u(\cdot|t)} J_N(x(\cdot|t), u(\cdot|t)) && (3.22a)\\
\text{subject to} \quad & x(0|t) = x(t), \quad s(0|t) = 0, && (3.22b)\\
& x(k+1|t) = f(x(k|t), u(k|t)), && (3.22c)\\
& s(k+1|t) = \rho s(k|t) + w(k|t), && (3.22d)\\
& w(k|t) = \tilde{w}_\delta(x(k|t), u(k|t), s(k|t)), && (3.22e)\\
& g_j(x(k|t), u(k|t)) + c_j s(k|t) \leq 0, && (3.22f)\\
& s(k|t) \leq \bar{s}, \quad w(k|t) \leq \bar{w}, && (3.22g)\\
& (x(N|t), s(N|t)) \in \mathcal{X}_f, && (3.22h)\\
& k = 0, ..., N-1, \quad j = 1, ..., p,
\end{aligned}$$

with J_N defined as in the following

$$J_N(x(\cdot|t), u(\cdot|t)) = \sum_{k=0}^{N-1} l(x(k|t) - x_s, u(k|t) - u_s) + V_f(x(N|t) - x_s). \tag{3.23}$$

The main idea is to predict the tube size $s \in \mathcal{R}_{\geq 0}$ online as part of the optimization problem. The evolution of the tube size is determined by the appearing noise and the contraction parameter ρ.

Assumption 3.6. *There exists a terminal controller κ_f, a terminal cost function V_f, a terminal set $\mathcal{X}_f$, and a constant $\bar{w}$ s.t. the following properties hold for all $(x, s) \in \mathcal{X}_f$, all $w \in [\bar{w}_{min}, \bar{w}]$ with $\bar{w}_{min} := \inf_{(x,u) \in \mathcal{Z}} \tilde{w}_\delta(x, u, 0)$, all $s^+ \in [0, \rho s - \rho^N w + \tilde{w}_\delta(x, \kappa_f(x), s)]$, and all d_w s.t. $V_\delta(x^+ + d_w, x^+, \kappa_f(x^+)) \leq \rho^{2N} w^2$:*

$$\begin{aligned}
& V_f(x^+) \leq V_f(x) - l(x, \kappa_f(x)), && (3.24)\\
& (x^+ + d_w, s^+) \in \mathcal{X}_f, && (3.25)\\
& \tilde{w}_\delta(x, \kappa_f(x), s) \leq \bar{w}, && (3.26)\\
& g_j(x, \kappa_f(x)) + c_j s \leq 0, \quad j = 1, ..., p, && (3.27)\\
& s \leq \bar{s}, && (3.28)\\
& \textit{with } x^+ = f(x, \kappa_f(x)). && (3.29)
\end{aligned}$$

Furthermore, the terminal set cost V_f is continuous on the compact set $\mathcal{X}_{f,x} := \{x | \exists s \in [0, \bar{s}], (x, s) \in \mathcal{X}_f\}$, i.e., there exists a function $\alpha_f \in \mathcal{K}_\infty$, s.t.

$$V_f(z) \leq V_f(x) + \alpha_f(||x - z||), \forall x, z \in \mathcal{X}_{f,x}. \tag{3.30}$$

With Assumption 3.6, in [36] it is shown that this RMPC formulation in (3.22) is recursively feasible, the constraints are satisfied and the origin is practically asymptotically stable for the resulting closed-loop system under practically relevant assumptions. For more details see [36].

Additive Disturbances In this work we only do RMPC design assuming and considering additive disturbances. This drastically reduces the complexity of the problem, not only for the MPC formulation itself but also for the calculation of the required parameters, e.g. the description of $\mathcal{W}$. For this simpler case, the tube size s can be explicitly written by using the formula for the geometric sum as:

$$s(k) = \frac{1-\rho^k}{1-\rho}\bar{w}, \tag{3.31}$$

with

$$\bar{w} := \sup_{z,v,v^+,d_w} \sqrt{V_\delta(f(z,v)+d_w, f(z,v), v^+)}, \tag{3.32}$$

$$s.t.(z,v) \in \mathcal{Z}, (f(z,v), v^+) \in \mathcal{Z}, d_w \in \mathcal{W}(z,v)). \tag{3.33}$$

This then leads to the following simplified RMPC formulation given in (3.34):

$$\begin{aligned}
V_N(x(t)) \quad = \quad & \min_{u(\cdot|t)} J_N(x(\cdot|t), u(\cdot|t)) && (3.34a)\\
\text{subject to} \quad & x(0|t) = x(t), && (3.34b)\\
& x(k+1|t) = f(x(k|t), u(k|t)), && (3.34c)\\
& g_j(x(k|t), u(k|t)) + c_j \frac{1-\rho^k}{1-\rho}\bar{w} \le 0, && (3.34d)\\
& x(N|t) \in \mathcal{X}_f, && (3.34e)\\
& k = 0, ..., N-1, \quad j = 1, ..., p.
\end{aligned}$$

Also the assumption for the terminal ingredients (compare Assumption 3.6) for guaranteeing stability now becomes simpler:

Assumption 3.7. *There exists a terminal controller κ_f, a terminal cost function V_f, a terminal set $\mathcal{X}_f$, s.t. the following properties hold for any $x \in \mathcal{X}_f$ and all d_w s.t. $V_\delta(x^+ + d_w, x^+, \kappa_f(x^+)) \le \rho^{2N}\bar{w}^2$:*

$$V_f(x^+) \le V_f(x) - l(x, \kappa_f(x)), \tag{3.35}$$

$$x^+ + d_w \in \mathcal{X}_f, \tag{3.36}$$

$$\frac{1-\rho^N}{1-\rho}\bar{w} \le \bar{s} = \sqrt{\delta_{loc}}, \tag{3.37}$$

$$g_j(x, \kappa_f(x)) + c_j \frac{1-\rho^N}{1-\rho}\bar{w} \le 0, \quad j = 1, ..., p, \tag{3.38}$$

$$\textit{with } x^+ = f(x, \kappa_f(x)). \tag{3.39}$$

Furthermore, there exists a function $\alpha_f \in \mathcal{K}_\infty$, s.t.

$$V_f(z) \le V_f(x) + \alpha_f(||x-z||), \forall x, z \in \mathcal{X}_f. \tag{3.40}$$

Describing the disturbances as additive ones reduces the complexity of the optimization problem and makes it equivalent to the corresponding nominal MPC scheme. The main disadvantage of it is the potential of introducing a lot of conservatism.

3.3 Learning - Theory

Machine learning (ML) is a tool which was successfully deployed in many different tasks in the last decades. In the last few years it attracted even more attention due to the recent successes in deep learning. Particularly impressive successes, e.g. in image processing, natural language processing and reinforcement learning, could arguably also be achieved thanks to access to a significant increase in computational resources.

The field of ML can be clustered in the following three subcategories: i) supervised learning, ii) unsupervised learning and iii) reinforcement learning. In our work we will only make use of supervised learning techniques; regression and classification. Therefore, in the following we will only give an introduction for the latter. For each of the topics, we will only provide a brief account.

3.3.1 Supervised Learning

Assume there exists a function $f(x)$. Supervised learning is a technique for finding $f(x)$ by providing a set of training examples $\mathbb{X}$ with p corresponding (potentially noisy) target samples $y^{(i)}, i = 1, ..., p$ of the function $f(x)$. For approximating this function, nowadays neural networks (NN) are used very often. NNs are trained by using back-propagation. This is done by inserting samples to the network, calculating its output at the current state of the network, computing the error e to the desired value the network should show at its output and then doing gradient descent on the weights of the activation functions in the network nodes.

Recent big successes with NNs were mainly possible thanks to deep learning techniques. Nowadays, with the help of modern graphic processing units (GPUs) it is possible to also train those big models in tractable amounts of time. Currently, the most popular choice for the optimizer of the training (which is e.g. responsible for finding the learning rate) is the ADAM optimizer [29]. As activation functions, usually rectified linear units (ReLu) functions are chosen, since they behave advantageous with respect to problems of training networks, such as the vanishing gradient problem.

Supervised Regression

Supervised regression denotes the special case of the previous introduction to supervised learning when the function $f(x)$ denotes a continuous valued function. This means, we really try to find a continuous function which maps values of a specific domain into its range. The corresponding neural networks are usually built by putting a linear activation at the output layer.

Supervised Classification

Classification is the problem of matching data points to classes, i.e. the function $f(x)$ has discretized (but possibly infinitely many) possible values. Since differentiable activation functions need to be used in the network, the output will still take continuous values. To obtain the desired classes, then a threshold is taken of this output. The normal choice for the activation of the output layer for classification tasks is usually a soft-max function.

3.3.2 Ability to Overcome the Curse of Dimensionality

In our practical example in Chapter 8 we need to be able to deal with relatively high input dimensions. E.g. already for simplest case of tracking an output reference, we need an input size of 7 or 11 for the case of using the simplified or the full kinematic formulation, respectively. By regarding the sampling of this formulation as a sampling of a multi-dimensional grid, this means that we are only able to sample significantly less than 10 points per dimension. We will do some more practical computations for our robotic use case in Section 9.2.3.

The neural networks used in our case might still be able to perform well in approximating the desired function, since they often have an impressive ability of projecting high dimensional problems to lower dimensional manifolds. To make this even more effective, it is usually necessary to make assumptions about the data and to exploit them in the models. A very good example for this are convolutional neural networks (CNNs), see [17], which e.g. assume important spatial relations of neighboring pixels in image processing.

3.3.3 Statistical Learning

Statistical learning theory represents a statistics-based method to investigate ML algorithms and is often able to unveil additional, possibly hidden, information.

Standard literature such as [18] describe the main concepts. However, since in this work we are mainly interested in validating the performance of our neural network, we want to make statistical statements about the reliability of our learned policy. Several inequalities are known for providing an upper bound to the probability for a specific deviation of the observed mean value. Examples are the Bienayme-Chebychev inequality and Chebyshev's inequality. In this work we will make use of the so called Hoeffding inequality [20]. In general, this inequality is useful, since it provides an upper probability bound to the scenario of having divergence of the real mean value of a distribution compared to the one observed from experiments. The corresponding inequality is given in the following:

$$\mathbb{P}\left[|\tilde{\mu} - \mu| \geq \epsilon_h\right] \leq 2e^{-2p\epsilon_h^2}. \tag{3.41}$$

In this case, $\tilde{\mu}$ denotes the empirical risk, i.e. in our case the observed mean value of the distribution of a collection of random variables, while μ is the actual mean value. To make this statement valid, p independent and identically distributed (i.i.d.) random variables need to be observed. ϵ_h describes the difference in the mean value of the observed and the real mean value. We will go into more detail about this for our specific use case in Section 5.3.2.

A comprehensive overview of concepts in statistical learning theory is given in [66], which also explains Hoeffding's inequality.

Chapter 4

RMPC Design

For the RMPC design we use the theory from Sec. 3.2.3. In the following, we will first show the used and simplified setup of our MPC design. Then in Section 4.2 we will give an high level overview of how the RMPC design can be done. Afterwards, we will provide more insights into the computation of the sets, values and parameters needed for getting a proper RMPC controller according to the paper in [36]. We will also introduce the continuous time (CT)-equivalent parameters, to do the computations independently from the specific sampling time used in the real-time implementation. A more compact version of the theory presented herein is presented in our corresponding paper [53].

4.1 Setup

Quadratic Incremental Lyapunov Function

For the incremental Lyapunov function V_δ, a quadratic function is chosen, i.e.

$$V_\delta(x, z) = |x - z|^2_{P_\delta}. \tag{4.1}$$

For this special case, Proposition 4.1 provides a direct method to compute $\tilde{w}_\delta$ for general nonlinear disturbances.

Proposition 4.1. *Let Assumption 3.3 hold. Now, suppose that Assumption 3.2 is satisfied with* $V_\delta(x, z, v) = |x - z|^2_{P_\delta}$. *Then Assumption 3.4 is satisfied with*

$$w_\delta(z, v, c) := \sup_{\{x \mid |x-z|_{P_\delta} \le c\}} \hat{w}(x, \kappa(x, z, v)). \tag{4.2}$$

Furthermore, the conditions in Proposition 3.1 are satisfied with

$$\tilde{w}_\delta(z, v, c) := \sup_{\{x \mid |x-z|_{P_\delta} \le c\}} \sup_{d_w \in \mathcal{W}(x, \kappa(x,z,v))} |d_w|_{P_\delta}. \tag{4.3}$$

This Proposition uses directly the shape V_δ and $\mathcal{W}$ to compute $\tilde{w}_\delta$, thus leads to less conservative bounds than many other approaches. In the following we will present this for additive disturbances.

Additive Disturbance

As mentioned earlier we will only consider additive disturbances. By doing so, the formulation in Equation 3.22 which contains the tube size as an additional state in the optimization problem simplifies to the form seen in Equation 3.34. The additive disturbance modifies the function f_w to the following:

$$f_w(x, u, d) = f(x, u) + d_w. \tag{4.4}$$

With this formulation and a quadratic incremental Lyapunov function, the Proposition 4.1 simplifies even further to the following:

$$\bar{w} := \sup_{z,v,d_w} \sqrt{|(f(z,v)+d_w) - f(z,v)|^2_{P_\delta}}, \tag{4.5}$$

$$s.t.(z,v) \in \mathcal{Z}, (f(z,v),v^+) \in \mathcal{Z}, d_w \in \mathcal{W}(z,v)). \tag{4.6}$$

Quadratic Stage Cost

For all of our MPC designs in this thesis we use a quadratic stage cost $l(x,u)$. This means that

$$l(x,u) = |x - x_e|^2_Q + |u - u_e|^2_R. \tag{4.7}$$

In this case x_e and u_e denote the reference state and input for both setups; when the reference is provided in state and input space as well as for the output set point tracking setting.

Polytopic State Constraints

For the state and input we consider polytopic constraints, i.e. constraints of the form

$$L_{j,x}x + L_{j,u}u \leq 1, \quad j = 1,...,r. \tag{4.8}$$

Nonlinear Output Constraints and Collision Avoidance

For being able to deal with the nonlinear output constraints and avoiding obstacles we deal with the general formulation for constraints (see Definition 3.1) on the output:

$$g_j(x,u) \leq 0, \quad j = r+1,...,p. \tag{4.9}$$

4.2 Procedure

Our presented RMPC approach mainly consists of two bigger parts; performing the offline computations as well as doing the online computations. In this section we will give an overview of the required components. Then later in this chapter, we will go into detail for all of the required components.

4.2.1 Algorithm for Offline Computation

Regarding the needed offline calculations, we refer the reader to Algorithm 1. In the very beginning, two main tuning parameters are given; the CT contraction rate ρ_c and the effect of the disturbance on the incremental Lyapunov function $\bar{w}_c$. Additionally it's possible to set the maximum value of c_j, e.g. to 1. In a next step, these conditions need to be formulated in LMIs. Using these LMIs as constraints, the optimal P_δ and K_δ can be found by maximizing the determinant of X, i.e. minimizing the determinant of P_δ. After computing or checking the values for c_j and $\bar{w}_c$ respectively, we can then compute required values for the terminal ingredients.

Details on where Algorithm 1 comes from and how the steps are exactly performed can be seen in the following sections.

4.2.2 Algorithm for Online Computation

After having calculated important values offline, we will now shortly explain how the actual online implementation is done. This can be seen in more detail in Algorithm 2. The modified optimization problem, potentially covering dynamic set point tracking, needs to be solved. After the solution has been obtained, we can then apply it to the system in addition to the prestabilization-input which is applied to the system in (almost) real-time.

Algorithm 1 Offline Calculations for RMPC Design

```
1: Define $\rho_c$ and potentially $\bar{w}_c$ and $c_j$.
2: Write the LMIs to enforce constraints on the resulting $P_\delta$ and $K_\delta$. The constraint on the
   contraction in Assumption 4.2 (more specifically in (4.15)) is needed. Constraints on $\bar{w}_c$, state
   constraints, input constraints and output constraints are optional but possibly result in a less
   conservative solution for the given circumstances. In order to formulate the LMIs, we use the
   standard substitution $X = P_\delta^{-1}$, $Y = KX$ and the Schur complement.
3: Minimize $-log(det(X))$ with respect to the LMIs, to get solutions for $P_\delta$ and $K_\delta$.
4: Compute $c_j$, $\forall j = 1, \dots, p$ (see (4.81) and (4.83)) or check whether constraint from LMI still
   holds.
5: Check whether $\rho_c$ satisfies the conditions (by using griding approach).
6: Compute $\bar{w}_c$ or check whether constraint from LMI still holds.
7: Compute the terminal ingredients: terminal cost (see Section 4.4.1) and compute $\bar{s}_f$ for the
   terminal set (Section 4.4.2).
8: Check whether the Lyapunov descent condition is fulfilled for the terminal cost within the
   terminal set.
9: Finally compute the DT parameters $\rho$ and $\bar{w}$ from $\rho_c$ and $\bar{w}_c$ respectively, using the given
   sampling time.
```

Algorithm 2 Online Calculations, execute at every time step $k \in \mathbb{N}$ during the sampling time interval of length h, starting at time t.

```
1: Solve the MPC problem from (4.53).
2: Apply the prestabilized input $u(t+\tau) = v^*_{MPC}(0|t) + K_\delta \cdot x(\tau|t),\ \tau \in [0,h]$ to the system
   (Section 4.3).
```

4.3 Computations in Continuous Time

In the following we will explain how we make use of the real-time behavior of our robotic control framework (Section 6.4). As you will see, we apply real-time prestabilizing feedback which then allows us to perform the offline calculations in CT.

Prestabilization Different to the typical nominal MPC formulation where the input $v_{mpc}(0|t)$ is directly applied to the system, prestabilized dynamics can be used. This means and has the big advantage that the system is stabilized in real-time along the horizon by a (nearly continuous) feedback law $\kappa(x)$, in addition to the applied piece-wise constant MPC control input. The dynamics can then be reformulated as

$$\dot{x} = f_\kappa(x, v_{mpc}) = f(x, v_{mpc} + K_\delta \cdot x), \quad g_{j,\kappa}(x, v_{mpc}) = g_j(x, v_{mpc} + K_\delta \cdot x), \tag{4.10}$$

where $g_{j,\kappa}$ is the function defining the compact nonlinear constraint set as defined in Def. 3.1. We therefore apply the real system input as

$$u(t+\tau) = v^*_{mpc}(0|t) + K_\delta \cdot x(\tau|t)),\ \tau \in [0,h], \tag{4.11}$$

in the sampling interval of length h starting at t. This system input is then also used in the stage cost $l(x, u(t), x_s, u_s)$.

Offline Calculations

Assumption 4.1. *We can implement the CT feedback $\kappa(x(t)) = K_\delta \cdot x(t)$.*

Under Assumpt. 4.1, we are doing the RMPC design parameter computation in CT to be independent of the actual sampling time. This is also new in comparison to the work in [19]. We will introduce the most important CT constants and design parameters in the following. According to (3.15), we use the following definition for our perturbed system:

$$\dot{x} = f(x,u,d), \quad (x,u) \in \mathcal{Z}, \quad d \in \mathbb{D}. \tag{4.12}$$

The general bound on the disturbance remains the same as denoted in Assumption 3.3. By going to CT, the criteria for incremental stability from Assumpt. 3.2 becomes the following:

Assumption 4.2. *Incremental stabilizability in CT: In analogy to Assumption 3.2. There exists a local control law $\kappa(x,z,v)$ for the incremental Lyapunov function from* (4.1)*, s.t. the following holds:*

$$\frac{d}{dt}V_\delta(x,z) = \frac{\partial V_\delta}{\partial x}|_{x,z}(f(x,v)+d_w) + \frac{\partial V_\delta}{\partial z}|_{x,z} f(z,v) \tag{4.13}$$

$$\leq -2\rho_c V_\delta(x,z) + 2\tilde{w}_\delta(z,v,c)\sqrt{V_\delta(x,z)} \tag{4.14}$$

(4.13)/(4.14) can be satisfied with the following two conditions:

$$\frac{\partial V_\delta}{\partial x}|_{x,z} f(x,v) + \frac{\partial V_\delta}{\partial z}|_{x,z} f(z,v) = 2(f(x,\kappa(x,z,v)) - f(z,v))^T P(x-z) \leq -2\rho_c V_\delta(x,z), \tag{4.15}$$

$$\frac{\partial V_\delta}{\partial x}|_{x,z} d_w \leq 2\tilde{w}_\delta(z,v,c)\sqrt{V_\delta(x,z)}. \tag{4.16}$$

Here, ρ_c is the continuous equivalent of ρ. They can be transformed for a known sampling time by using the following relation:

$$\rho = e^{-\rho_c h}. \tag{4.17}$$

Using the description in Equation 4.1 for V_δ, for the continuous disturbance bound we obtain the following:

$$\bar{w}_c := \sup_{z,v,d_w} \sqrt{V_\delta(f(z,v)+d_w, f(z,v))} = \sup_{z,v,d} \sqrt{||f_w(z,v,d) - f(z,v)||^2_{P_\delta}}. \tag{4.18}$$

The tube size also becomes a continuous description (compare to Equation 3.31):

$$s(t) = \frac{1-e^{-\rho_c t}}{\rho_c}\bar{w}_c, \text{ equivalent to DT with } \bar{w} = s(h) = \frac{1-e^{-\rho_c h}}{\rho_c}\bar{w}_c. \tag{4.19}$$

With the CT stabilizing feedback (Section 4.3) and incremental Lyapunov function, we can now apply the DT RMPC scheme according to Equation 4.19.

4.4 Terminal Ingredients

For the RMPC design we also need appropriate terminal ingredients, i.e. $(V_f, \mathcal{X}_f, \kappa_f, \bar{w})$. In contrast to the nominal case (compare Sec. 3.1.1), this time also the tightened constraints need to be satisfied for the terminal ingredients. We need to find a robust positively invariant (RPI) terminal set. For more information on set theory in control we refer to [6]. For the general case of arbitrary disturbances, the terminal ingredients need to satisfy Assumption 3.6. However, as we limit ourselves to the case of additive disturbances, the terminal ingredients need to satisfy the simpler Assumption 3.7. First, we will show how to compute the terminal cost V_f and its corresponding local terminal controller. Then, we will show two ways for constructing the terminal set.

4.4.1 Terminal Cost - Literature Review

In this section, we will shortly explain methods for computing the terminal cost known in the literature. This covers linear and nonlinear system dynamics as well as constant and varying set points.

Linear System Dynamics

Computing the terminal cost for linear system dynamics is the simplest case. The terminal cost has the task to bound the infinite horizon closed-loop cost of the MPC controller. Therefore, we can simply use the infinite horizon cost of the LQR controller (compare Sec. 3.1.1). We only need to make sure that state and input constraints are satisfied within the terminal set.

Nonlinear System with Constant Set Point

For the problem of steering nonlinear system dynamics with quadratic stage cost, quadratic terminal cost $V_f(x) = ||x||_P^2$ to a preknown set point, we can compute a terminal set that locally satisfies Assumption 3.7. This can be done using standard methods [9, 55].

Without loss of generality, we consider the Jacobi linearization of the system around the set point $x_s = 0$, $u_s = 0$:

$$\dot{x} = Ax + Bu, \quad A := \frac{\partial f}{\partial x}|_{0,0}, B := \frac{\partial f}{\partial u}|_{0,0}. \tag{4.20}$$

If (A, B) Equation 4.20 is stabilizable, then we can find a stabilizing (linear) terminal controller s.t. $A_K = A + BK$ is asymptotically stable. In [9] it is shown that the Lyapunov Equation with Q^* being positive-definite and symmetric and $\kappa \in [0, -\lambda_{max}(A_K))$

$$(A_K + \kappa I)^T P + P(A_K + \kappa I) = -Q^*, \quad Q^* = Q + K^T RK, \tag{4.21}$$

admits a unique positive definite and symmetric solution P. The infinite horizon cost $J^\infty(x, u)$ for any x at time t lying in the terminal set is then bounded from above by

$$J^\infty(x, u) = \int_t^\infty ||x(t)||_Q^2 + ||u(t)||_R^2 dt \leq x^T Px. \tag{4.22}$$

The value function $V(x)$ is given as in the following:

$$V(x) = J(x, t, t + T_p), \tag{4.23}$$

Chen and Allgoewer show the stability property of this cost function

$$V(x(t + \delta)) - V(x(t)) \;\leq\; -\int_t^{t+\delta} l(x(\tau), u(\tau))d\tau \;\leq -\delta\gamma, \tag{4.24}$$

with $\gamma > 0$.

We only need to make sure that the state and input constraints are not violated within the terminal set and that the terminal cost V_f is a control Lyapunov function. If this does not hold, the terminal set needs to be shrinked. The latter can be checked using the following condition (see [9]):

$$x^T P(f(x, Kx) - A_K x) \leq \kappa x^T Px. \tag{4.25}$$

In our case we choose the LQR controller as feedback controller and get the terminal cost as

$$V_f(x(N|t)) = |x(N|t)|_P^2. \tag{4.26}$$

Nonlinear Systems with Varying Set Points

For general nonlinear systems and variable set points, the computation is more difficult.

For a simple approach using a LTV description of the nonlinear system close to the steady-state manifold, we refer to [70, 69]. More general, in [43] the steady-state manifold is split into different intervals and for each interval, a constant P, K are computed using a description of LTV systems. Alternatively, in [32] the terminal ingredients P, K are continously parameterized and computed using quasi-LPV methods. Since we are not using this approach, we won't show these techniques in more detail.

4.4.2 Terminal Set - New Approach Based on Incremental Lyapunov Function

Since we need to be able to do robust set point tracking with varying set points, we need to find a suitable, non conservative terminal set for our online computations. For this, we got inspired by the work in [36] which uses the incremental Lyapunov function to find a terminal set for constant set points.

Constant Set Point

In [36], a Proposition states that by using

$$\mathcal{X}_f = \{(x, s) \in \mathbb{R}^{n+1} | s \in [0, \bar{s}_f], V_f(x) \leq \gamma_1\} \tag{4.27}$$

as the terminal set, Assumption 3.7 is satisfied for specific γ_1. As we've seen before we can calculate the terminal cost and the terminal controller using standard methods [9]. For the computation of the terminal set, i.e. γ_1, the maximal tube size $\bar{s}_f$ is needed to make sure that the tightened constraints are satisfied within the terminal set. The required conditions for γ_1 are described in [36]. Since we need to handle varying set points for our robotic use case, we are not able to use this approach and won't describe it in more detail here.

New Approach for Varying Set Points

We now want to compute a terminal set for varying set points. Similar work was done in [35]. Since we do not know the desired set point in advance and therefore can not simply compute a non-conservative terminal set size for every offline point, the idea of our approach here is to include the size of the terminal region in the optimization problem. This approach differs from existing approaches in the following ways:

1. Our terminal set are sublevel sets of V_δ which significantly simplifies the conditions on the terminal set. The idea of using sublevel sets of V_δ was also introduced in [30].
2. We optimize the terminal set size online, i.e. it is part of the optimization problem, compare [35].

To the best of our knowledge this has not been done before for the cases we cover here.

Notation Let us denote the non-constant set point in state and input as x_s and u_s, respectively. We consider a terminal set as a function of x_s and u_s of the following form:

$$\mathcal{X}_f(x_s, u_s) := \{x | V_\delta(x, x_s) \leq \gamma_2(x_s, u_s)\}. \tag{4.28}$$

Let us introduce the following notation:

$$\mathcal{Z}_k := \{(x, u) | g_j(x, u)) + c_j s(k) \leq 0\}, \text{ with } s(k) = \frac{1 - \rho^k}{1 - \rho}, \tag{4.29}$$

$$c_{max} = \max_j c_j, \tag{4.30}$$

$$\bar{s}_f \overset{\text{(Add. Disturbances)}}{=} \frac{1 - \rho^N}{1 - \rho} \bar{w}. \tag{4.31}$$

Requirements for Terminal Set For a proper terminal set, the following conditions need to be satisfied:

1. The terminal set needs to be robust positively invariant (RPI) for a given set point (x_s, u_s), i.e. once a trajectory entered the RPI set, it will never leave it again. This can be formulated as:

$$x \in \mathcal{X}_f(x_s, u_s) \Rightarrow f(x, \kappa(x, x_s, u_s)) + d_w \in \mathcal{X}_f(x_s, u_s), \ \forall |d_w|_{P_\delta} \leq \rho^N \bar{w}. \tag{4.32}$$

2. The tightened constraints are satisfied within the terminal set, i.e.

$$(x, \kappa(x, x_s, u_s)) \in \mathcal{Z}_N, \quad \forall x \in \mathcal{X}_f(x_s, u_s). \tag{4.33}$$

3. The terminal cost is a continuous Lyapunov function in the terminal set $\mathcal{X}_f$ satisfying

$$V_f(f(x, \kappa(x, x_s, u_s)), x_s) - V_f(x, x_s) \leq -l(x, \kappa(x, x_s, u_s), x_s, u_s),\ \forall x \in \mathcal{X}_f(x_s, u_s). \tag{4.34}$$

Approach We choose the following ansatz for the terminal set as defined in Equation 4.28 including the tube size at the end of the horizon $\bar{s}_f$ to write the following formulation with respect to the set point (x_s, u_s):

$$\mathcal{X}_f(x_s, u_s) := \{x | \sqrt{V_\delta(x, x_s)} + \bar{s}_f \leq \alpha(x_s, u_s)\} = \{x | |x - x_s|_{P_\delta} + \bar{s}_f \leq \alpha(x_s, u_s)\}. \tag{4.35}$$

Together with the explicit formulation of the tube size for additive disturbances from Equation 3.31 this results in the following:

$$\mathcal{X}_f(x_s, u_s) := \{x | |x - x_s|_{P_\delta} \leq \alpha(x_s, u_s) - \frac{1-\rho^N}{1-\rho}\bar{w}\}. \tag{4.36}$$

Derivation In the following we will derive the conditions for $\alpha(x_s, u_s)$, leading to Equation 4.35 being a proper terminal set. For this purpose, the 3 criteria defined before need to be satisfied. Due to our simplifying assumptions it holds that $V_\delta(x, x_s) = |x - x_s|^2_{P_\delta}$.

1. The set needs to be RPI. It holds $x \in \mathcal{X}_f$:

$$\max_{d_w} |(x^+ + d_w) - x_s|_{P_\delta} + \bar{s}_f^+ \tag{4.37}$$

$$\overset{\text{Triangle Inequality}}{\leq} |x^+ - x_s|_{P_\delta} + \max_{d_w} |d_w|_{P_\delta} + \bar{s}_f^+ \tag{4.38}$$

$$\overset{\text{Ass. 3.7}}{\leq} |x^+ - x_s|_{P_\delta} + \rho^N \bar{w} + \bar{s}_f^+ \tag{4.39}$$

$$\overset{\text{Def. of s(k+1)}}{=} |x^+ - x_s|_{P_\delta} + \rho^N \bar{w} + \rho \bar{s}_f + \bar{w} - \rho^N \bar{w} \tag{4.40}$$

$$\overset{\text{Ass. 3.2}}{\leq} \rho |x - x_s|_{P_\delta} + \rho \bar{s}_f + \bar{w} \tag{4.41}$$

$$= \rho(|x - x_s|_{P_\delta} + \bar{s}_f) + \bar{w} \leq \rho\alpha + \bar{w} \overset{!}{\leq} \alpha \tag{4.42}$$

$$\Leftrightarrow \frac{\bar{w}}{1-\rho} \leq \alpha. \tag{4.43}$$

For this α value, the terminal set is RPI.

2. All states in the terminal set need to satisfy the tightened constraints, i.e.

$$g_j(x, u) + c_j \bar{s}_f \leq 0,\ \forall |x - x_s|_{P_\delta} \leq \alpha. \tag{4.44}$$

This also strongly depends on the set point x_s:

$$g_j(x, u) + c_j \bar{s}_f \overset{\text{Ass. 3.5}}{\leq} g_j(x_s, u_s) + c_j \sqrt{V_\delta(x, x_s)} + c_j \bar{s}_f \tag{4.45}$$

$$\overset{\text{Equation 4.35}}{\leq} g_j(x_s, u_s) + c_j \alpha \overset{!}{\leq} 0 \tag{4.46}$$

$$\Leftrightarrow \alpha \leq -\frac{g_j(x_s, u_s)}{c_j}. \tag{4.47}$$

3. The terminal cost can be calculated as seen before. For the special case of linear systems, it's simply the infinite horizon cost of the corresponding LQR controller.

Resulting Conditions Therefore we have the two conditions on α, again summarized here:

$$\frac{\bar{w}}{1-\rho} \leq \alpha \leq -\frac{g_j(x_s,u_s)}{c_j}, \quad \forall j = 1, ..., p. \tag{4.48}$$

The RPI condition provides a lower bound on alpha and therefore requires a sufficiently large terminal set, whereas the constraint satisfaction bounds the size of the terminal set from above.

Remark. *These constraints implicitly constrain the set of set points x_s to the ones that are feasible.*

Formulation for the Optimization Problem As we want our terminal set to be as large as possible we always aim for the maximum admissible size. Therefore, the optimal value for α would be:

$$\alpha(x_s,u_s) = \max_j -\frac{g_j(x_s,u_s)}{c_j}. \tag{4.49}$$

We can include the terminal set as defined in Equation 4.28 with $\gamma_2 = (\alpha - \bar{s}_f)^2$. However, since we know (x_s, u_s) only after the optimization, we need to include the bounds on alpha in the optimization problem. The terminal constraint set therefore becomes:

$$\mathcal{X}_f(x_s,u_s) := \{x| \quad \sqrt{V_\delta(x,x_s,v)} + \bar{s}_f = |x - x_s|_{P_\delta} + \bar{s}_f \leq \alpha\} \tag{4.50}$$

$$\Rightarrow \mathcal{X}_f(x_s,u_s) := \{x| \quad V_\delta(x,x_s,v) = |x - x_s|^2_{P_\delta} \leq \gamma_2 = (\alpha - \bar{s}_f)^2\}, \tag{4.51}$$

$$\text{with } \frac{\bar{w}}{1-\rho} \leq \alpha \leq -\frac{g_j(x_s,u_s)}{c_j}, \quad \forall j = 1, ..., p. \tag{4.52}$$

4.5 Summary - Resulting Optimization Problem

4.5.1 Constant Set Point

The RMPC formulation with suitable terminal ingredients for the simpler case of static ingredients is exactly the one from (3.34). We use this formulation for our simulation example in Chapter 7.

4.5.2 Varying Set Point

The resulting optimization problem including the set point reference tracking, the output constraints as well as our special terminal ingredients can be found in the following:

$$\begin{aligned}
V_N(x(t),y_t) = \quad & \min_{u(\cdot|t),x_s,u_s,\alpha} \; J_N(x,y_t;u(\cdot|t)*,y_s,x_s,u_s,\alpha) && (4.53a)\\
\text{subject to} \quad & x(0|t) = x(t), && (4.53b)\\
& x(k+1|t) = f(x(k|t),u(k|t)), && (4.53c)\\
& g_j(x(k|t),u(k|t)) + c_j\frac{1-\rho^k}{1-\rho}\bar{w} \leq 0, && (4.53d)\\
& x_s = f(x_s,u_s), \quad y_s = h(x_s,u_s), && (4.53e)\\
& \frac{\bar{w}}{1-\rho} \leq \alpha \leq -\frac{g_j(x_s,u_s)}{c_j}, \quad \forall j = 1,...,p && (4.53f)\\
& |x(N|t) - x_s|^2_{P_\delta} \leq (\alpha - \bar{s}_f)^2, && (4.53g)\\
& k = 0,...,N-1, \quad j = 1,...,p,
\end{aligned}$$

with J_N as introduced in Section 3.1.2 and repeated here:

$$J_N(x,y_t;u(\cdot|t),y_s,x_s,u_s) = \sum_{k=0}^{N-1} l(x(k|t)-x_s,u(k|t)-u_s)+V_f(x(N|t)-x_s,y_s)+V_O(y_s-y_t). \tag{4.54}$$

4.6 Derivations and Computations of Required Parameters - A Comprehensive Collection

In this section we will now present the required computations needed to be in a position to do the calculations for the algorithms introduced in 4.2.

4.6.1 Incremental Lyapunov Function

Our goal is to compute P_δ and K_δ for the incremental Lyapunov function $V_\delta(x,z) = |x-z|^2_{P_\delta}$ and the linear feedback $K_\delta x$, used as pre-stabilization. These matrices can be found by solving a minimization problem for $-log(det(X))$, where $X = P_\delta^{-1}$ under LMI conditions.

Formulating Suitable Conditions For theory on LMIs in system theory refer to [7] and for a similar use case as ours refer to [32, 31]. It's beneficial to include pre-known constraints into the LMIs needed for computing P_δ and K_δ, since this allows to choose less conservative parameters. For the incremental Lyapunov function we know conditions which should hold:

1. From Ass. 4.2 and specifically Equation 4.15 we get the requirement for the incremental Lyapunov function:

$$2(f(x,\kappa(x,z,v)) - f(z,v))^T P_\delta (x-z) \leq -2\rho_c V_\delta(x,z). \tag{4.55}$$

   For a linear system with linear state feedback this becomes

$$\Leftrightarrow 2(A(x-z) + BK_\delta(x-z))^T P_\delta (x-z) \leq -2\rho_c V_\delta(x,z) \tag{4.56}$$

$$\overset{\Delta x = x-z}{\Leftrightarrow} \Delta x^T((A+BK_\delta)^T P_\delta + P_\delta(A+BK_\delta))\Delta x \leq -2\rho_c \Delta x^T P_\delta \Delta x \tag{4.57}$$

$$\Leftrightarrow \Delta x^T((A+BK_\delta)^T P_\delta + P_\delta(A+BK_\delta) + 2\rho_c P_\delta)\Delta x \leq 0. \tag{4.58}$$

$$\Leftrightarrow (A+BK_\delta)^T P_\delta + P_\delta(A+BK_\delta) + 2\rho_c P_\delta \leq 0. \tag{4.59}$$

2. From Ass. 4.2 and specifically Equation 4.16 we get the requirement for the incremental Lyapunov function:

$$\frac{\partial V_\delta}{\partial x}|_{x,z} d_w \leq 2\bar{w}_c(z,v,c)\sqrt{V_\delta(x,z)} \tag{4.60}$$

$$\Leftrightarrow \frac{\partial}{\partial x}(x-z)^T P_\delta (x-z) d_w = 2(x-z)^T P_\delta d_w \overset{!}{\leq} 2\bar{w}_c |x-z|_{P_\delta} \tag{4.61}$$

$$\overset{P_\delta \text{ pos. def. and symm.}}{\Leftrightarrow} (x-z)^T P_\delta^{1/2} P_\delta^{1/2} d_w = (P_\delta^{1/2}(x-z))^T P_\delta^{1/2} d_w \tag{4.62}$$

$$\overset{\text{Cauchy-Schwarz Inequ.}}{\leq} |P_\delta^{1/2}(x-z)|_2 \cdot |P_\delta^{1/2} d_w|_2 = |x-z|_{P_\delta} \cdot |d_w|_{P_\delta} \overset{!}{\leq} \bar{w}_c |x-z|_{P_\delta} \tag{4.63}$$

$$\Leftrightarrow |d_w|_{P_\delta} \leq \bar{w}_c. \tag{4.64}$$

3. Since we have constraints on the states and inputs and potentially on the output function, it makes sense to also include those in the finding process of P_δ and K_δ to potentially get a less conservative solution for our problem. By doing so, we can limit the values of the

corresponding c_j parameters, $\forall(z,v) \in \mathcal{Z}$ and $\forall r \in \mathcal{Z}$:

$$g_j(x,\kappa(x,z,v)) - g_j(z,v) \leq c_j\sqrt{V_\delta(x,z)} = c_j|x-z|_{P_\delta} \text{ from (3.21)} \tag{4.65}$$

$$\Leftrightarrow g_j(x,\kappa(x,z,v)) - g_j(z,v) \overset{\Delta x = x-z}{\approx} (\frac{\partial g_j}{\partial x}|_r + \frac{\partial g_j}{\partial u}\frac{\partial \kappa}{\partial x}|_r)\cdot \Delta x \leq c_j|\Delta x|_{P_\delta} \tag{4.66}$$

$$\text{and with } |\Delta x|_{P_\delta} = \sqrt{\Delta x^T P_\delta^{1/2} P_\delta^{1/2}\Delta x} = \sqrt{(P_\delta^{1/2}\Delta x)^T(P_\delta^{1/2}\Delta x)} = |P_\delta^{1/2}\Delta x|_2 \tag{4.67}$$

$$\Leftrightarrow (\frac{\partial g_j}{\partial x}|_r + \frac{\partial g_j}{\partial u}\frac{\partial \kappa}{\partial x}|_r)\cdot \Delta x \leq c_j|P_\delta^{1/2}\Delta x|_2 \tag{4.68}$$

$$\overset{\Delta\tilde{x} = P_\delta^{1/2}\Delta x}{\Leftrightarrow} (\frac{\partial g_j}{\partial x}|_r + \frac{\partial g_j}{\partial u}\frac{\partial \kappa}{\partial x}|_r)P_\delta^{-1/2}\cdot \Delta\tilde{x} \tag{4.69}$$

$$\leq |(\frac{\partial g_j}{\partial x}|_r + \frac{\partial g_j}{\partial u}\frac{\partial \kappa}{\partial x}|_r)P_\delta^{-1/2}|_2 \cdot |\Delta\tilde{x}|_2 \overset{!}{\leq} c_j|\Delta\tilde{x}|_2 \tag{4.70}$$

$$\Leftrightarrow |(\frac{\partial g_j}{\partial x}|_r + \frac{\partial g_j}{\partial u}\frac{\partial \kappa}{\partial x}|_r)P_\delta^{-1/2}|_2 \leq c_j \tag{4.71}$$

$$\Leftrightarrow |(\frac{\partial g_j}{\partial x}|_r + \frac{\partial g_j}{\partial u}\frac{\partial \kappa}{\partial x}|_r)P_\delta^{-1/2}|_2^2 \leq c_j^2 \tag{4.72}$$

$$\Leftrightarrow c_j^2 - (\frac{\partial g_j}{\partial x}|_r + \frac{\partial g_j}{\partial u}\frac{\partial \kappa}{\partial x}|_r)P_\delta^{-1}(\frac{\partial g_j}{\partial x}|_r + \frac{\partial g_j}{\partial u}\frac{\partial \kappa}{\partial x}|_r)^T \geq 0. \tag{4.73}$$

Formulating LMI Conditions Analogous to the work in [32], we pick the following choice for the substitution of P_δ and K_δ:

$$X = P_\delta^{-1}, \quad Y = K_\delta P_\delta^{-1} = K_\delta X. \tag{4.74}$$

With this choice we can use the LMIs of the following equations written in variables X and Y:

1. $$AX + BY + (AX+BY)^T + 2\rho_c X \leq 0, \text{ (from (4.59))}. \tag{4.75}$$

2. $$\begin{pmatrix} X & d_w \\ d_w^T & w_c^2 \end{pmatrix} \geq 0, \text{ (from (4.64))}, \tag{4.76}$$

   which must be checked for all vertices d_w in $\mathcal{W}$.

3. $$c_j^2 - \left(\frac{\partial g_j}{\partial x}|_r + \frac{\partial g_j}{\partial u}\frac{\partial \kappa}{\partial x}|_r\right) X \left(\frac{\partial g_j}{\partial x}|_r + \frac{\partial g_j}{\partial u}\frac{\partial \kappa}{\partial x}|_r\right)^T \geq 0, \text{ (from (4.73)}. \tag{4.77}$$

   This is not an LMI yet, but can be transformed to one:

   $$\overset{\text{Schur complement}}{\Leftrightarrow} \begin{pmatrix} c_j^2 & \frac{\partial g_j}{\partial x}|_r + \frac{\partial g_j}{\partial u}\frac{\partial \kappa}{\partial x}|_r X \\ \left(\frac{\partial g_j}{\partial x}|_r + \frac{\partial g_j}{\partial u}\frac{\partial \kappa}{\partial x}|_r X\right)^T & X \end{pmatrix}. \tag{4.78}$$

   E.g. for a polytopic constraint on the state we get

   $$\frac{\partial g_j}{\partial x}|_r + \frac{\partial g_j}{\partial u}\frac{\partial \kappa}{\partial x}|_r = L_x \tag{4.79}$$

   $$\rightarrow \begin{pmatrix} c_j^2 & L_x X \\ (L_x X)^T & X \end{pmatrix} \geq 0. \tag{4.80}$$

Remark. *Usually it makes sense to describe d_w limited by its ∞-norm. This implies that none of the vector entries can exceed a certain boundary. Therefore, the possible set for the disturbance is given by a polyhedron. Note that for a polyhedron it's only necessary to consider its vertices for the LMI seen before.*

4.6.2 Constraint Tightening

As seen in the formulation of our optimization problem in (4.53), we need to find parameters $c_j,\ j = 1, \ldots, p$. These parameters define how much each of the constraints needs to be tightened to still be in a position to guarantee the desired robustness properties.

Polytopic State Constraints

Using polytopic constraints significantly simplifies the calculation of c_j for the j-values corresponding to the states. Putting in the polytopic constraints to Equation 3.21 of Assumption 3.5 gives us the following relation:

$$c_j \geq \frac{L_{j,x}(x-z) + L_{j,u}\kappa(x,x,v)}{\sqrt{V_\delta(x,z)}}, \quad \forall (x,z,v) \text{ with } V_\delta(x,z,v) \leq \delta_{loc}. \tag{4.81}$$

For the practical computation of c_j, we therefore get for our setup (see (4.71)):

$$c_j := |(L_{j,x} + L_{j,u}K_\delta)P_\delta^{-1/2}|_2. \tag{4.82}$$

Nonlinear Output constraints

As we want to enforce constraints on our output which is usually highly nonlinear, we also need to find a c_j for its tightening. The general condition can be found in the following:

$$c_j \geq \frac{g_j(x,\kappa(x,z)) - g_j(z,v)}{\sqrt{V_\delta(x,z)}}, \quad \forall (x,z,v) \text{ with } V_\delta(x,z,v) \leq \delta_{loc}. \tag{4.83}$$

By looking at (4.71) we can again write this as:

$$c_j = \max_r |(\frac{\partial g_j}{\partial x}|_r + \frac{\partial g_j}{\partial u}\frac{\partial \kappa}{\partial x}|_r)P_\delta^{-1/2}|_2. \tag{4.84}$$

Since in principle we need to include all $r \in \mathcal{Z}$, we again sample this to get the correct value.

Collision Avoidance

In principle our approach would also be expandable to exact collision avoidance. In contrast to what we do, collision avoidance does not require to find a differentiable function which bounds the constraint but more general and practical relevant formulations are possible, e.g. also box constraints. This approach was introduced in [75] and works by reformulating non-differentiable constraints collision avoidance constraints into smooth nonlinear constraints by using strong duality of convex optimization while not introducing additional approximations. A robust formulation of this approach can be found in [62] by Soloperto et al..

4.6.3 Check Exponential Decay Rate

Before actually applying the controller in practice, it turned out to be very useful to check the calculations done before once again. This reduces the risk of possible mistakes significantly.

Linear systems

For linear systems this is straightforward. We need to check that the following really holds:

$$(A + BK)^T P + P(A + BK) + 2\rho_c P \leq 0. \tag{4.85}$$

Since we are considering linear state dynamics for the robotic use case, A and B is an exact representation. We can modify this condition to the following:

$$(A + BK_\delta)^T P_\delta + P_\delta(A + BK_\delta) + 2\rho_c P_\delta \leq 0 \tag{4.86}$$

$$\Leftrightarrow P_\delta^{-1/2}(A + BK_\delta)^T P_\delta^{1/2} + P_\delta^{1/2}(A + BK_\delta)P_\delta^{-1/2} + 2\rho_c I_{n\times n} \leq 0 \tag{4.87}$$

$$\Leftrightarrow P_\delta^{-1/2}(A + BK_\delta)^T P_\delta^{1/2} + P_\delta^{1/2}(A + BK_\delta)P_\delta^{-1/2} \leq -2\rho_c I_{n\times n} \tag{4.88}$$

$$\Leftrightarrow \lambda_{max}\left(P_\delta^{-1/2}(A + BK_\delta)^T P_\delta^{1/2} + P_\delta^{1/2}(A + BK_\delta)P_\delta^{-1/2}\right) \leq -2\rho_c. \tag{4.89}$$

Nonlinear Systems

For the nonlinear case we can recompute the real value for ρ_c to check whether our imposed value during the optimization holds in practice. For this, a surrounding Δz of x defined by the incremental Lyapunov function is investigated and then ρ_c is calculated according to the following rule:

$$\rho_c = min\left(\rho_c, -\frac{\Delta z^T P_\delta(\dot{z} - \dot{x})}{\Delta z P_\delta \Delta z}\right). \tag{4.90}$$

This needs to be done in a sampling fashion since it only allows to make statements locally.

4.6.4 Terminal Ingredients

The terminal ingredients consist of terminal cost and terminal set. The terminal cost can be computed according to [9] as described earlier. The terminal set can then be calculated as described in Section 4.4.2 for dynamic set points or as given in [36] for constant set points.

Chapter 5

AMPC Approach

In this chapter we introduce the idea of an AMPC by combining the contents of the preceding Chapters 3.1 and 3.3. As mentioned earlier, the idea of this thesis to approximate the RMPC controller by ML regression is based on the work in [19]. Our focus is more practical and one of our goals is to demonstrate this new approach in practice on a complex real world system, the Apollo robot. Additionally, we base our RMPC controller on the work in [36] instead of [33], as it was done in [19]. Also our validation procedure for the AMPC was modified compared to the earlier work of Hertneck et al. by not considering the error in the approximated input π_{approx}, but instead the deviation of the DT state at the next time step $x_{\text{approx}}(t+1)$. Therefore, we use the true induced error along the trajectory which allows us to be less conservative. Additionally, our RMPC problem formulation including the constraint tightening is computed in CT, allowing for sampling time independent statements. Furthermore, for the MPC formulation itself we use prestabilized dynamics in (pseudo) CT with a feedback controller $K_\delta \cdot x$. For the Apollo implementation we build upon a special MPC reference tracking formulation [43]. Finally, the whole AMPC implementation is done in an efficient and fast C++ implementation using ACADO and CASADI for solving MPC problems and TensorFlow C++ API for approximating it.

In the following we highlight the major improvements compared to [19].

5.1 Problem Setting

The main idea of the AMPC formulation is borrowed from [19]. For the sake of simplicity and the used validation procedure, we write this chapter in discrete time even though we are deriving the RMPC quantities in continuous time.

We consider the nonlinear discrete-time system

$$x(t+1) = f(x(t), u(t)), \quad x \in \mathbb{R}^n, \quad u \in \mathbb{R}^m, \quad t \in \mathbb{N} \tag{5.1}$$

and the perturbed discrete-time system

$$x(t+1) = f_w(x(t), u(t), d(t)), \quad d \in \mathcal{D}. \tag{5.2}$$

In contrast to the work in [19], where compact polytopic input and state constraints

$$\mathcal{X} = \{x \in \mathbb{R}^n | Hx \leq 1_p\}, \quad \mathcal{U} = \{u \in \mathbb{R}^m | Lu \leq 1_q\} \tag{5.3}$$

are addressed, we additionally cover nonlinear constraints of the form

$$g_j(x, u) \leq 0, \quad j = r+1, ..., p. \tag{5.4}$$

Our control objective is to ensure stability of x_s, constraint satisfaction and to optimize some cost $J_N(x; u^*)$ for the regular MPC problem and $J_N(x, y_t; u^*, y_s)$ for the Apollo robot tracking formulation. For this purpose, and as seen in the last chapter, we design an RMPC which is robust to additive noise on $f(\cdot,\cdot)$ within chosen bounds. Note that this also accounts for inaccurate/disturbed inputs. This RMPC is then sampled offline over the set of feasible states $\mathcal{X}_{\text{feas}}$, delivering the optimal solution $\pi_{MPC}(x)$. This policy is then approximated using supervised learning techniques, NNs in our case. This yields an AMPC function $\pi_{approx} : \mathcal{X}_{feas} \to \mathcal{U} | u = \pi_{approx}(x)$ with a closed loop system given by

$$x(t+1) = f(x(t), \pi_{approx}(x(t))). \tag{5.5}$$

Thanks to the RMPC design, robust constraint satisfaction and stability are guaranteed if the impact of the disturbance on the system dynamics is smaller than what was considered during the design procedure (compare Sec. 3.2.3).

5.2 Procedure

The algorithm for designing the AMPC is similar to Algorithm 1 in [19]. However, for the validation we use the condition in (5.17) instead of (5.9).

For the RMPC design we use the scheme described in the last chapters, based on [36]. We choose this approach to compensate for the influence of appearing disturbances. As a short recap of Assumption 3.3, we account for disturbances of the following form to preserve the guarantees of our controller:

$$f_w(x,u,d) - f(x,u) \in \mathcal{W}(x,u), \quad \text{with a compact set } \mathcal{W}(x,u) \subset \mathbb{R}^n. \tag{5.6}$$

There exists a scalar function $\hat{w}$ that satisfies the following:

$$|d_w| \leq \hat{w}(x,u), \ \forall \ d_w \in \mathcal{W}(x,u), \tag{5.7}$$

for a given norm $|\cdot|$. For the sake of simplicity we only consider the case of additive disturbancees, i.e. the perturbed system from (5.2) becomes the following:

$$x(t+1) = f_w(x(t), u(t), d(t)) = f(x(t), u(t)) + d_w, \text{ with } d_w \in \mathcal{W}. \tag{5.8}$$

Remark. *The main difference between using additive and general disturbances is denoted by using $d_w \in \mathcal{W}$ instead of $d_w \in \mathcal{W}(x(t), u(t))$ for the disturbed system $f_w(x(t), u(t), d)$.*

5.3 Previous Work [19]

5.3.1 Validation Criterion

In [19], the authors derived a criterion to compensate for the inaccurate input approximation $\pi_{MPC}(x)$. This robustness criterion is very intuitive for the setting of developing an approximate MPC. The criterion is given in the following:

$$|\pi_{approx}(x) - \pi_{MPC}(x)|_\infty \leq \eta, \tag{5.9}$$

i.e. this implies that

$$\pi_{approx}(x) = \pi_{MPC}(x) + d, \text{ with } |d|_\infty \leq \eta. \tag{5.10}$$

Here, η is a user determined parameter which defines how big the deviation might get without losing the given guarantees for all $x \in \mathcal{X}$. This is possible due to an additional assumption in [19] which requires that there exists a Lipschitz constant $\lambda \in \mathbb{R}$, s.t. $\forall x \in \mathcal{X}, \forall u \in \mathcal{U}, \forall u + d \in \mathcal{U}$ the following holds:

$$|f(x, u+d) - f(x,u)| \leq \lambda |d|_\infty. \tag{5.11}$$

Hence, for this setup the influence of the input inaccuracies to the deviation of $x(k+1)$ is described by introducing an additional Lipschitz constant. Therefore, the input inaccuracy is transformed to a system disturbance in our RMPC setup. Since this constant needs to satisfy the disturbance bound everywhere, this can introduce additional conservatism compared to the case of just bounding the influence on $x(k+1)$ as seen in (5.8).

5.3.2 Statistical Guarantees

For the statistical guarantees, in [19] the statistical verification was done for whole trajectories, i.e. trajectories

$$X_i := \{x(t), t \in \{0, ..., T_i\} : x(0) = x_i \in \mathcal{X}_{feas}, x(T_i) \in \mathcal{X}_f,\ x(t+1) = f(x(t), \pi_{approx}(x(t)))\}. \quad (5.12)$$

As it can be seen, only the nominal model without additional disturbances was covered. To be in a position to observe statistically meaningful information, an indicator function is introduced:

$$I(X_i) = \begin{cases} 1, & \text{if } |\pi_{MPC}(x) - \pi_{approx}(x)|_\infty \leq \eta,\ \forall x \in X_i \\ 0, & \text{otherwise.} \end{cases} \quad (5.13)$$

Applying Hoeffding's Inequality

The empirical risk is given as

$$\tilde{\mu} := \sum_{j=1}^{p} I(X_j). \quad (5.14)$$

Together with Hoeffding's inequality, given as

$$\mathbb{P}\left[|\tilde{\mu} - \mu| \geq \epsilon_h\right] \leq 2e^{-2p\epsilon_h^2}, \quad (5.15)$$

the following statement can be derived:

$$\mathbb{P}\left[I(X_i) = 1\right] \geq \mu_{crit},\ \text{with } \mu_{crit} \leq \tilde{\mu} - \epsilon_h = \tilde{\mu} - \sqrt{-\frac{ln\left(\frac{\delta_h}{2}\right)}{2p}} \quad (5.16)$$

holds at least with confidence level $1 - \delta_h$.

This result was taken from [19]. For more information on Hoeffding's inequality, see Section 3.3.

5.4 Validation

5.4.1 New Validation Criterion

We now present the new validation criterion, which is not as intuitive as the one explained before but more close to the formulation of our RMPC design and hence, less conservative. We can check the overall system disturbance in the space of the incremental Lyapunov function, i.e. directly with respect to the norm we are interested in, which is the least conservative measurement for this approach.

This criterion is given in the following:

$$\sqrt{V_\delta(f_w(x, \pi_{approx}, d), f(x, \pi_{MPC}))} = \sqrt{V_\delta(f(x, \pi_{approx}) + d_{w,model}, f(x, \pi_{MPC}))} \quad (5.17)$$

$$= |d_{w,approx} + d_{w,model}|_{P_\delta} = |d_w|_{P_\delta} \leq \bar{w}. \quad (5.18)$$

Here, $\bar{w}$ is the maximum admissible disturbance in this norm, which results from our assumption of the overall occuring disturbance d_w. In the ideal case d_w would be a vector of zeros, whereas in practice it takes values unequal to zeros due to the approximation error ($d_{w,approx}$) and the model mismatch and measurement noise ($d_{w,model}$).

Remark. *By comparing our new validation criterion from* (5.17) *to the old one in* (5.9) *it is obvious that we look at the full disturbance including the error of the approximation as well as additional disturbances such as model mismatch and measurement noise. In the old validation criterion, solely the approximation error was covered.*

5.4.2 Statistical Guarantees

If we would do it the same way as in [19], the indicator function (compare (5.13)) for our trajectory would look as following:

$$I(X_i) = \begin{cases} 1, & \text{if } |f_w(x, \pi_{approx}, d) - f(x, \pi_{MPC})|_{P_\delta} = |d_w|_{P_\delta} \leq \bar{w}, \ \forall x \in X_i \\ 0, & \text{otherwise.} \end{cases} \tag{5.19}$$

Discussion

As mentioned before, it is important to say that our solution also covers additional disturbances such as the model mismatch. To be in a position to give the statistical guarantees from the last section, we need the following:

1. The system needs to be sampled along closed loop trajectories.
2. The model mismatch needs to be deterministic, i.e. $d_{w,model}$ along the trajectory needs to be deterministically determined for a given starting point.

Remark. *Due to the fact that we use Hoeffding's inequality for the validation, the trajectories needs to be i.i.d.. Since we sample the start points of the trajectories randomly, the trajectories are also i.i.d. if the overall mapping to the indicator function is deterministic. Additional uncertainty in the real world system can lead to the case of non deterministic behavior and therefore to trajectories not being i.i.d. anymore.*

Due to the need of having a deterministic function, we decided to do our validation on our robot simulator, trying to mimic the real world scenario. It approximates effects neglected by our kinematic model such as inertia and friction but is still deterministic, why our arguments still hold. To be in a position to do the validation on the real world system, modifications would be needed.

Advantages Nevertheless, this approach has several advantages over the one in the previous work. It is

1. less conservative since the influence of the input does not need to be described by an upper bounding constant,
2. also accounts for the integration error in the simulation,
3. it covers the model mismatch between our simplified kinematic model and the real identified system given in the robotic simulation (SL, compare Chapter 6)
4. and it could even be used to detect in real-time whether our model assumptions are still satisfied.

5.5 New Ways of Sampling

Later on in this thesis, we will both show, a simulation example (the same as in [19]) used to validate our frameworks and add further extensions as well as a practical example; controlling a robotic arm on Apollo robot. Due to the different nature of the two examples with respect to the state dimensionality we apply different techniques for doing the sampling. E.g. the chemical stirred-tank reactor (CSTR) has only 2 dimensions and its policy is easily visualizable and interpretable while the robot has much higher dimensions.

For both approaches we developed new approaches for doing the sampling. For the continuous stirred-tank reactor (CSTR) we introduced a recursive approach for the sampling enabling vanishingly small approximation errors while saving computational costs. For the robot experiments we first do random sampling (makes it easier to add data afterwards or to use data while the sampling has not finished) and then randomly sample closed-loop trajectories to get more related data to our real world scenario and our validation procedure.

We will explain each of them in the corresponding chapters (Section 7.2.6 and Section 9.2.3) in more detail and outline the main differences compared to the previously conducted sampling in [19].

5.6 Improved Neural Network Approximation

Also in this case we introduced new techniques (especially for the simulation example) and advantageous practices for the neural network regression, trying to learn the RMPC policy. The structure of the underlying policy as well as the dimensionality of the simulation example and the robot experiment is quite different. Therefore, we describe the improvements and considerations in the corresponding chapters (Section 7.2.5 and Section 9.2.3).

Chapter 6

Frameworks

6.1 Overview

As described earlier in Chapter 1, one of the main tasks of this Master Thesis is to develop and implement an AMPC approach with guarantees on Apollo robot (see Fig. 1.1) and to deploy it in practice. Due to the high time critical demands of the robot (all hardware related command signals needs to be updated at a frequency of $1kHz$), the whole robotic control framework SL (Sec. 6.4) is implemented in real-time C++. To be compatible with this framework and also to fulfill the demanding requirements, we decided in the very beginning to also implement all of the code which will actually be needed to run on the robot in C++. Some other offline calculations, e.g. for training the network or validating theoretical ideas, are implemented in Python and MATLAB.

Detailed instructions on how to use the created code can be found in our corresponding user manual which is given in Appendix A of this thesis.

6.2 Model Predictive Control Framework

We are able to solve optimal control problems (OCPs) in C++ to avoid error-proneness due to required interfaces and to not introduce additional delay. Otherwise, effort in handling the communication of different frameworks or potentially even programming languages would have been needed. In particular, this would have become difficult, since we need to be able to deploy our code in a real-time environment (Section 6.4).

6.2.1 ACADO

After doing some research and comparison between CasADi and ACADO [21], we decided to do our programming using ACADO in C++. The important reason for this decision was the expected faster evaluation of ACADO, the fact that it's tailored for optimal control problems as well as the potential real-time iteration scheme promising evaluations in the magnitude of $1ms$ [23, 67, 14, 68]. However, it still unveiled some difficulties in the practical usage. It seems as if the online support by the developers has stopped several years ago. For ordinary use cases, useful information can be found in the official ACADO manual [22]. However, for more specific problems and questions it turned out to require quite some trial and error, especially due to the fact that the user manual is not fully complete towards the end.

When we started implementing code for the robot control, we encountered bigger problems using ACADO. On the one hand, the underlying quadratic program (QP) solver qpOases had some difficulties solving our optimization problem, potentially due to the highly nonlinear and non quadratic output function. On the other hand, it was also really difficult to formulate the control problem in a way such that it would satisfy our mathematical formulation. E.g. even the usage of additional, tailored decision variables is not trivial in ACADO.

6.2.2 CasADi

CasADi [1] is a general purpose optimization problem solver using symbolic variables. It is not tailored for MPC problems such as ACADO. However, in the meanwhile it also offers the *opti* package which simplifies writing code for optimal control problems and makes the syntax more intuitive. It is possible to introduce additional decision variables, define the optimization objective in a desired way and much more. The standard underlying solver is *iPOPT*. It offers APIs for Python, MATLAB, C++ and octave. We used CasADi in the very beginning for solving optimization problems in MATLAB and planned to use ACADO for the C++ implementation. However, for the more complicated case of our robotic control we had difficulties in writing our control problem due to the previously mentioned challenges (Section 6.2.1). Therefore, we also switched to CasADi for the C++ robot implementation. It is also worth mentioning that the C++ documentation of CasADi is really poor and the authors of the software advice the users against deploying the C++ API. Also the examples given in the source code for the C++ cases are very limited, so it took a while to figure out how we could implement our relatively complex optimization problem. Since also the Python and MATLAB versions are using the same C++ backend, it was clear that the C++ API must also offer the same functionality.

6.3 Machine Learning Framework - TensorFlow

Since this project contains a big learning part, a suitable ML framework is needed. Our goal was to develop the whole software framework in C++, hence, desirably also the ML framework should have a C++ API to avoid programming language interfaces. We are using NNs for the approximation of our AMPC controller. One of the most powerful and most common frameworks for the usage of NNs is TensorFlow which also provides a C++ API. Therefore, we decided in the very beginning to use Tensorflow. Alternatives would have been PyTorch or Caffe.

In our case we are using TensorFlow 1.13. Multiple APIs are provided by TensorFlow. The recommended and most comprehensive one is the Python API. Especially for training and creating custom models this is the way to go. For the training we mainly use the KERAS NN library which nowadays is part of TensorFlow's core library and offers a higher-level set of abstractions which makes it easier to rapidly develop NN-ML models. Despite the skeptical opinion in the web regarding the C++ API, we decided to deploy it for the inference in our own C++ programming framework.

6.3.1 Training - Python

The most complete API of TensorFlow is certainly the Python API. It offers a wide range of functionalities and - maybe most importantly - can deployed by using the KERAS front end. Therefore, we used TensorFlow Python for doing the training.

6.3.2 Inference - C++

Following the same argumentation as in Section 6.2, we aimed for having a full C++ implementation in the end to achieve the desired performance and avoid problems with combining seperate prgramming languages. Luckily, one of the most powerful learning frameworks to date offers a C++ API; the TensorFlow C++ API. To be in a position to use this API, the graph trained with KERAS front-end needs to be frozen. This has the additional advantage that the evaluation becomes incredibly fast. An evaluation step of big NNs with millions of decision variables on a CPU only takes less than $1ms$. It was also possible to successfully integrate this in our software framework. However, for using the C++ API, TensorFlow must be built from source, which turned out to be a challenge. The whole building process is done by the open-source release of the Google internal building system which is called *Bazel*. More information on how to build TensorFlow from source and how to use it in your catkin C++ framework can be found in the Appendix; Section A.3.4.

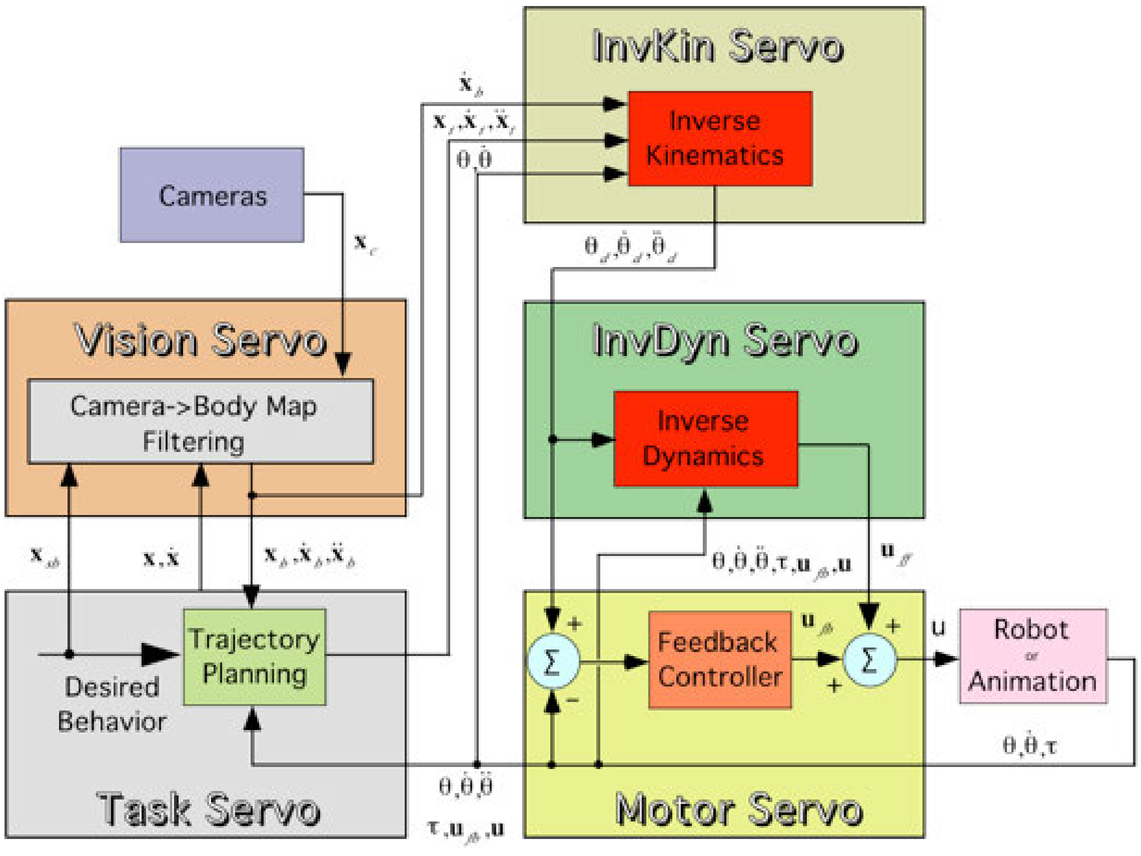

Figure 6.1: Block diagram of the software modules in SL and their communication among each other. Image taken from [58].

6.4 Real Time Robot Control Framework - SL

For the control of our robot we are partly dependent on the framework which is currently used to control the robot. In our case, this is the Simulation Laboratory (SL) [58]. In this section we only introduce aspects that are important for the choice of the system, the influence of the control signal and the dynamic behavior. In [58], many different aspects of the control framework are explained. However, in our opinion most important from an engineering perspective is the block diagram illustration of the different software modules, depicted in Figure 6.1. The motor servo takes on the task of calculating the low level motor commands from the desired quantities Θ_d, $\dot{\Theta}_d$, u_{ff} and the current state Θ, $\dot{\Theta}$ of the robot [58]. The task servo is the environment where the user is intended to influence the system. This is where the control law is implemented, even though very often the low level (e.g. PD) part is done by the motor servo. In here, it's also possible to cancel out the low level control commands and control the whole system by applying the feed-forward command u_{ff}. The inverse dynamics servo can be used to create feed-forward commands according to the desired Θ_d, $\dot{\Theta}_d$, $\ddot{\Theta}_d$. Note that in this formulation also the desired acceleration is used. Furthermore, we are not using the inverse kinematics servo and the vision servo of SL. The perception we need is also done in the task servo by spawning a separate thread to not threaten the real time demands.

In the beginning, we were considering to only command accelerations and to use the inverse dynamics servo only. However, due to bad feed-forward estimates on the real world system - arising from non ideal system identification - we decided to also calculate reference angles and angular velocities, commanding them to the low level controllers in the motor servo.

6.4.1 Real Time

Since this framework is real-time critical - the robot stops operation when it does not get any signal for more than one interval - we needed to take this into account for the design of our software. We decided not to use a potential real-time ROS implementation but instead to spawn real-time threads updating the values of the needed variables. The whole framework functionalities are packaged within a class. An instance of this class is then created in our SL task and its member variables are read out containing the important information.

6.4.2 Modularity

For us it was really important to write a code which is as modular as possible. It is possible to run different configurations, e.g. with or without the NN control, without rebuilding the project. For this purpose we decided to store the configurations in a YAML file which is read into the memory at the beginning of the program execution.

6.4.3 Simulation

In the very beginning we also investigated the use of the control toolbox [16]. It is a toolbox provided by the *IDRL* lab at ETH Zurich and provides efficient and useful numerical methods and control design functionalities. Especially in terms of simulating our system we considered the usage of this toolbox. However, in the end we decided to write own simulations using integrators in the orders of up to 8, and the simulation environment of SL which also considers inertia of the robotic system as well has the ability to directly test the functioning of our framework.

6.5 Motion Tracking - Vicon

Since we also wanted to be able to perform an interactive demonstration, we needed to address the perception part. We considered using the camera or *kinect* system built in to Apollo. However, since this should not be the core of this thesis, we decided to first use a more straightforward approach. We decided to use the Vicon system for tracking the obstacles and reference with respect to the robot frame.

6.5.1 Vicon Bridge

The Vicon system uniformly streams its information into the network. Then, on any computer in the same network it is possible to access this provided data. For the purpose of decoding these network signals, a useful package is provided; the Vicon bridge. It takes the network signals as inputs, decodes them and then publishes them locally in ROS. In our perception thread, we are then able to listen to this information.

6.6 Developed Frameworks

We developed several different code sources reaching from C++ code for the CSTR simulation, the robot experiments and simulation over MATLAB code used for doing the offline calculations for the RMPC design to Python code for plotting the logged data and training the NNs. More information about the different parts of our code can be found in Appendix A. All code is available on the AMD gitlab server.

6.6.1 Conclusion

From an implementation perspective it was more difficult than expected to use the C++ API of *TensorFlow*. First of all the API itself is quite poorly documented. Furthermore at the time of this Master Thesis *TensorFlow* needed to be built from source by using *Bazel* to get the needed libraries for the C++ API. Additionally also CasADi has a poor documentation for its C++ usage. Therefore we needed to spent some days on finding correct and efficient ways of implementing our optimization problem.

Chapter 7

Simulation Example - CSTR

To be in a position to reach the goals of this thesis, i.e. to demonstrate the RMPC as well as the AMPC approach on a real world robotic system, we decided to first implement the whole pipeline in C++ for a smaller and less complex simulation example. We were aiming for a fast acting pipeline from the offline to the online calculations. For the sake of comparability we decided to investigate the same system as already done in [19], however with some minor implementation modifications.

The efficiency and speed of the approach in [19] was limited and it was bound to MATLAB which is unsuitable if fast behavior is needed or the pipeline is meant to be applied on a real world system in a C++ environment. Additionally the main contributions in [19] lay more in theory, such as successfully proposing statistical guarantees for the AMPC controller, than in optimizing the algorithms and frameworks, e.g. parallelization was not really considered. As we are interested in the functioning of the pipeline, we will not show too many intermediate results but focus on the resulting learned AMPC controller and its validation.

In contrast to the system formulation for the real world robotic example in Section 9.1 we also need to handle nonlinear system dynamics in this case. Once again, this shows the variety of the underlying RMPC scheme in [36].

7.1 System Formulation

We use the same example as in [19] which is originally taken from [47]. It is a continuous stirred-tank reactor (CSTR) which is a common benchmark for MPC control design. The system is described by:

$$\dot{\vec{x}} = \begin{pmatrix} \dot{x_1} \\ \dot{x_2} \end{pmatrix} = \begin{pmatrix} \frac{1-x_1}{\Theta} - kx_1 e^{-\frac{M}{x_2}} \\ \frac{x_f - x_2}{\Theta} + kx_1 e^{-\frac{M}{x_2}} - \alpha u(x_2 - x_c) \end{pmatrix}, \tag{7.1}$$

with given parameters[1]. Our goal is the same as in [19]; to stabilize the unstable steady state $x_e = (0.2632, 0.6519)^T$ with steady state input $u_e = 0.7853$. Constraints are present on the input u and on the transformed system state $x_t = x - x_e$:

$$\mathcal{X}_t = [-0.2, 0.2] \times [-0.2, 0.2],\ \mathcal{U} = [0, 2]. \tag{7.2}$$

7.1.1 Continuous Time Formulation

As it was already observable in (7.1), we decide to use the CT formulation of the system. We make this choice with the real world robotic example in mind, for which a fast sampling rate of the software framework (i.e. 1kHz) and a significantly smaller sampling rate of the RMPC controller are given. Therefore we are able to model the prestabilizing feedback as continuous and hence, to do the RMPC offline calculations in CT.

[1] $\Theta = 20, k = 300, M = 5, x_f = 0.3947, x_c = 0.3816, \alpha = 0.117$

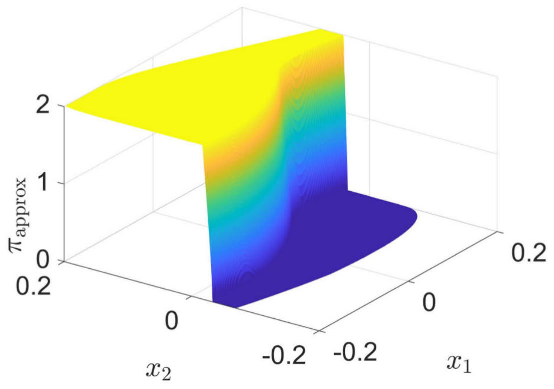

Figure 7.1: Groundtruth taken from [19]. This Fig. depicts the continuous function learned by the neural network. The approximation has no problems to properly mimic the function due to the high number of sampling points. IEEE control systems letters©.

7.2 Setup

For this example, our main goal is to mimic the result of the simulation example in [19] to reveal bugs in the implementation. Therefore, we do not include dynamic set point tracking in the design.

7.2.1 Groundtruth

Due to the low dimensionality - the state and input dimensions are 2 and 1 respectively - in [19] the set was simply sampled uniformly with a grid size of $2.5 \cdot 10^{-4}$ obtaining $1.6 \cdot 10^6$ feasible out of $2.56 \cdot 10^6$ possible data points $(x, \pi_{MPC}(x))$. On average one evaluation for them took 0.71s which solely leads to a runtime of more than 500 hours. The function learned from these samples is depicted in Fig. 7.1.

7.2.2 Assumed Disturbance

In [19] the used RMPC controller was an input robust MPC design. As a result, a Lipschitz constant is needed to bound its influence on the resulting deviation of the next state (compare Section 5.3.1). In the given work, Hertneck et al. determined the Lipschitz constant as $\lambda = 5.5 \cdot 10^{-3}$. With the underlying RMPC design this ends up in an admissible bound on the input disturbance of $\eta = 5.1 \cdot 10^{-3}$ to still guarantee stability, recursive feasibility and constraint satisfaction.

Since we are using the scheme in [36] for the RMPC design instead of [33], we are able to tolerate an $\eta = 6.4 \cdot 10^{-3}$, i.e. 25% more compared to the previous work when bounding the induced disturbance (of the input approximation) by the same parameter λ. Determining $\bar{w}_d$ from this according to $\bar{w}_d = \lambda\eta$ returns $\bar{w}_d = 0.0226$ for our calculations. Directly checking whether the input disturbance introduced by the neural network is smaller than η is more conservative than checking the deviation of the next step with respect to $\bar{w}_d$. Later in this Chapter we will also investigate whether there exists a measurable difference during the validation procedure.

7.2.3 Incremental Stabilizability

The assumption of the incremental stabilizability can be verified as explained in [34] and was already done in [19].

7.2.4 RMPC Design

For the RMPC design we need to handle nonlinear system dynamics. Contrary to [19], we base our design on the work in [36].

Formulation

The resulting RMPC optimization problem can be seen in (7.3). Principally it is equivalent to the general formulation in (3.34) as introduced in [36] for additive disturbances.

$$\begin{aligned}
V_N(x(t)) \quad = \quad & \min_{u(\cdot|t)} J_N(x(\cdot|t), u(\cdot|t)) && \text{(7.3a)}\\
\text{subject to} \quad & x(0|t) = x(t), && \text{(7.3b)}\\
& x(k+1|t) = f(x(k|t), u(k|t)), && \text{(7.3c)}\\
& g_j(x(k|t), u(k|t)) + c_j \frac{1-\rho^k}{1-\rho}\bar{w} \leq 0, && \text{(7.3d)}\\
& x(N|t) \in \mathcal{X}_f, && \text{(7.3e)}\\
& k = 0, ..., N-1, \quad j = 1, ..., p,
\end{aligned}$$

with J_N as introduced in Section 3.2.3 and repeated here:

$$J_N(x(\cdot|t), u(\cdot|t)) = \sum_{k=0}^{N-1} l(x(k|t) - x_s, u(k|t) - u_s) + V_f(x(N|t) - x_s). \tag{7.4}$$

Constraints

In this example we only need to consider polytopic state and input constraints that are given in (7.2). We can write the constraints as $g_j(x, u) \leq 0$ for $j \in \{1, \ldots, p\}$. We need the Jacobians for the required LMIs needed to compute the incremental Lyapunov function (see (4.77)) and again to calculate c_j for $j = 1, ..., p$ using (4.84). However, since the Jacobian of polytopic constraints is constant, this simplifies to the form in (4.82).

7.2.5 Learning - Combining Regression and Classification

By looking at Figure 7.1 we thought about ways of potentially not approximating the whole area using regression. For the naive learning approach of approximating the whole state space with regression, dense sampling needs to be given in all areas. Therefore, we investigate the introduction of a supervised classification method, in our case also given by a NN.

The potential improvement looks as follows: In regions of changing policies we would need to have a properly working regression network, in flat regions we would assign the corresponding value of the detected class, according to the classifying network. This would also induce the necessity of only sampling very finely in these regions, where we expect a fast changing policy. The advantage is that a classification approach needs less examples in flat regions to produce suitable results, compared to regression. As a motivation we show an exemplary classification in Figure 7.3. To make sure that we always apply the regression input when needed, it is also possible to increase the width of the middle region (see Figure 7.4b).

7.2.6 Alternative Sampling

In the last section we introduced the idea of a combination of classifying the regions and using the regression in the interesting regions where the policy is changing. For this idea to be useful, we also need to be able to profit from it, i.e. we need to be able to only sample the interesting regions. For this we propose a sampling consisting of two steps.

Simple Uniform Sampling

The simplest approach and to generally reproduce the results is to uniformly sample the MPC also in our case. In our specific case, the finest resolution we sampled uniformly is $8 \cdot 10^{-4}$. A plot of all the samples can be seen in Fig. 7.2a.

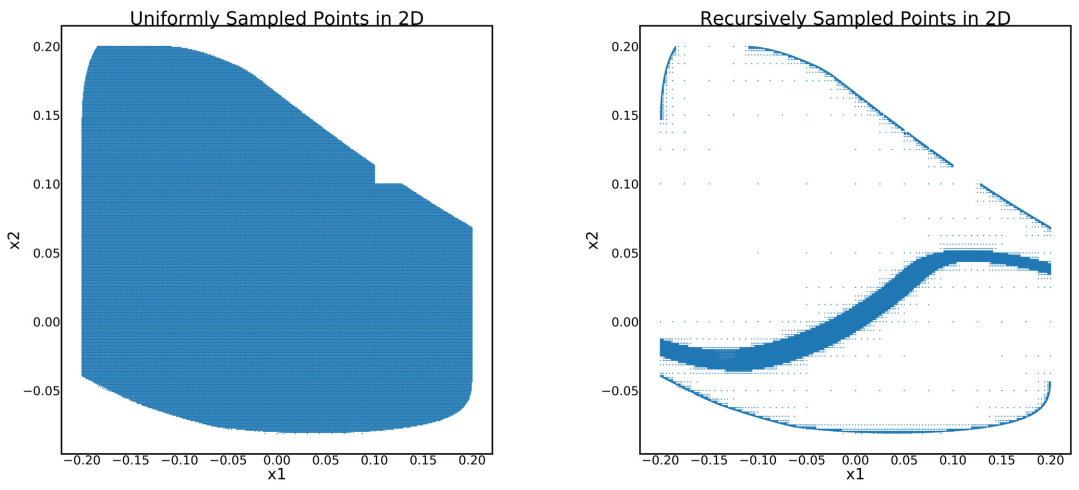

(a) Uniformly sampled points with grid resolution $8 \cdot 10^{-4}$.

(b) Recursively sampled points up to grid resolution $2.5 \cdot 10^{-4}$.

Figure 7.2

New Recursive Approach

Even though we might have a good classification for the different regions, we still need an approximation for the remaining fast changing area. Therefore we introduce a recursive approach which locally increases the resolution as long as neighboring values are still differing. For this we start with a square, i.e. 4 points and its corresponding computed MPC values. Then if the increase resolution criteria is fulfilled, 5 more points are introduced and its MPC values are computed. The used criteria is given in Algorithm 3. The difficult part about this implementation is to make full use of parallelism and to not recompute solutions at the same points multiple times. Additionally

Algorithm 3 Recursive sampling.

```
1: In advance: define the desired set of data which should be sampled
2: Sample the 4 corner of the set and evaluate its ideal RMPC conrol commands. Write those
   commands to the log.
3: IF resolution $\geq$ resolution$_{max}$: create a new square for each of the previous given points and
   sample call recursively again 3.
4: ELSE: Compare the returned values of the corners.
5: IF either one of them was infeasible or deviates from the mean value of the 4 control commands
   go again to 3.
6: ELSE: Terminate.
```

a finest grid resolution is defined in advance. In our case, we choose $2.5 \cdot 10^{-4}$ as in [19] for the whole grid. This means, in the interesting regions we obtain the same grid resolution as in their approach. The resulting grid can be seen in Fig. 7.2b. Overall, only 111459 points need to be sampled for the recursive approach instead of the $2.56 \cdot 10^{6}$ of the brute force approach. This leads to an overall sampling time, including the more sparse sampling in Figure 7.2a, of 9 hours instead of 500 hours. This is not only achieved by using this recursive approach but also because of faster algorithms and parallelization which allows us to sample approximately 8 times faster compared to [19].

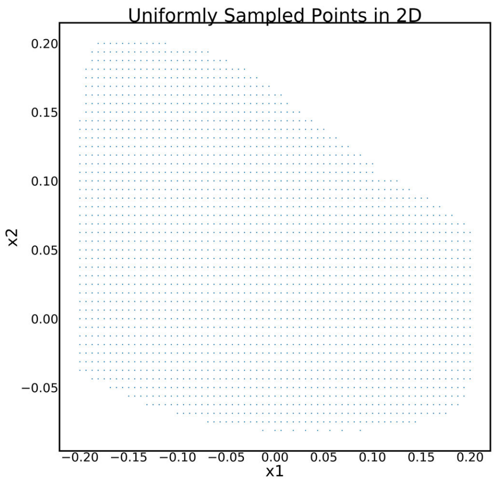

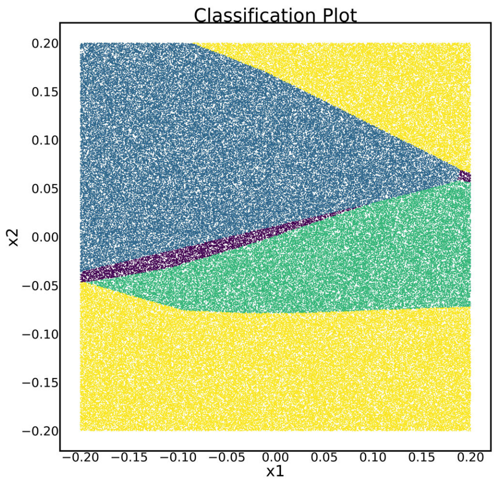

(a) Sampling of 2500 points with grid resolution $8 \cdot 10^{-3}$.

(b) Classification result obtained from training with few points, evaluated on 200,000 random points. Yellow: infeasible; Green/blue: saturated at min/-max; Violet: continuous

Figure 7.3

7.3 Results

In this section we will shortly show the results we could obtain for the simulation example.

7.3.1 New Learning Approach

It can be clearly seen in Fig. 7.1 that most of the regions of this controller lie in saturation. Actually, this is typical for controllers aiming for optimal behavior. Learning all flat regions for good response in regression requires many samples, even though the function is trivial in these regions. As a result, we present the idea of determining these areas in terms of classification. If the points in the set are not classified wrongly, i.e. free of noise, the regions are geometrically clearly defined. Therefore only few points are needed to achieve good classification results for the flat regions. At the boundaries, more points lead to sharper and more precise edges. This is demonstrated in Fig. 7.3, where only 2500 points are used for training. Looking at Fig. 7.4a shows an example which is trained on the uniformly sampled set from Fig. 7.2a. It is visible that the edges are more clearly evaluated on random points compared to Fig. 7.3. With this approach we can already cover most of the area with less samples than before. To make classification robust, we can increase the width of the continuous region afterwards by adding an additional percentage to the corresponding output label of the middle region for each point. This can be seen in Fig. 7.4b.

7.3.2 Pure Regression

For the training of the regression network we used the combined data from Fig. 7.2a and Fig. 7.2b. The resulting approximation can be found in Fig.7.5a. It is clear that the result in the flat regions is not as good as for the uniform sampling with high grid resolution. However, this is not a problem since we can make use of the classification in these regions if we want to.

For the validation we use $70,000$ randomly sampled points visualized in Fig. 7.5b.

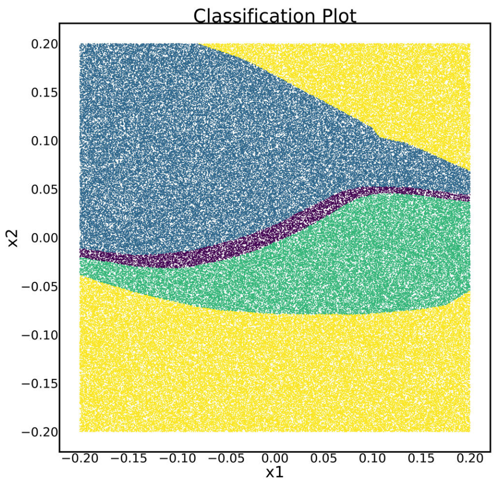

(a) Classification trained on uniformly sampled points with grid resolution $8 \cdot 10^{-4}$ (compare Fig. 7.2a), evaluated on 200,000 random points. As it can be seen, the middle region is less wide than in Figure 7.4b.

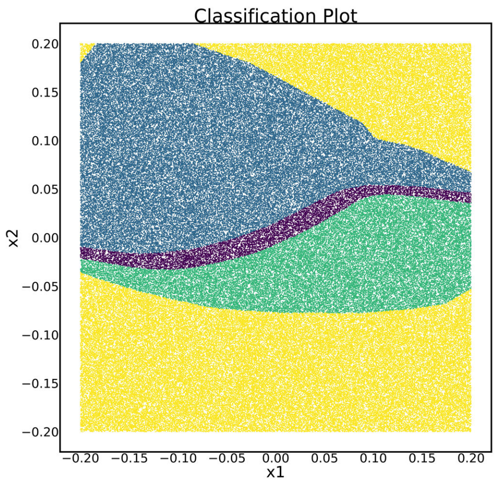

(b) Classification trained on the same amount of uniformly sampled points. In this case the middle region is widened afterwards to make sure that we do not erroneously classify an interesting point as saturated.

Figure 7.4

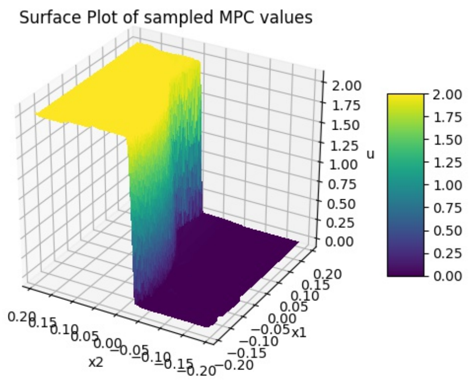

(a) Surface Plot of the Regression over the Set.

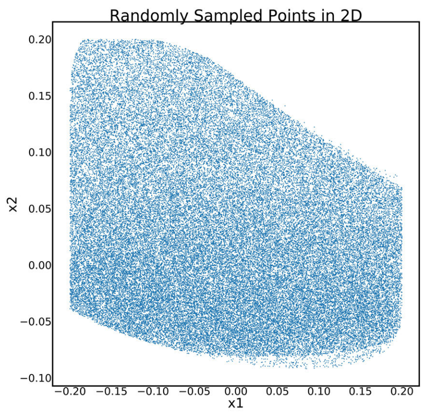

(b) Recursively sampled points.

Figure 7.5

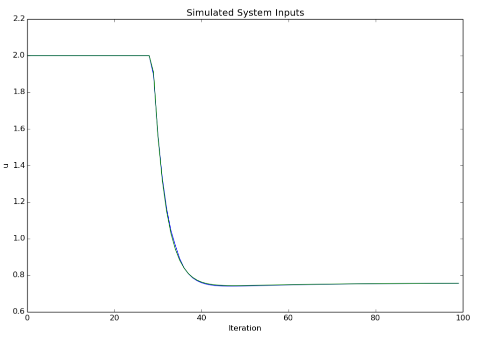

(a) Inputs of MPC and AMPC controllers along the trajectory.

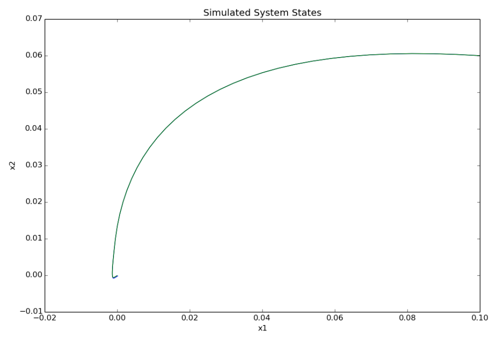

(b) State Trajectory of MPC and AMPC controllers along the horizon for $x_{t,0} = [0.1, 0.06]^T$.

Figure 7.6

7.3.3 Simulation

A simulation of the trajectory for the MPC and the AMPC controllers can be seen in Fig. 7.6. It is visible that even though the control input deviates, the trajectory is almost indistinguishable. This can be interpreted as an empirical confirmation of why the new validation criterion, based on the state evolution, is less conservative than the previous one based on the input deviation.

7.3.4 Validation

For this example, we sample 42518 feasible trajectories to full convergence, i.e. not only until the state reached the terminal set. The old validation criterion from [19] satisfies the conditions for our learned AMPC along 24785 trajectories, i.e.

$$\tilde{\mu}_{\text{old-val-criterion}} = 58.293\%, \text{ for } p = 42518. \tag{7.5}$$

Our new validation criterion is significantly less conservative and violates the conditions not along a single trajectory, i.e.

$$\tilde{\mu}_{\text{new-val-criterion}} = 100.0\%, \text{ for } p = 42518. \tag{7.6}$$

Hence, our new proposed validation criterion outperforms the previous one significantly with respect to conservatism for practical use cases.

7.3.5 Overall Comparison

New RMPC Approach Basing the work on [36] instead of [33] allows us to give a less conservative bound η on the input disturbance, i.e. without considering any other factors. The values for η now become:

$$\eta = 1.4 \cdot 10^{-2} \tag{7.7}$$

instead of

$$\eta = 5.1 \cdot 10^{-3} \tag{7.8}$$

in [19].

New Validation Criterion This new criterion is less conservative than the old one. In our validation, we achieve to satisfy the new validation criterion along 100.0% of the 42518 sampled trajectories, compared to 58.293% for the old criterion along the same trajectories.

Overall Speed-Up Due to parallelization and novel sampling, we are able to push down the 500 hours for the sampling in [19] to less than 9 hours with our approach. This is mainly due to the recursive sampling, more efficient code and parallelization.

Furthermore, since the network needs to achieve lower precision, less points need to be sampled in the critical regions and therefore additional speed-up can be achieved.

Chapter 8

Introducing Apollo Robot

The robot we are using for showing the abilities of our RMPC and AMPC approach is the Apollo robot which is located at the MPI in Tübingen. An image of the robot can be seen in Figure 8.1. The robot is equipped with two KUKA LBR4+ robotic arms. However, for our experiments we will only deploy one of them (always the right arm).

8.1 Geometry

In this section we introduce the geometry of the robotic arm to give an idea about what movements the robot is able to perform. In Figure 8.2 an illustration of the arm is found. For introducing the coordinate systems, it is common to use the Denavit-Hartenberg (DH) convention. By doing so, the derivation of the resulting kinematics is less tedious than by arbitrarily introducing the coordinate systems. The coordinate frames seen in Figure 8.2 were chosen according to this convention.

8.2 Robot Description

As seen in Section 6.4, using the robot control framework is not trivial and we need to adhere to it when deciding for our robot description. It is possible to identify a model of the robot. In literature, there are several works about System Identification of the KUKA LBR4+ robot. However, since the integration would have been non trivial with no guarantees of the result satisfying our requirements, we decided to choose a kinematic approach, to do the control with desired accelerations and leave the task of the feedback linearization to the inner loop low-level controllers. For the sake of potential future work, yet we will shortly describe our findings and works regarding system identification of the KUKA LBR4+ robotic arm.

Remark. *Even when considering the dynamic model of the robot, the CT prestabilizing feedback κ can always be chosen in a way such that the resulting system dynamics f_κ are also linear.*

8.2.1 Identification of the Dynamics Equations

A comprehensive overview of nonlinear system identification can be found in [59]. It is written as a survey where the authors give guidelines in nonlinear system identification and also a lot of background information to better understand the challenges as well as their origin. The work also covers additional topics such as the impact of structural model errors and process noise on the system identification. The article also covers an overview of possible models, such as - among others - deterministic differential algebraic equation (DAE) models, stochastic state space models, semi-physical modeling, linearization based models, linear parameters varying (LPV) models, black box models and many more. It also shows the design excitation signals validation of the model and collection of examples.

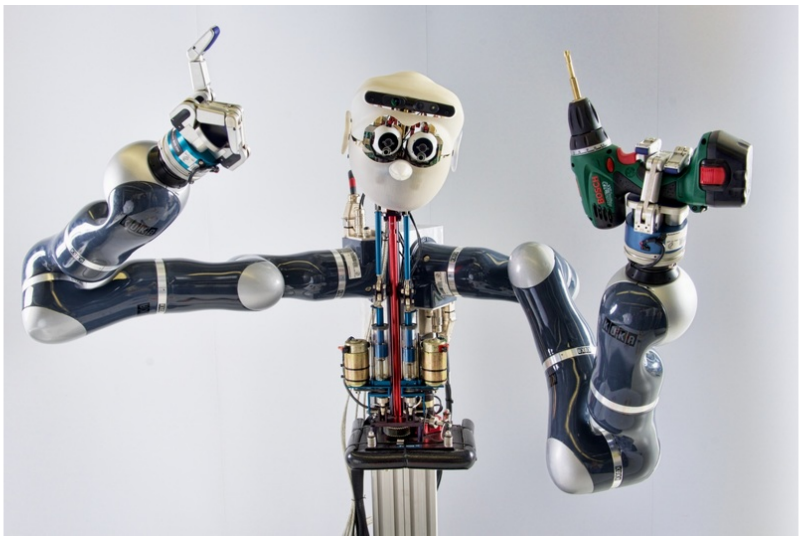

Figure 8.1: Image of the robot we are using for our practical robot experiments. Max Planck Institute for Intelligent Systems©.

Getting more to the actual topic of interest, the system identification of the KUKA LBR4+ robotic arm, brings us first to the work of Gaz et al. [15]. In this work, the authors present an approach for the model identification of this robotic arm (denoted as KUKA LWR IV in the paper). On that account they present a general procedure for determining the structure as well as an identification of the values of the dynamic coefficients used by the manufacturer (i.e. KUKA). The authors refer to this approach by calling it *reverse engineering*, since they try to match the numerical data provided by the software interface to a suitable symbolic model. The identification results as well as the training and validation results are publicly available.

Another relevant work was presented by Bargsten et al. [3], in which the authors describe a full structured approach for model-based controller design of the KUKA LBR4 robotic arm, including the system identification. Also a control application is presented to show validity of the proposed system identification. Along with this paper, also a freely available model toolbox for this robotic arm is published, which might be interesting for future work.

Another paper trying to estimate the system dynamics of the KUKA LWR robot can be found in [25]. In this work the authors try to utilize the presence of joint torque sensors data offered by the KUKA robotic arm. Traditional identification methods only take into account the motor position and the motor torques, computed as a result of the current reference signal multiplied by the joint drive gains. In this paper, in contrast they are directly using the joint torque data measured by sensors and compare the results to the traditional approach as well to using both sources of information. Surprisingly they can show that using motor torques calculated from electric currents lead to the same accuracy as using usually expensive torque sensors.

The last work we want to cite in this chapter is done by Stürz et al. [64]. In this work, the authors also perform system identification, however not on the KUKA LBR4 but on its successor LBR iiwa. Similar to the robot we are using, it is also equipped with torque sensors in each joint. This paper presents an identification of the minimal set of needed parameters as well as a consistent set of parameters for the physics robot, not neglecting friction. In this work, the parameters are obtained by solving a nonlinear optimization problem with additional constraints to ensure physical feasibility.

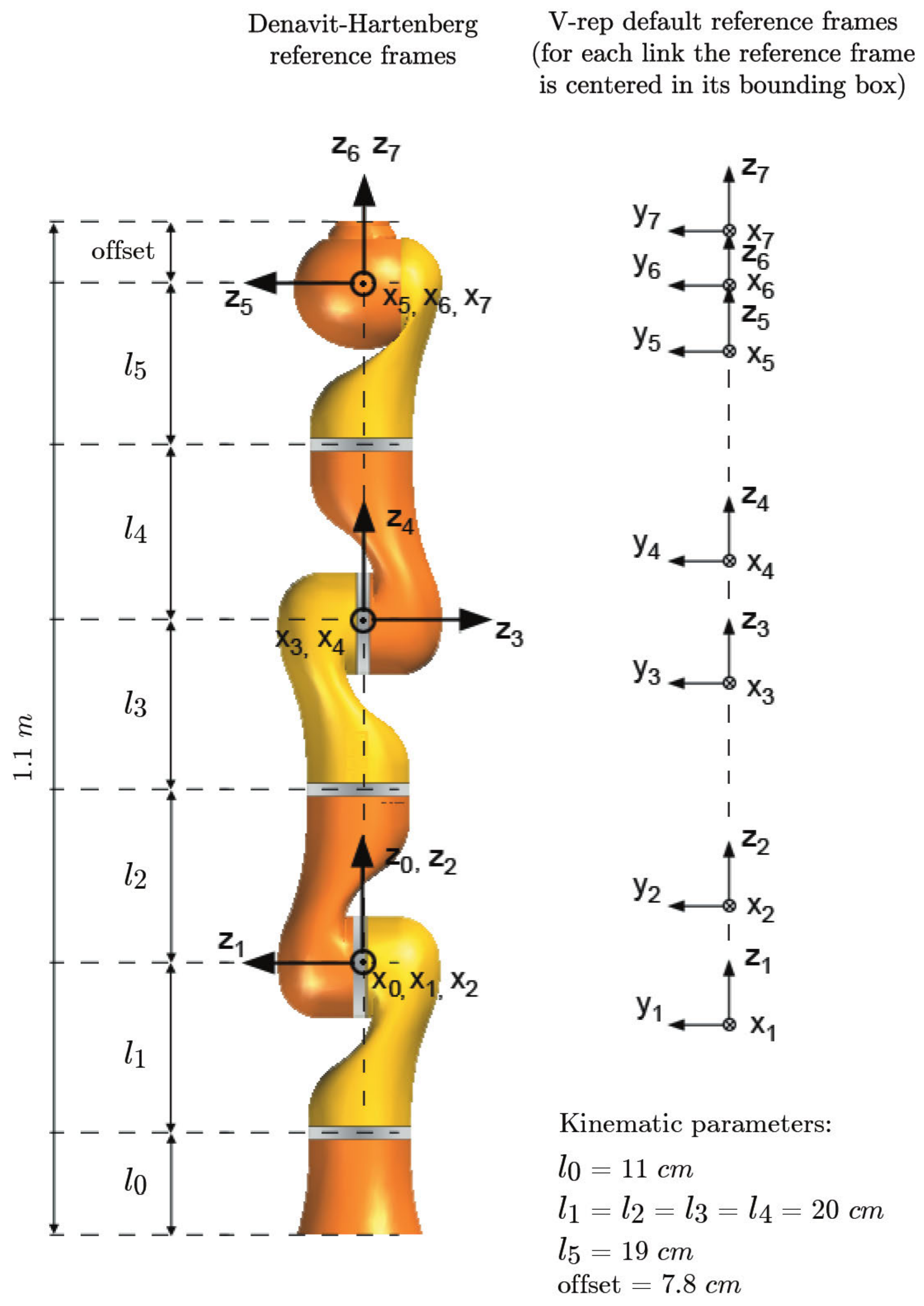

Figure 8.2: Illustration of the geometry and local coordinates of the KUKA LBR4 robotic arm. Image taken from the *Notes on the KUKA LWR4 dynamic model* document from Coppelia Robotics GmbH and Massimo Cefalo (`http://www.coppeliarobotics.com/contributions/LBR4p_dynamic_model.pdf`).

8.3 General Kinematics of KUKA LBR4+

As shortly mentioned before, we perform the control task on the kinematic model and hence, leave some of the tasks to the inner control loop, consisting of the low level controllers. The exact model will be introduced in the next chapter. Nevertheless we will present the position of the end-effector already in this section. More information about the derivation of kinematics can be found in these two standard references [60, 61].

We aim for the position of the end effector, given the joint angles. This highly nonlinear function can be derived using the DH convention, as introduced in Section 8.1 and is given in (8.1):

$$o_{end-eff}(\Theta) = \left(\begin{matrix} -0.4\cos(\Theta_1)\sin(\Theta_2) - 0.39\sin(\Theta_4)(\sin(\Theta_1)\sin(\Theta_3) \\ 0.39\sin(\Theta_4)(\cos(\Theta_1)\sin(\Theta_3) + \cos(\Theta_2)\cos(\Theta_3)\sin(\Theta_1)) \\ 0.4\cos(\Theta_2) + 0.39\cos(\Theta_2)\cos(\Theta_4) + 0.31 \end{matrix} \right. \\ \left. \begin{matrix} -\cos(\Theta_1)\cos(\Theta_2)\cos(\Theta_3)) - 0.39\cos(\Theta_1)\cos(\Theta_4)\sin(\Theta_2) \\ -0.4\sin(\Theta_1)\sin(\Theta_2) - 0.39\cos(\Theta_4)\sin(\Theta_1)\sin(\Theta_2) \\ +0.39\cos(\Theta_3)\sin(\Theta_2)\sin(\Theta_4) \end{matrix} \right). \tag{8.1}$$

Remark. *Also the orientation of the end effector could be included in the output function. Its dimensionality would then expand to 6 (instead of 3). However, since we are not using the orientation for our control task, we decided not to show the derivation here.*

The derived position of the end-effector given in (8.1) denotes the position of the origin of coordinate systems 5, 6 and 7 in Figure 8.2, i.e. the middle of the last spherical part of the robot.

However, in our use case we are interested in the position of the middle of the palm of the barrett hand. If the last three joints are fixed at $\Theta_{5,6,7} = 0$, we can write its position only dependent on Θ_i, for $i = 1, \dots, 4$ as in the following:

$$o_{hand-palm}(\Theta) = \left(\begin{matrix} -0.4\cos(\Theta_1)\sin(\Theta_2) - 0.578\sin(\Theta_4)(\sin(\Theta_1)\sin(\Theta_3) \\ 0.578\sin(\Theta_4)(\cos(\Theta_1)\sin(\Theta_3) + \cos(\Theta_2)\cos(\Theta_3)\sin(\Theta_1)) \\ 0.4\cos(\Theta_2) + 0.578\cos(\Theta_2)\cos(\Theta_4) + 0.31 \end{matrix} \right. \\ \left. \begin{matrix} -\cos(\Theta_1)\cos(\Theta_2)\cos(\Theta_3)) - 0.578\cos(\Theta_1)\cos(\Theta_4)\sin(\Theta_2) \\ -0.4\sin(\Theta_1)\sin(\Theta_2) - 0.578\cos(\Theta_4)\sin(\Theta_1)\sin(\Theta_2) \\ +0.578\cos(\Theta_3)\sin(\Theta_2)\sin(\Theta_4) \end{matrix} \right). \tag{8.2}$$

This is also the position we are using for controlling the robot later on.

8.4 SL Specifics and Constraints

8.4.1 Joint Offset DH convention to SL

We do all of our control actions on the DH model derived in Section 8.3. Though, the angles are defined differently in SL and therefore need conversion. The shift between the two angle definitions can be seen in Table 8.1. With these shifted values we can obtain the angles for SL using the transformation in (8.3):

$$\Theta_{joint,SL} = \Theta_{joint,DH} + \Delta\Theta_{joint}. \tag{8.3}$$

Table 8.1: Shift between angles in SL and our DH convention.

Joint	lbr-0	lbr-1	lbr-2	lbr-3	lbr-4	lbr-5	lbr-6
$\Delta\Theta_{joint}$ [rad]	0	-1.57	1.05	0	-1.57	0	0

8.4.2 Joint Limits

As a matter of principle, the angular joint limits are given by the constraints of the hardware: the joints are not able to do more than one full rotation. Nevertheless, for our angular joint limits we use the joint constraints as given in SL, to not violate any internal constraints. Those angular joint limits observed from SL are given in Table 8.2. The angular velocity is not really limited in

Table 8.2: Angular joint limits of the KUKA LBR4 defined in SL's Joint Space.

Joint	lbr-0	lbr-1	lbr-2	lbr-3	lbr-4	lbr-5	lbr-6
Min [rad]	-2.96	-3.1	-1.9	-2.09	-3.1	-2.09	-2.96
Max [rad]	2.96	-0.1	4.0	2.09	1.35	2.09	2.96

the same way and is not clearly restricted in SL. Nevertheless, after reaching a certain too high velocity, the KUKA controller kicks in and stops the robot. Based on experience, the robot is able to move at high speeds before reaching that point. Therefore, we arbitrarily define these values as design parameters, also dependent on the speed of our controller. We define the values as it can be seen in Table 8.3. If we use a more comprehensive system state dynamics, as seen in the next

Table 8.3: Angular velocity joint limits, used as design parameters.

Joint	lbr-0	lbr-1	lbr-2	lbr-3	lbr-4	lbr-5	lbr-6
Max [|rad/s|]	2.3	2.3	2.3	2.3	2.3	2.3	2.3

chapter in (9.2), we can also enforce bounds on the acceleration. In this case we choose the ones seen in Table 8.4.

Table 8.4: Angular acceleration joint limits, used as design parameters.

Joint	lbr-0	lbr-1	lbr-2	lbr-3	lbr-4	lbr-5	lbr-6
Max [$\|rad/s^2\|$]	8	8	8	8	8	8	8

Remark. *As it can be seen in the next chapter, we assume to be in a position to control the angular velocity or the angular acceleration (depending on the model) of the joints directly. Therefore, the limitations in angular velocity and angular acceleration are a powerful and important way to limit the model uncertainty.*

8.4.3 Robot frame to DH convention

Additionally, since reference and obstacles are given in the robot frame, we need to transform them to our DH robot arm coordinate system. The robot frame coordinate system is located between the shoulders of the robot, with z axis pointing upwards and x-axis pointing horizontally.

Let us denote the transformation subscripts as following: $x_{arm} = T_{arm-apollo} \cdot x_{apollo}$. In our case, the transformation between the robot frame and the DH robot arm is static. This static transformation for points in the Apollo frame to points in the DH frame is derived in the following by inspection:

$$R_{arm-apollo} \cdot \begin{pmatrix} 1 \\ 0 \\ 0 \end{pmatrix} = \begin{pmatrix} 0 \\ 1/2 \\ \sqrt{3}/2 \end{pmatrix}, \; R_{arm-apollo} \cdot \begin{pmatrix} 0 \\ 1 \\ 0 \end{pmatrix} = \begin{pmatrix} 0 \\ -\sqrt{3}/2 \\ 1/2 \end{pmatrix}, \tag{8.4}$$

$$R_{arm-apollo} \cdot \begin{pmatrix} 0 \\ 0 \\ 1 \end{pmatrix} = \begin{pmatrix} 1 \\ 0 \\ 0 \end{pmatrix}. \tag{8.5}$$

This results in the following rotation matrix

$$\Leftrightarrow R_{arm-apollo} \cdot \begin{pmatrix} 1 & 0 & 0 \\ 0 & 1 & 0 \\ 0 & 0 & 1 \end{pmatrix} = R_{arm-apollo} = \begin{pmatrix} 0 & 0 & 1 \\ 1/2 & -\sqrt{3}/2 & 0 \\ \sqrt{3}/2 & 1/2 & 0 \end{pmatrix}. \tag{8.6}$$

Additionally we can observe the following translation vector by inspection:

$$t_{arm-apollo} = 0.05813 \cdot \begin{pmatrix} 0 \\ 1/2 \\ -\sqrt{3}/2 \end{pmatrix}. \tag{8.7}$$

8.5 Controlling the Robot

As seen in Section 6.4 we use SL for the robot control. SL integrates low-level PID controllers for controlling the state and acceleration by taking a reference and transforming it to voltage commands for the motors of the KUKA LBR4+ robotic arms. In our experience, they work reliably if a smooth and continuous state trajectory is set as reference. We are not using the underlying dynamic model of the robotic arms but leave that to the low level controllers. The solution of the MPC controller grants access to the optimal input $u^*(0|t)$ in the form of a reference velocity $\dot{x}_r$ (compare (9.1)) or acceleration $\ddot{x}_r$ (compare (9.2)). Since the low-level PID controllers take a reference state x_r and velocity $\dot{x}_r$ as input, we need to infer the state (compare (9.1)) or the state and the velocity (compare (9.2)) from the obtained input $u^*(0|t)$. We can take the desired acceleration into account by using the inverse dynamics function of SL to obtain a feedforward command (compare Figure 6.1), which is directly applied to the KUKA robotic arm.

Simplified System ((9.1)) For this formulation introduced in (9.1), the input $u^*(0|t)$ describes the desired velocity. According to the system definition, we directly obtain the following as an output of the optimization problem:

$$\dot{x}_r = u^*(0|t). \tag{8.8}$$

As the velocity reference might be discontinuous in this simple setting, it is not easy to get a reasonable estimate for the acceleration. We decided to set it to zero:

$$\ddot{x}_r = 0. \tag{8.9}$$

Using the inverse dynamics function still offers some gain, e.g. due to gravity compensation. In particular, this helps the low level controllers in arm positions close to horizontal. The desired speed can easily be targeted in real time (i.e. 1ms) in the MPC sampling time interval with the following policy:

$$x_r^+ = A_{d,1ms} x_r + B_{d,1ms}(u^*(0|t) + K_\delta x_{real}). \tag{8.10}$$

$A_{d,1ms}$ and $B_{d,1ms}$ denote the matrices of the discretization, corresponding to a sampling time of 1ms. At the beginning of an interval, of course we then set $x_r = x_{real}$.

Full System ((9.2)) In this setting the output of the system directly describes the acceleration

$$\ddot{x}_r = u^*(0|t). \tag{8.11}$$

The desired velocity and state can be calculated accordingly:

$$x_r^+ = A_{d,1ms} x_r + B_{d,1ms}(u^*(0|t) + K_\delta x_{real}), \tag{8.12}$$

where x_r contains both the angle and the angular velocity and $A_{d,1ms}$, $D_{d,1ms}$ denote the discretization for the system, given a sampling time of 1ms.

Remark. *The exact discretization for a piecewise constant input signal* $u^*(0|t)$ *over an arbitrary long time horizon would be*

$$x^+ = A_{cl,d}x + B_{cl,d}u^*(0|t), \tag{8.13}$$

where $A_{cl,d}$ *and* $B_{cl,d}$ *denote the matrices for the exact discretization of the continuous time system* $\dot{x} = (A + BK_\delta)x + Bu^*(0|t)$. *Therefore, normally the expression in* (8.10) *and in* (8.12) *would only be an approximation due to a non constant input term* $K_\delta x_{real}$. *However, in this specific case we are calculating the next state after 1ms. And since the internal rate of the framework is also given as 1ms,* x_{real} *is constant within this interval.*

Chapter 9

Experimental Results on Apollo Robot

In this chapter we present our results on the robotic system we introduced in the last chapter. Our goal is to control the position of the arm under constraints in the state and input space as well as constraints regarding the position of the end-effector. In Section 9.1 we will frame this task as a control problem. In Section 9.2 we will introduce the RMPC design and the learning architectures before we will present the results in Section 9.3. Further results and a more condensed version of our work can be found in our corresponding paper [53].

9.1 System Formulation

9.1.1 System State Dynamics

In the following, we will present two ways of formulating the problem as a control task. One simplified one where we assume to be able to directly control the velocity of the joints, and another more realistic one where we use the joint accelerations as control signal. The motivation for the first one is mainly to reduce dimensions, in order to be in a more comfortable position to sample the state space for the learning approach. The robot has 7 degrees of freedom, nevertheless, we only control the first 4 joints and keep the joints 5-7 constant. This is sufficient for controlling the position but becomes a restriction when control of the end-effector orientation would be desired.

Simplified Formulation

For the kinematic control of Apollo robot, we define the system state vector and its derivative as in (9.1). We assume being able to control the velocity of the joints directly relying on the low level joint controllers.

$$x = \begin{pmatrix} x_1 \\ x_2 \\ x_3 \\ x_4 \end{pmatrix} = \begin{pmatrix} \Theta_1 \\ \Theta_2 \\ \Theta_3 \\ \Theta_4 \end{pmatrix}, \quad \dot{x} = f(x,u) = \begin{pmatrix} \dot{\Theta}_1 \\ \dot{\Theta}_2 \\ \dot{\Theta}_3 \\ \dot{\Theta}_4 \end{pmatrix} = \begin{pmatrix} u_1 \\ u_2 \\ u_3 \\ u_4 \end{pmatrix}. \tag{9.1}$$

We define the corresponding output function as the end-effector position of the robotic arm as this is the item of interest. Its arithmetic expression was derived in Section 8.3 in (8.2).

In practice this formulation of the state dynamics only makes sense under the following assumption.

Assumption 9.1. *The underlying controller which controls the speed of the robot joints is fast enough, i.e. also possibly discontinuous or fast changing velocity commands are reached in the system by applying the underlying low level controllers.*

Remark. *As we will see in Section 9.2.1 this model is realistic for low absolute velocities, leading to smaller steps in the velocity reference. Additionally it becomes more and more unrealistic, the more we decrease the sampling time of the MPC controller, since the rise time of the controller becomes less negligible.*

9.1.2 Full Formulation

Alternatively it is possible to use the accelerations as input signal. This has two big advantages:

1. It is more related to direct dynamics control.
2. The speed profile is automatically continuous, and hence, is more realistic and easier to control.

For this purpose, a new state dynamics formulation is needed:

$$x = \begin{pmatrix} x_1 \\ x_2 \\ x_3 \\ x_4 \\ x_5 \\ x_6 \\ x_7 \\ x_8 \end{pmatrix} = \begin{pmatrix} \Theta_1 \\ \Theta_2 \\ \Theta_3 \\ \Theta_4 \\ \dot\Theta_1 \\ \dot\Theta_2 \\ \dot\Theta_3 \\ \dot\Theta_4 \end{pmatrix}, \quad \dot x = f(x,u) = \begin{pmatrix} \dot\Theta_1 \\ \dot\Theta_2 \\ \dot\Theta_3 \\ \dot\Theta_4 \\ \ddot\Theta_1 \\ \ddot\Theta_2 \\ \ddot\Theta_3 \\ \ddot\Theta_4 \end{pmatrix} = \begin{pmatrix} x_5 \\ x_6 \\ x_7 \\ x_8 \\ u_1 \\ u_2 \\ u_3 \\ u_4 \end{pmatrix}, \tag{9.2}$$

with the same output function.

Remark. *It is worth mentioning that this formulation would be completely equivalent to the pure dynamic model if an exact feedback linearization would be applied to the latter. However, for this to be viable, a model with a good quality needs to be identified.*

9.1.3 Output Function

We define the position of the end palm of the robot hand as the output of the system. This function was derived using the DH convention in the last chapter and is repeated in (9.3):

$$y = h(x,u) = \begin{pmatrix} -0.4\cos(\Theta_1)\sin(\Theta_2) - 0.578\sin(\Theta_4)(\sin(\Theta_1)\sin(\Theta_3) \\ 0.578\sin(\Theta_4)(\cos(\Theta_1)\sin(\Theta_3) + \cos(\Theta_2)\cos(\Theta_3)\sin(\Theta_1)) \\ 0.4\cos(\Theta_2) + 0.578\cos(\Theta_2)\cos(\Theta_4) + 0.31 \\ - \cos(\Theta_1)\cos(\Theta_2)\cos(\Theta_3)) - 0.578\cos(\Theta_1)\cos(\Theta_4)\sin(\Theta_2) \\ - 0.4\sin(\Theta_1)\sin(\Theta_2) - 0.578\cos(\Theta_4)\sin(\Theta_1)\sin(\Theta_2) \\ + 0.578\cos(\Theta_3)\sin(\Theta_2)\sin(\Theta_4) \end{pmatrix}. \tag{9.3}$$

9.2 Setup

9.2.1 Determination of the Disturbance

To be in a position for designing the RMPC controller, we first need to identify the disturbance magnitude of the system, i.e. what was denoted as d_w earlier. For this purpose, we randomly sample trajectories and analyze disturbance values for both system formulations.

Simplified Formulation

First we will have a look at the simplified formulation from (9.1).

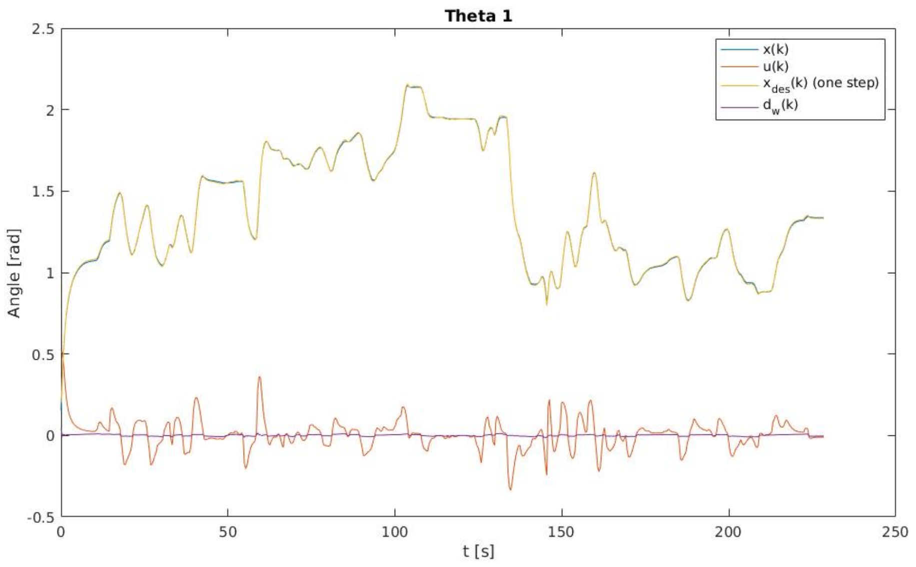

Figure 9.1: Disturbance (i.e. error) and trajectory of Θ_1 of the real robot when limiting the velocity to $0.7 rad/s$. It is especially large when the system accelerates or brakes abruptly, e.g. in the very beginning.

Disturbance of Real Robot For designing the RMPC we first wanted to find out how big the real disturbance on the system can get. For this purpose we sampled the state space on the real robot to get an idea of how big the deviation of the real system is compared to our assumed nominal system. To get an idea about this, please look at Figure 9.1. We only show the measurements on Θ_1, which is representative for the behavior of all joints. It is likely that the error becomes larger with increasing demanded accelerations, since the system is not able to accelerate instantly (and without delay) to the desired velocity. Looking at Figure 9.1 unveils that Assumption 9.1 is at least partly fulfilled for low velocities and a slow sampling rate of $0.4s$, since the disturbance remains moderate.

When trying to design a suitable RMPC controller the deviation of the disturbed function $x_{k+1} = f_w(x, u, w)$ compared to the nominal system $x_{k+1} = f(x, u)$ is the important characteristic. To guarantee safety, we need to be in a position to account for all possible disturbances along the horizon.

Disturbance as Function of the Velocity We came up with the idea that very likely the disturbance is related to the velocity; higher velocity means higher disturbances. In this case the error seems to be mainly created due to high intractable acceleration. Nevertheless, high acceleration steps can also be avoided by limiting the velocity.

We sample random trajectories in simulation and plotted the ∞-norm of the disturbance against the ∞-norm of the joint velocities (in $\frac{rad}{s}$). This is visualized in Figure 9.2. In order to design a suitable and sufficient RMPC controller, we limited the speed of the joints to a value only giving rise to manageable disturbances. We perform a reverse approach: we check, for which disturbances we are still able to design a suitable controller. Then afterwards, we limit the velocity to make sure to keep the disturbance within these bounds.

Remark. *Note that for this thesis we are only properly looking at the disturbance values in simulation. We found the model to be relatively accurate in this respect and since we are doing the validation in simulation only, we are mainly interested in this value within this work.*

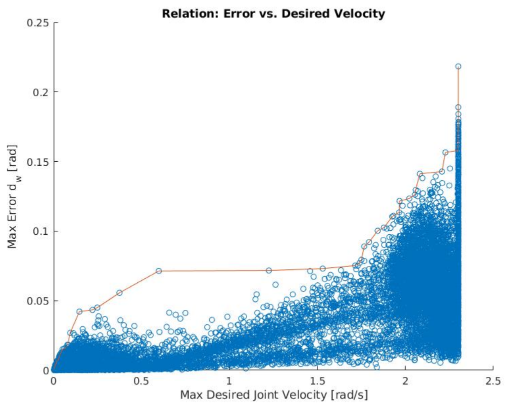

Figure 9.2: Disturbance in relation to the joint velocities for the simulation.

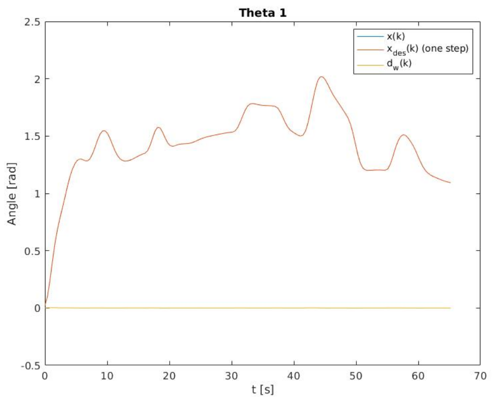

(a) Disturbance of Θ_1 for the simulation.

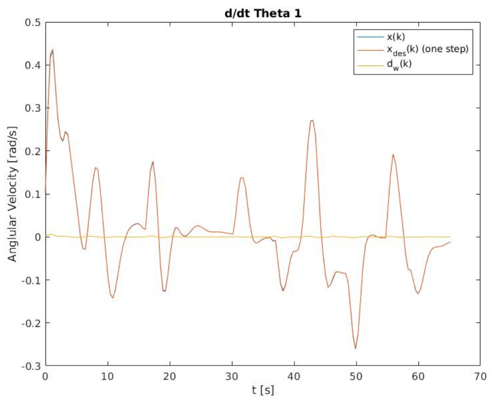

(b) Disturbance of $\dot{\Theta}_1$ for the simulation.

Figure 9.3

Full Formulation

This time, we use the full description with 8 states as seen in (9.2).

Disturbance of the Real Robot In the very beginning we wanted to find out how the real system is behaving compared to our assumptions. For this purpose, we limited the joint velocity to $0.7\frac{rad}{s}$ and the angular acceleration to $0.7\frac{rad}{s^2}$. In Figure 9.3 we can see the deviation on the state (angle and angular velocity) of the first joint of the real robot.

Disturbance as Function of the Velocity and Acceleration We proceed in a similar manner as in the last subsubsection for the simplified formulation. However, this time we are not only plotting the disturbance against the velocity, but against the velocity and the acceleration. This makes sense, since these are the values of interest, which we are able to control. The corresponding plots for the control problem formulation can be seen in Figure 9.4a and Figure 9.4b.

All in all, it also becomes clear that the error of this full formulation is much smaller than the one of the simplified case. The explanation for this is that it is physically possibe to control the accelerations by applying a specific torque on the electric motors leading to a continuous angle and angular velocity profile. In contrast, it is not possible to directly control the velocity; the shorter the sampling time gets, the more negative impact is created by the not infinitesimal rise time of the low level controllers, leading to a deviation from the expected state.

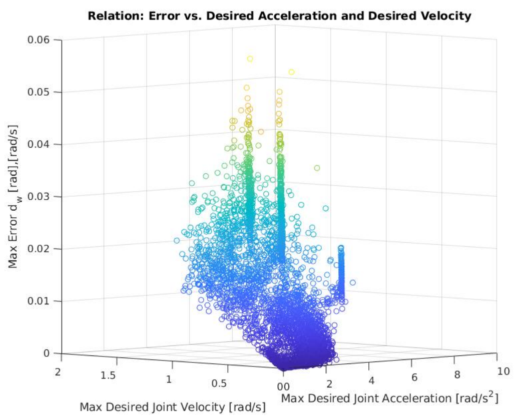

(a) Disturbance as a function of the velocity and the acceleration for the simulation from perspective 1.

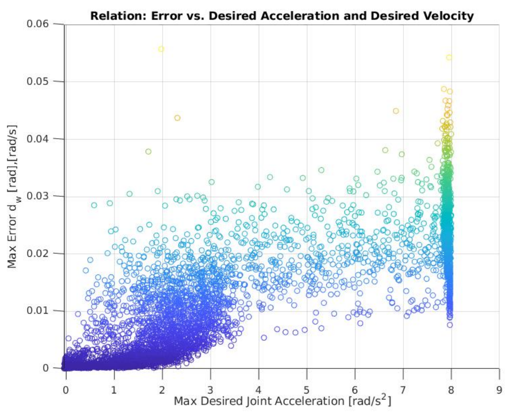

(b) Disturbance as a function of the velocity and the acceleration for the simulation from perspective 2.

Figure 9.4

9.2.2 RMPC Design

The main theory for the used RMPC scheme was introduced in Section 3.2 and the needed knowledge and calculations for its design were introduced in Chapter 4. Since our goal is to control the output function and we do not have explicit knowledge about the corresponding state x_s, we include the dynamic set point tracking as introduced earlier (Section 3.1) in our RMPC scheme. Additionally, we need to consider constraints on the state, input and output functions. The constraints on the output function are of nonlinear nature, due to the fact that the output function itself is nonlinear.

Formulation

The resulting RMPC optimization problem in (9.4) is analogous to the one derived in Section 4.5. It contains everything we need to be in a position to track the output function and therefore, to control the robot, while satisfying all constraints and guaranteeing recursive feasibility under disturbances.

$$V_N(x(t), y_t) = \min_{u(\cdot|t), x_s, u_s, \alpha} J_N(x, y_t; u(\cdot|t)*, y_s, x_s, u_s, \alpha) \tag{9.4a}$$

$$\text{subject to} \quad x(0|t) = x(t), \tag{9.4b}$$

$$x(k+1|t) = f(x(k|t), u(k|t)), \tag{9.4c}$$

$$g_j(x(k|t), u(k|t)) + c_j \frac{1-\rho^k}{1-\rho} \bar{w} \leq 0, \tag{9.4d}$$

$$x_s = f(x_s, u_s), \quad y_s = h(x_s, u_s), \tag{9.4e}$$

$$\frac{\bar{w}}{1-\rho} \leq \alpha \leq -\frac{g_j(x_s, u_s)}{c_j}, \quad \forall j = 1, ..., p \tag{9.4f}$$

$$|x(N|t) - x_s|^2_{P_\delta} \leq (\alpha - \bar{s}_f)^2, \tag{9.4g}$$

$$k = 0, ..., N-1, \quad j = 1, ..., p,$$

with J_N as introduced in Section 3.1.2 and repeated here:

$$J_N(x, y_t; u(\cdot|t), y_s, x_s, u_s) = \sum_{k=0}^{N-1} l(x(k|t) - x_s, u(k|t) - u_s) + V_f(x(N|t) - x_s, y_s) + V_O(y_s - y_t). \tag{9.5}$$

In this case, the function $f(\cdot, \cdot)$ describes either the dynamics in (9.1) or in (9.2). The function $h(\cdot, \cdot)$ denotes the output function from(9.3), describing the 3D position in the Cartesian space.

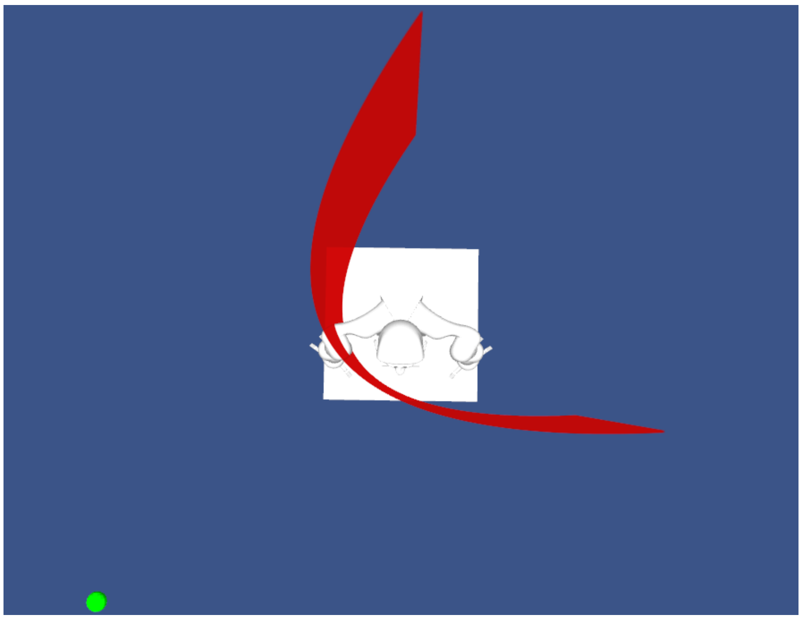

Figure 9.5: Visualization of the nonlinear output constraint which avoids that the robot could hit itself.

Constraints

As seen in (9.4d), we include the constraints in a robust way in our optimization problem (i.e. by tightening them). We will introduce the constraints in the following.

State and Input Constraints For the state constraints refer to Table 8.2, and for the full formulation from (9.2) also to Table 8.3. For the input constraints consider either (for the simplified formulation (9.1)) Table 8.3 or (for the full formulation (9.2)) Table 8.4. All of these constraints are of polytopic nature and can be written as $g_j(x,u) \leq 0$ for $j \in \{1,\dots,p-3\}$ (there will be 3 output constraints).

More interesting are the constraints on our output function, since they describe the space where the robot is supposed to operate in. In the following, we will derive the function $g_q(x,u)$ for $q = p-2$, $g_r(x,u)$ for $r = p-1$ and $g_p(x,u)$ and their derivatives with respect to x, i.e. the state of the system. $y_1(x)$, $y_2(x)$ and $y_3(x)$ denote the first, second and third entry of the system output (i.e. the x, y and z coordinates of the robot hand palm), which are a function of the system state. With (4.84), we can then calculate the c_j values corresponding to those constraints.

Robot Body Avoidance We use the constraint description to make sure that the robot does not hit its own body with the end effector. y^b denotes the base of the quadratic function which defines where the robot is allowed to move and where it is not. A visualization of the constraint can be seen in Figure 9.5.

In the coordinate system of the robotic arm this can be written as the following condition:

$$y_3 - y_3^b \geq -(y_2 - y_2^b)^2. \tag{9.6}$$

We want to transform this condition to the expected form for $g_q(x,u)$: $g_q(x,u) \leq 0$. With this

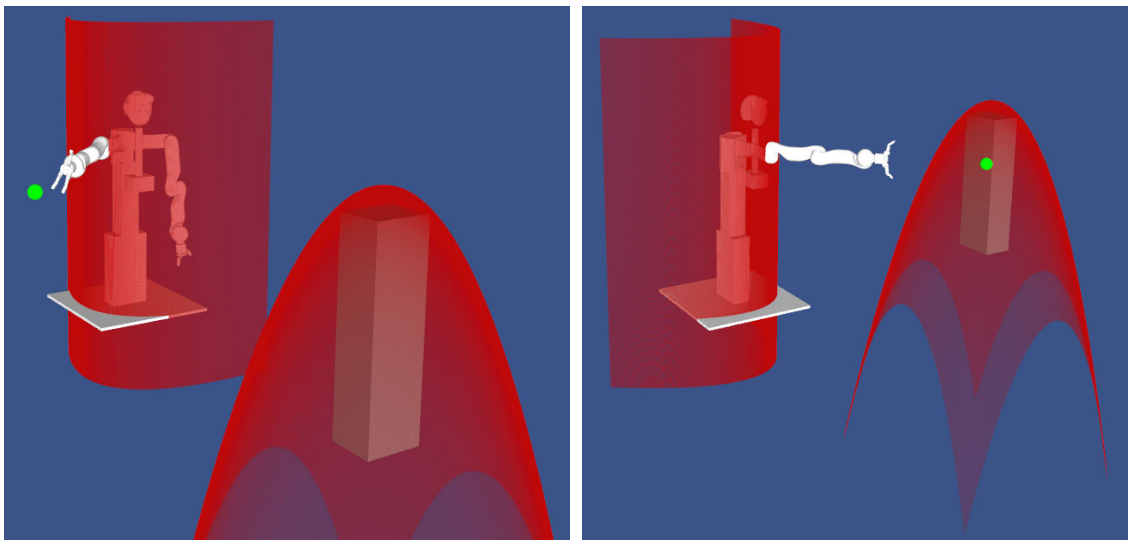

Figure 9.6: Visualization of the body constraint as well as the vertical obstacle constraint.

prerequisite we get:

$$g_q(x,u) = -y_3 + y_3^b - y_2^2 - (y_2^b)^2 + 2y_2^b y_2 \tag{9.7}$$

$$= -y_3 - y_2^2 + 2y_2^b y_2 + y_3^b - (y_2^b)^2 \tag{9.8}$$

$$\overset{y_1^b = y_2^b = 0}{=} -y_3 - y_2^2 \underbrace{+y_3^b}_{const} \overset{!}{\leq} 0. \tag{9.9}$$

Now we are interested in the Jacobian of this function (see (4.84) for more information), which can be written as the following:

$$\frac{\partial g_q(x,u)}{\partial x} = -\frac{\partial y_3}{\partial x} - 2y_2 \frac{\partial y_2}{\partial x}. \tag{9.10}$$

Obstacle Avoidance Additionally we use quadratic constraints to avoid obstacles in the operation space. In principle, we are able to handle any obstacle which can be described by a differentiable function. In this specific case we do the calculations for two types: horizontal and vertical obstacles. A visualization of a vertical obstacle can be seen in Figure 9.6. Herein, y^o denotes the position of the apex of the function, defining the position of the obstacle. In our case we define the obstacles with the help of quadratic functions. The constant C defines the steepness of the quadratic function, we choose it to be 2.

The calculations for the horizontal obstacle can be done as in the following:

$$y_3 - y_3^o \leq C(y_1 - y_1^o)^2 + C(y_2 - y_2^o)^2. \tag{9.11}$$

The corresponding function $g_r(x,u)$ is defined as follows:

$$g_r(x,u) = y_3 - y_3^o - Cy_1^2 - C(y_1^o)^2 + 2Cy_1^0 y_1 - Cy_2^2 - C(y_2^o)^2 + 2Cy_2^o y_2 \tag{9.12}$$

$$= y_3 - Cy_1^2 - Cy_2^2 + 2Cy_1^o y_1 + 2Cy_2^o y_2 \underbrace{-C(y_1^o)^2 - C(y_2^o)^2 - y_3^o}_{const} \overset{!}{\leq} 0. \tag{9.13}$$

For the derivative we get:

$$\frac{\partial g_r(x,u)}{\partial x} = \frac{\partial y_3}{\partial x} - 2C(y_1 - y_1^o)\frac{\partial y_1}{\partial x} - 2C(y_2 - y_2^0)\frac{\partial y_2}{\partial x}. \tag{9.14}$$

Now we do the calculations for the vertical obstacle:

$$y_1 - y_1^o \geq -C\left((y_3 - y_3^o)^2 + (y_2 - y_2^o)^2\right) \tag{9.15}$$

and therefore

$$g_p(x,u) = -y_1 - Cy_2^2 + 2Cy_2y_2^o - Cy_3^2 + 2Cy_3y_3^o + \underbrace{y_1^o - C\left(y_2^o\right)^2 - C\left(y_3^o\right)^2}_{const} \overset{!}{\leq} 0. \tag{9.16}$$

For the derivative we get:

$$\frac{\partial g_p(x,u)}{\partial x} = -\frac{\partial y_1}{\partial x} - 2C(y_2 - y_2^o)\frac{\partial y_2}{\partial x} - 2C(y_3 - y_3^o)\frac{\partial y_3}{\partial x}. \tag{9.17}$$

It is obvious that we still have the location of the obstacle in this derivatives of g_r and g_p. However, since the function is linear in this argument and we are interested in the extrema for finding c_r and c_p we only need to consider the maximum and minimum values of y_1^o and y_2^o. Since the robot arm only has a total length of $1.288m$ (to the palm of the hand), we choose the following bounds:

$$-1.4 \leq y_1^o \leq 1.4, \text{ and } -1.4 \leq y_2^o \leq 1.4, \text{ and } -1.4 \leq y_3^o \leq 1.4. \tag{9.18}$$

RMPC Offline Computations

We need to do some offline calculations to get the required parameters for our RMPC controller. Of course we designed many RMPC controllers along the way: for 4 dimensions, for 8 dimensions, with a sampling time of $0.4s$ for the RMPC robot control, with a sampling time of $0.01s$ and $0.04s$ (for the controller we used to train the neural network), and so on. We will demonstrate the design exemplary for one specific configuration: sampling time of $h = 0.4s$ and 8 dimensions, i.e. the full formulation from (9.2). The code for doing the offline computations as well as the results for the other designs can be found in the code coming with this thesis.

Remark. *As already described earlier, we assume for all of the calculations a CT prestabilization, due to the fact that it can be applied at a frequency of* $1ms$*. If this would not be possible, the prestabilization would also need to be included in the calculations in DT.*

1. The choice of the CT contraction rate is very important for the behavior of the system. Higher contraction rates enable the system to compensate for larger disturbances. However, when the contraction rate is significantly higher than the time constant of the system or the sampling time, this can lead to jerky behavior, since the end effector is slowing down by a large amount within the sampling interval before accelerating again. For this specific example, we choose a contraction rate of $\rho_c = 2.5$ (i.e. the time constant corresponding to the RMPC sampling rate). To always finish our calculations within the sampling time, we choose a relatively time horizon of only $T = 1.2$, i.e. 3 steps into the future. According to Figure 9.4a, we see that the maximum DT error is given as $d_w = 0.06$ (rad or rad/s). For a sampling time of $0.4s$, this is equivalent to $d_{w,c} = 0.15$. We put some tolerance on top and choose $d_{w,c} = 0.25$.

2. After having chosen the important design parameters, we need to calculate suitable P_δ and K_δ (refer to Section 4.6.1). In here, we consider the condition on the contraction rate as well as the constraints on our state and input (see Section 8.4). Furthermore, we require $\bar{w}_c$ to be smaller than a specific value, 0.32 in our case. This is the smallest bound on $\bar{w}_c$ which still preserves feasibility of the offline-calculations optimization problem. We get the following

two matrices:

$$P_\delta = \begin{pmatrix} 4.7311 & 0 & 0 & 0 & 0.9776 & 0 & 0 & 0 \\ 0 & 4.7311 & 0 & 0 & 0 & 0.9776 & 0 & 0 \\ 0 & 0 & 4.7311 & 0 & 0 & 0 & 0.9776 & 0 \\ 0 & 0 & 0 & 4.7311 & 0 & 0 & 0 & 0.9776 \\ 0.9776 & 0 & 0 & 0 & 0.3911 & 0 & 0 & 0 \\ 0 & 0.9776 & 0 & 0 & 0 & 0.3911 & 0 & 0 \\ 0 & 0 & 0.9776 & 0 & 0 & 0 & 0.3911 & 0 \\ 0 & 0 & 0 & 0.9776 & 0 & 0 & 0 & 0.3911 \end{pmatrix}, \quad (9.19)$$

$$K_\delta = \begin{pmatrix} -12.0983 & 0 & 0 & 0 & -5 & 0 & 0 & 0 \\ 0 & -12.0983 & 0 & 0 & 0 & -5 & 0 & 0 \\ 0 & 0 & -12.0983 & 0 & 0 & 0 & -5 & 0 \\ 0 & 0 & 0 & -12.0983 & 0 & 0 & 0 & -5 \end{pmatrix}. \quad (9.20)$$

3. As a next step we compute the required values for c_j. We have the following contraints:

   - Constraints $1, \dots, 16$ are the polytopic state constraints according to Table 8.2 transformed to our DH convention used for the control (Table 8.1).
   - Constraints $17, \dots, 24$ are the input constraints. As we have seen in the last section we limit those to $8\frac{rad}{s^2}$ for each of the 4 joints.
   - Constraint 25 is the constraint on the output function to avoid the robot hitting itself (compare (9.9)).
   - Constraint 26 is the constraint on the output function to avoid the robot hitting any horizontal obstacle at position y^o (compare (9.13)).
   - Constraint 27 is the constraint on the output function to avoid the robot hitting any vertical obstacle at position y^o (compare (9.16)).

   The resulting values for c_j are summarized in Table 9.1, 8.4 and 9.2.

   Table 9.1: Values for c_j of the state and input constraints, i.e. for $j = 1, \dots, 24$.

j	1,2	3	4	5,6	7,8	9...24
c_j	0.2234	0.4498	0.4322	0.2242	0.3164	1.0

   Table 9.2: Values for c_j of the output constraints, i.e. for $j = 25, 26, 37$.

j	25	26	27
c_j	0.7906	4.2143	4.5535

4. We check that ρ_c and w_c satisfy our requirements.
5. We calculate $\bar{w}_{c,allowed} = \frac{\rho_c}{c_{max}} = 2.5$, which is bigger than the $\bar{w}_c$ we imposed.
6. We check whether $\bar{w}_{c,allowed,output} = \frac{-g_j(x_{test}, u_{test})}{c_j}$ is bigger than $\bar{w}_c$ for realistic (x_{test}, u_{test}).
7. We compute the maximum tube size $\bar{s}_f = \frac{1-e^{-\rho_c T}}{\rho_c} w_c = 0.1188$.
8. We define the matrices Q and R as following: $Q = I_{8\times 8}$, $R = I_{4\times 4}$.

9. Finally, we compute the terminal cost, which is the exact infinite horizon cost using the corresponding K_δ-controller. This results in:

$$P_f = \begin{pmatrix} 16.1534 & 0 & 0 & 0 & 6.0905 & 0 & 0 & 0 \\ 0 & 16.1534 & 0 & 0 & 0 & 6.0905 & 0 & 0 \\ 0 & 0 & 16.1534 & 0 & 0 & 0 & 6.0905 & 0 \\ 0 & 0 & 0 & 16.1534 & 0 & 0 & 0 & 6.0905 \\ 6.0905 & 0 & 0 & 0 & 3.8181 & 0 & 0 & 0 \\ 0 & 6.0905 & 0 & 0 & 0 & 3.8181 & 0 & 0 \\ 0 & 0 & 6.0905 & 0 & 0 & 0 & 3.8181 & 0 \\ 0 & 0 & 0 & 6.0905 & 0 & 0 & 0 & 3.8181 \end{pmatrix}. \quad (9.21)$$

10. Compute the DT equivalents of the parameters: $\rho_d = e^{-\rho_c \cdot h} = 0.3679$, $\bar{w}_d = \frac{1-e^{-\rho_c h}}{\rho_c}\bar{w}_c = \frac{1-\rho_d}{\rho_c}\bar{w}_c = 0.0791$.

9.2.3 Learning

Curse of Dimensionality

At this place we do a small calculation example to underline one main problem for the learning.

Including parallelization, we assume a computing time of $0.05\frac{s}{sample}$. This results in $72,000\frac{samples}{hour}$ or $1,728,000\frac{samples}{day}$. If we want the calculations not to take longer than 7 days we can approximately evaluate a maximum of

$$\#_{max} = 1.2 \cdot 10^7 \ samples. \quad (9.22)$$

Sample State Space If we now use the more comprehensive system description from (9.2), we already get 8 state dimensions 3 reference dimensions, fully neglecting the possibility of having additional obstacle positions. With the maximum number of samples from (9.22) it is clear that in any case only few samples can be gridded per dimension. E.g. if we look at the simplified system description from (9.1) and we want to sample the 3D reference we get a sampling space of 7 dimensions (4 state and 3 output). This leads to the following amount of samples for each dimension:

$$\#_{dim1} = \left(1.2 \cdot 10^7\right)^{1/7} = 10.26\frac{\text{samples}}{\text{state dimension}}. \quad (9.23)$$

For the more comprehensive full formulation this only leads to

$$\#_{dim1} = \left(1.2 \cdot 10^7\right)^{1/11} = 4.4\frac{\text{samples}}{\text{state dimension}} \quad (9.24)$$

samples per dimension. However, as we have shortly explained in Section 3.3.2, neural networks are often still able to learn suitable function mappings.

Sample in Output Space Another approach is to sample in the output space, i.e. we set realistic end-effector positions and then calculate the input for a given reference and state. By doing so, we have only 3 dimensions we are sampling over. In principle this leaves us space to get

$$\#_{dim2} = (1.2 \cdot 10^7)^{1/3} = 228.9\frac{\text{samples}}{\text{output dimension}} \quad (9.25)$$

samples for each of the six dimensions. in practice we would implement this by simulating realistic trajectories. Our hope is then, that we cover most of the relevant state space areas for being able to learn a working policy. This is similar to the work in [28], where the authors also sampled full trajectories for learning an approximation.

Sampling

For the sampling, we first start with simplified systems to get a feeling about how well the network is able to approximate the implicit MPC policy function. We started with a 2D-2D configuration, i.e. only enabling the first two joints while providing as a two dimensional reference lying in a plane in front of the robot. After we found out that we are able to properly learn an approximation of the RMPC control policy we increased the dimensions. Most of the sampling rounds we started were 4D-3D, i.e. all 4 joints and a 3 dimensional output reference for the simplified formulation in (9.1) without any obstacles or for the full formulation 9.2 without any obstacles.

Random Sampling On the one hand, we chose to randomly sample the possible dimensions. We had two main reasons in mind:

1. By sampling it randomly, the NN has at least a rough idea of how to approximate each region. Since in our validation a sampled trajectory counts as violated as soon as on AMPC step along this trajectory does not guarantee stability we especially strongly interested in avoiding outliers.
2. We chose random sampling over griding, since this easily allows the addition of further points afterwards. For griding, introducing more points would not be trivial and you need to wait every time until the whole space is sampled. Otherwise this would lead to an imbalanced sample point distribution.

Sampling Trajectories When trying to fit the network to the randomly sampled policy points from the last paragraph, we encountered some difficulties (more information in Section 9.3.3). Therefore, we decided to additionally sample random trajectories, i.e. to repeatedly choose a random starting point and to sample the subsequent trajectory until steady state is reached. This has the big advantage that our samples better represent the robot use case and therefore lead to a smaller approximation error. By doing so, it is possible to reach better performance and to simplify the validation.

Network Architecture

For the network architecture we only try standard fully connected neural networks. We vary them a lot with respect to size, deepness, the loss function, the training procedure and the batch size. The following plots are all taken with respect to the training of the 4-dimensional simplified formulation.

Configuration For the activation functions within the network we choose ReLu activations. Only in the last layer, as typical for regression problems, we choose a linear activation. As an optimizer we use Adam [29], as most people are doing at the moment. Our error function is a mean squared error (MSE).

Network Size For the performance in general it seems that a specific network size is required. However, after a specific epoch (approximately epoch 11 for this example) the performance improvement saturates. This can be seen in Figure 9.7 where we show the training result of different network configurations from 157 hidden units ($5,760$ trainable parameters) through to 2700 hidden units ($1,103,804$ trainable parameters). It is clear that bigger network lead to better performance until a specific point of stagnation. All networks shown in this plot have between 4 and 8 hidden layers.

Depth of the Networks Even though we reach nice convergence and proper results, we are not able to get the training error fully down to 0. This is also not necessarily needed since we only need to get good enough results such that our assumptions from the RMPC design are satisfied. Still, we try to further decrease the validation loss by choosing even deeper networks. Deep networks

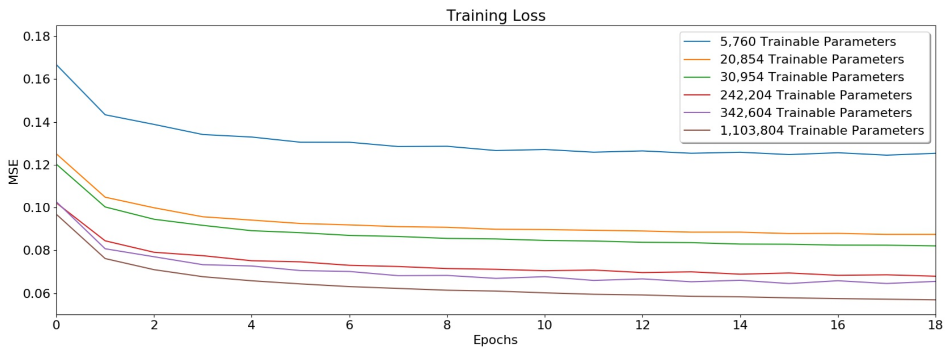

Figure 9.7: Training loss for different network configurations of different size. The bigger the network, the lower the loss. This training was done on the simplified 4-dimensional system without any prestabilization, i.e. the overall values the network should learn have moderate values in magnitude (between -2.3 and 2.3)

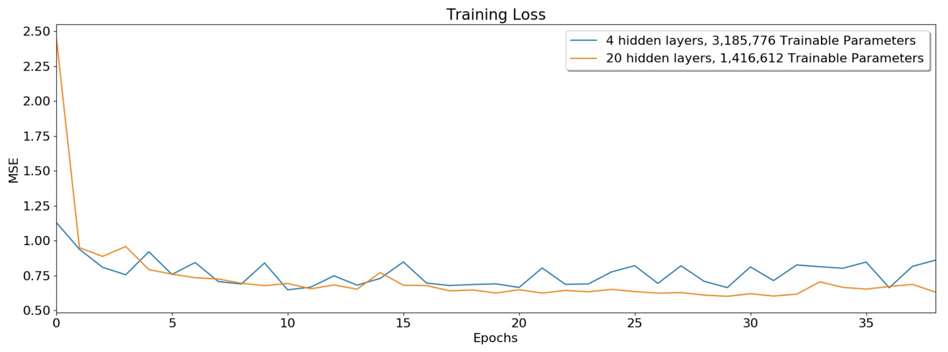

Figure 9.8: Training loss for two networks with very different depth. The deeper network converges slower but reaches about the same performance. In this case, again the learning for the simplified 4-dimensional system is shown. This time, we learn the full output, including the prestabilization, leading to larger signals, which explains the higher loss compared to Figure 9.7.

usually have higher potential expressiveness but take longer to train. As it can be seen in Figure 9.8, their learning curve looks typical for training deep networks; slower training but good convergence. For this specific example they are not able to achieve significant higher performance than shorter networks with similar number of hidden neurons.

Overfitting In general, we do not encounter big problems regarding overfitting. An exemplary comparison of the training and validation set can be seen in Figure 9.9.

Regularization Regularization helps to keep the size of the weights smaller, compared to the case without regularization. Since overfitting is not a big problem in our case, there is also no real need for regularization. Anyhow, we tried it but only encountered a small decrease in performance.

Network Training

The network training turns out to be quite important. As we use the prestabilized dynamics, our system input to be learned becomes the following:

$$u_{sys}(\tau|t) = v_{RMPC} + K_\delta x(\tau|t),\ \forall \tau \in [0, T). \tag{9.26}$$

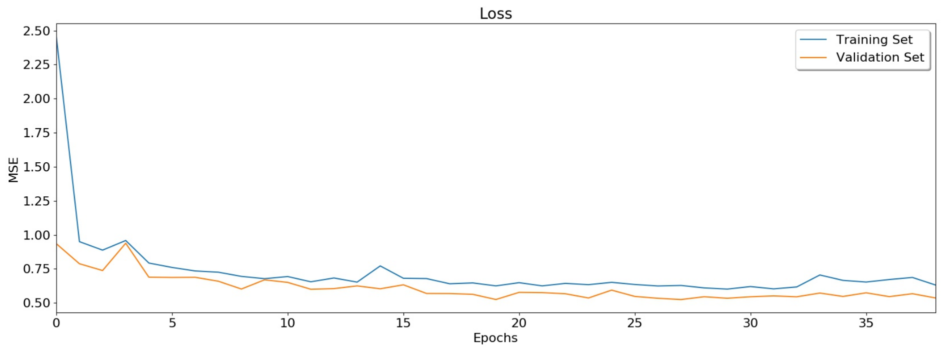

Figure 9.9: Visualization of the performance on the training and validation set. We do not face big problems problems in terms of overfitting for this learning problem. The performance on the whole validation set is calculated after the epoch, while the performance on the training set is the average of the error during the training interval (one epoch). This explains why the error of the validation set is sometimes smaller, compared to the training set error.

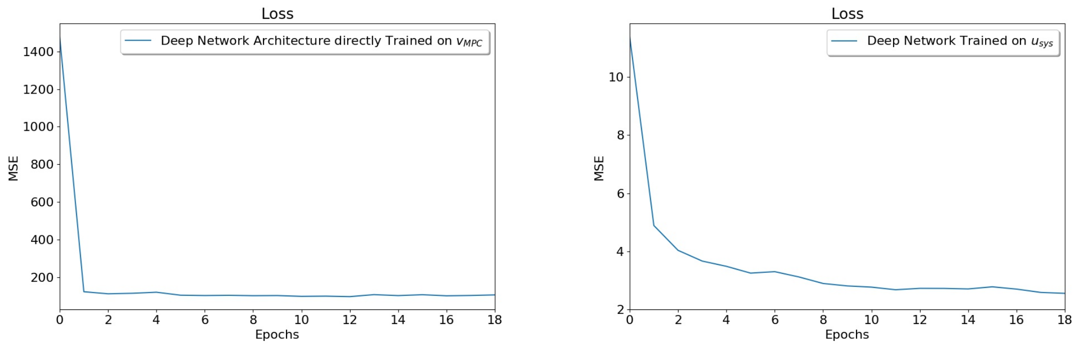

(a) Value of the loss function on the training set when directly learning v_{MPC}

(b) Value of the loss function on the training set when learning u_{sys}.

Figure 9.10

Since we impose limits on u_{sys}, this also means that the absolute values of the entries of v_{RMPC} can become relatively large (i.e. values in the scale of 100, 200). This is particularly problematic for a strong prestabilization we impose in order to achieve fast operation.

Naively using v_{RMPC} for the training often produces decent results but still retains a big MSE error, since the overall output can be increased by several magnitudes. We know that the values of v_{RMPC} need to include an offset to compensate for $K_\delta x(0|t)$ at the beginning of the interval. This term $K_\delta x(0|t)$ keeps $u_{sys}(0|t)$ and $u_{sys}(h|t)$ within the bounds. We can equalize for this RMPC internal compensation by simply adding $K_\delta x(0|t)$ to v_{RMPC}, which is equivalent to directly learning $u_{sys}(0|t)$ (see (9.26)).

The big advantage of this is that we enable the network to get a better precision with respect to the actual unknown core of the approximated policy. The comparison of the error of the two plots can be seen in Figure 9.10. As a consequence, in the online implementation we then need to subtract $K_\delta x(0|t)$ to get v_{RMPC}.

9.2.4 Validation

For the validation we use the results from Section 5.4. For this thesis we do the validation in simulation but also considering the model mismatch, the delay of the controller as well as additional errors, e.g. induced by the integrators. In the next section (9.3) we will show our approach to find AMPCs for the simplified formulation (9.1) as well as for the full formulation (9.2).

Sampling Trajectories

The validation in simulation is done as following: We use the feedback gain K_δ to steer the system to a random state; the starting point of the trajectory. When we are approximately in a steady state, we start the trajectory control trying to reach a random output set point. As soon as we reached the state well enough, we sample the next trajectory and so on.

Criterion

The validation is done according to Section 5.3.2, in particular using the indicator function of (5.19). In our validation procedure we need the different trajectories to be i.i.d.. Since the resulting trajectory is deterministic with respect to the start state of the trajectory and the desired end-effector position, also the trajectories are i.i.d. for i.i.d. sampled start points and desired references.

In our specific case, we not only have the error due to the erroneous approximation of the neural network as in [19], but also additional errors such as the model mismatch. We have two possible ways of how to deal with this.

Full Validation along Trajectories This formulation is most straight forward. We sample our trajectories in deterministic simulation as described before and then validate the following criterion:

$$|f_w(x, \pi_{approx}, d) - f(x, \pi_{MPC})|_{P_\delta} = |d_w|_{P_\delta} \leq \bar{w}, \; \forall x \in X_i. \tag{9.27}$$

Bound Model Mismatch For the other formulation we need the following assumption.

Assumption 9.2. *For the ideal input π_{MPC}, the disturbance caused by model mismatch, time delay and integrator errors, are bounded according to the following condition:*

$$|f_w(x, \pi_{MPC}, d) - f(x, \pi_{MPC})|_{P_\delta} = |d_{w,model}|_{P_\delta} \leq \bar{w}_{model} \; \forall x, \; \textit{with } \pi_{MPC} = u^*(0|t). \tag{9.28}$$

We can now sample the trajectory in the same way as described before. However, at every time step we are not comparing the expected following state $x^+ = f(x, \pi_{MPC})$ with the observed system state $x_w^+ = f_w(x, \pi_{approx}, d)$, but instead with the expected state when applying the approximated input $x_{w,approx}^+ = f(x, \pi_{approx})$ to the nominal system.

Theorem 9.1. *Assume we have the admissible bound $\bar{w}_{model}$ for our RMPC controller error. If*

$$|f(x, \pi_{approx}) - f(x, \pi_{MPC})|_{P_\delta} \leq \bar{w}_{approx} = \bar{w} - \bar{w}_{model}, \tag{9.29}$$

with $\bar{w}$ from our RMPC design and $\bar{w}_{model}$ from Assumption 9.2 holds, then the guarantees of our underlying RMPC design also hold for the deployed AMPC.

Proof.

$$|f_w(x, \pi_{approx}, d) - f(x, \pi_{MPC})|_{P_\delta} \tag{9.30}$$
$$= |f_w(x, \pi_{approx}, d) - f(x, \pi_{approx}) + f(x, \pi_{approx}) - f(x, \pi_{MPC})|_{P_\delta} \tag{9.31}$$
$$\overset{\text{Triang. ineq.}}{\leq} |f_w(x, \pi_{approx}, d) - f(x, \pi_{approx})|_{P_\delta} + |f(x, \pi_{approx}) - f(x, \pi_{MPC})|_{P_\delta} \tag{9.32}$$
$$\overset{Ass.\ 9.2}{\leq} \bar{w}_{model} + \bar{w}_{approx} \overset{(9.29)}{=} \bar{w}. \tag{9.33}$$

And therefore according to our RMPC design, we know that the requirements are satisfied. □

9.2.5 Implementation

In the beginning we planned to use ACADO for the solving of our RMPC problem. It has several advantages such as faster computations and performance functionalities such as the real time iteration (see Section 6.2.1 for more information). Since our optimization problem is relatively complex with many additional non-standard decision variables and the nonlinear and non-quadratic output function, we encountered problems. As a results, we decided to use the CasADi C++ API for our experiments.

For the RMPC implementation, being at time step k, we always predict the state at step k+1 and solve the RMPC problem for this predicted step. In the next interval this input is applied. For the AMPC implementation, we compute the input at the beginning of the interval (based on the current state) and directly apply it during this interval. This is reasonable since the evaluation of the AMPC takes less than $1ms$.

9.3 Results

We started our robot experiments with the state dynamics formulation in (9.1) in the hope that Assumption 9.1 is fulfilled. We used this approach to set up our pipeline and to test it in simulation as well as on the real robot. We observed a computation time of approximately $250ms$ and hence, decided to choose a sampling time of $400ms$. By making the code more efficient but at the same time introducing more complex functionalities, we decided to keep this sampling time for the RMPC control for all experiments. For the AMPC approach, we use the simplified formulation (9.1) due to a smaller number of dimensions, i.e. easier training. Nevertheless, we also implement an AMPC version based on the full description (9.2).

In the following, we will only explain the final version of the RMPC controller in more detail which is based on the full 8 dimensional state description (9.2). Additionally we will show results for the AMPC approaches based on both formulations.

9.3.1 RMPC Control of the Apollo Robot

One of the main goals of this Master Thesis is to show a well working RMPC-based control scheme for Apollo robot.

WorkFlow

Our workflow for deploying our approach on the robot is structured in an iterative manner, i.e. we start by controlling the joint angels without considering the position of the robotic hand and then go to more complicated use cases. In terms of simulation, we start based on very simple integrator simulations. For an example of the simplified formulation, refer to Figure 9.11. In a next step, we integrate the output set point tracking herein, before moving to the more advanced simulation in SL (e.g. also including inertias etc.), see Figure 9.12. Moving to SL is particularly difficult, since our software framework needs to meet the standards regarding command communication and real time behavior.

Before actually moving to a robust formulation, also the code for calculating the offline parameters needs to be developed (compare Section 9.2.2). From a theoretical perspective, there are also some challenges such as the nonlinear output constraints and the RPI terminal set for non static set points. During the project, we were also considering to integrate robust collision avoidance, however, in the end we kept the formulation as described in Section 9.2.2 for all experiments.

Final Result

To make the final RMPC controller work for our use case on Apollo robot involves most of the steps described in this thesis, especially in Chapter 4 and in this chapter. The result is a working framework which controls the robot in a dynamic way, being able to robustly satisfy all constraints in state, input and output, even allowing the arm to avoid obstacles. The framework is written in

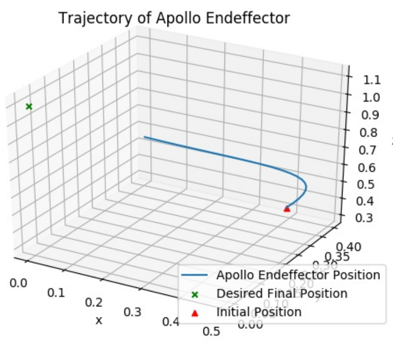

(a) Simulation of MPC for angle set point tracking with $T = 20$, $\Delta t = 0.5$ and $u_{max} = 0.05$. The horizon is not long enough to reach the desired position.

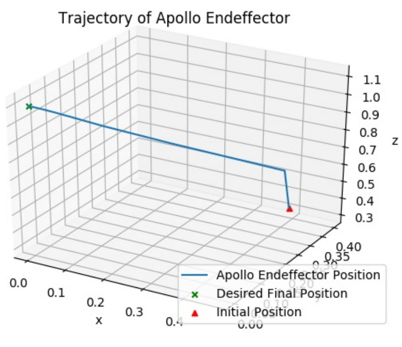

(b) Simulation of MPC for angle set point tracking with $T = 20$, $\Delta t = 0.5$ and $u_{max} = 1$. In this case the horizon is long enough.

Figure 9.11

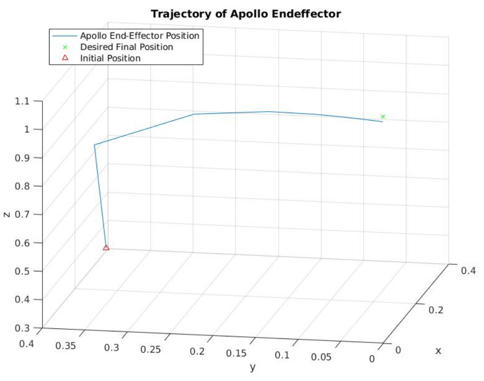

(a) Real set point tracking to reach the endeffector position $[0, 0, 11/10]^T$. $T = 10$, $\Delta t = 0.5$.

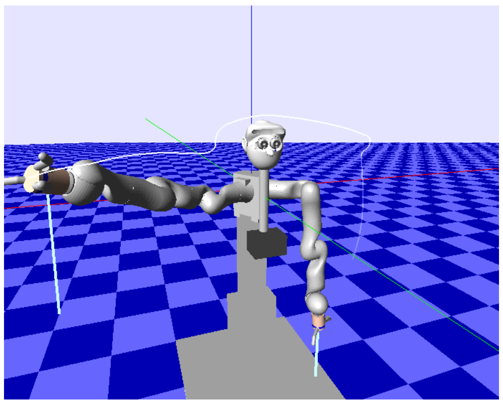

(b) Simulation in SL. The white lines depicts the trajectory of the robotic arm in the last few seconds.

Figure 9.12

a modular way, making it easy to also include further constraints, consider multiple obstacles or to aim for even faster movements by further decreasing the sampling time. In terms of timing we certainly admit for improvement.

The final results can be observed online[1].

9.3.2 AMPC Control of the Simplified Formulation

Workflow

In the beginning of this work we were skeptical regarding the curse of dimensionality (compare Section 9.2.3). This is the reason why we additionally also model the system very simplistic, only containing a 4 dimensional state vector (9.1).

During the development of the RMPC controller (we did it for the simplified as well as for the full formulation in parallel) this formulation turned out to work in practice. Therefore we also train an AMPC controller from this simplified description. Since our goal is to show that the

[1]`https://youtu.be/c5EekdSl9To`

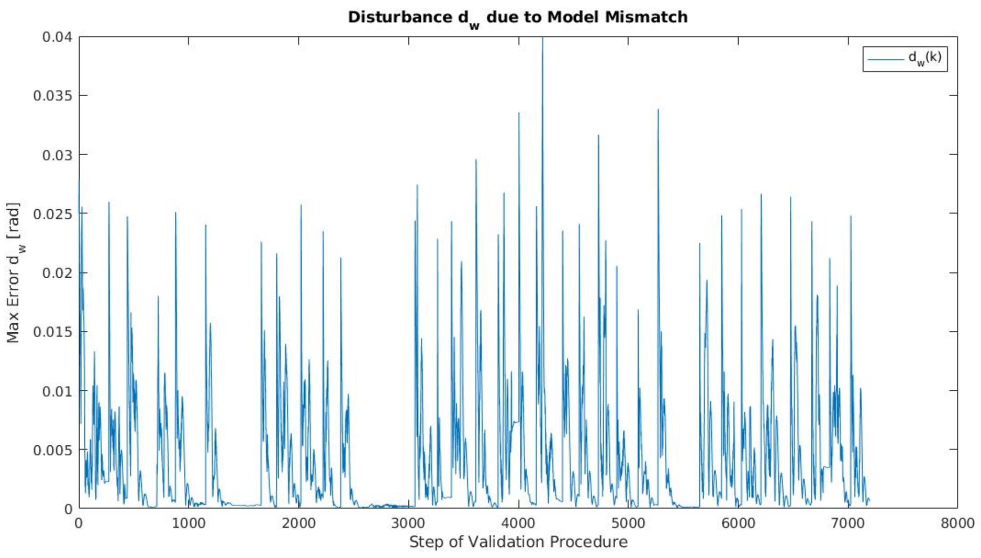

Figure 9.13: Disturbance d_w due to model mismatch for the choice of $10ms$ as sampling time. Unfortunately, the disturbances are too big to give any useful guarantees.

AMPC formulation can bring a huge gain in performance, we directly move to the faster variant: prestabilization and a sampling rate of just $0.01s$.

As described before, we perform the offline calculations under the assumption of having continuous time prestabilizing feedback. Therefore, also the allowed threshold on the disturbance is in continuous time. As described in Section 9.2.2 we think that $d_{w,c} = 0.25$ is a good measure of the disturbance. At the same time we easily find a corresponding RMPC design for this choice.

For another examples, we chose $d_{w,c} = 1.3$. Our goal for this design simply is to make the underlying RMPC controller as robust as possible. For $\rho_c = 100$, this $d_{w,c}$ marks the maximum feasible value.

Validation

Special about the AMPC is that it is the first time we see the system operating at this speed, since we were not able to simulate it realistically using the original RMPC controller, which is too slow.

When investigating the AMPC controller trained with $d_{w,c} = 0.25$, the error turns out to be bigger than expected. The main difficulty lies in the fact, that we are not able to test the error in advance without training the NN as a result of the lacking speed of the RMPC computations.

In Figure 9.13 it is possible to see the overall disturbance over time, occuring from the model mismatch only (under the assumption that our AMPC control command is perfect). This figure depicts the ∞-norm of the disturbance during the validation process. The maximum errors are approximately 0.04. For comparison: $d_{w,c} = 0.25$, approximately means in this case $d_w = 0.0025$, even though we are not looking for the infinity norm in the validation but rather on the incremental Lyapunov function (Section 5.4).

This is also the reason for the second design round including stronger prestabilization and a much higher admissible value for the disturbance, i.e. $d_{w,c} = 1.3$.

Since we are validating trajectories, we would need a percentage close to zero. Also for the redesigned AMPC controller the results in this case are not good enough; the model error is just too big. One explanation for this is that Assumption 9.1 is not valid anymore for such short sampling intervals.

This is also the reason why we decide to use the full formulation for designing the AMPC controller in the next section (9.3.3).

9.3.3 AMPC Control of the Full Formulation

Workflow

After the two detailed iteration steps for the simplified formulation described in the last section, we give it another try with the full eight dimensional formulation. Here, we expect to be able to bring down the model mismatch significantly, since the model is physically tractable and therefore the CT disturbance should be more or less invariant to the sampling time.

We design the controller for disturbances of $d_{w,c} = 1.0$ together with a contraction rate of $\rho_c = 10$. Furthermore, we design this controller for a sampling time of $T = 40ms$. This means exactly a speed-up by a factor of 10 compared to the RMPC-based control.

Validation

As introduced in Section 5.4, for the validation we need to sample i.i.d. trajectories. However, in this framework it is not as simple as for the other case, since also the velocity is included in our starting point of the coordinate system. In our case, we are setting the velocity in the starting point to zero and are therefore only able to give statistical guarantees for full trajectories, starting with zero velocity.

Since we do not do any state predictions for the usage of the AMPC controller (instead, we really calculate the input in the current interval based on the real system state), the validation even incorporates the non zero computational delay of the network, which is even neglected for most practical RMPC computations. Thanks to the fact that the evaluation takes less than $1ms$, the influence of this delay on the whole interval of $40ms$ is rather small.

The validation procedure itself is more promising for this setting, since the worst case model mismatch is much smaller. Nevertheless, performing the validation is still not simple. This occurs mainly due to two reasons:

1. The whole problem is now higher dimensional, since we have now a 8 dimensional formulation of the state vector compared to the 4 dimensional on in the simplified case. This leads to the fact that our sampled data regarding the sample dimensions is even more sparse than in the simplified formulation.

2. Since we operate at high sampling rates (i.e. either 10ms or 40ms) the underlying controller is able to control the system in a much more dynamic way. Looking at the data, it seems that the controller is acting like a *bang-bang* kind of controller when the corresponding position in the task space of the state is far away from the reference set point. Since we can operate at high speeds, this distance is much smaller than for the case of a sampling time of $400ms$, hence also the proportion of the controller acting at its input limits is much higher. This is confirmed by the experiments, which show that the NN AMPC controller performs well in the beginning of each trajectory and poorly towards the end. We explain this by the fact that the NN has mainly seen states and references far away from each other and therefore, inputs lying at their constraints, since we sampled randomly in state and reference.

   In this case it might be helpful to use the classification approach again as introduced in Chapter 7 for the chemical stirred-tank reactor.

Unfortunately we are also not able to provide statistical guarantees for this setting, at this point.

Sampling Trajectories For sampling data points, we decide to use a combination of randomly sampled data points and sampling trajectories. We sample approximately $45,000,000$ randomly chosen independent points and additional $45,000,000$ points by sampling over trajectories. For the final phase of the training, we decide to use 45 million more points, by sampling over trajectories, resulting in overall approx. 135 million points. In total, this takes 30 days of sampling on 2 computers. The points sampled over trajectories turn out to be practically more relevant.

Training Also the training turns out to be more difficult than expected. One reason is the previously mentioned curse of dimensionality. As you can see in Table 9.3, we do not manage to get down the mean squared error (MSE) below 0.7 for the validation set, even though we apply the technique of not learning v_{MPC} directly, but rather $u_{sys}(0|t)$. Since we are not really interested in the loss of our trained network but more in the worst case scenarios, we also try to train the network using different loss functions, e.g. the mean-quartic-error (MQE). Unfortunately this also does not help.

We observe that training in bigger batches can lead to significantly lower losses on the training set, since we are doing the gradient descent in more relevant directions. Unfortunately, the network is not able to generalize this decrease in the error also to the validation set. Therefore, using too big batches leads to overfitting. The full overview of our attempts can be seen in Table 9.3.

Final Result

Results for our AMPC controller can be observed online[2].

[2] `https://youtu.be/c5EekdSl9To`

Table 9.3: Overview of all of our training attempts. It can be seen that deeper networks usually lead to better performance, but take longer to train, compare [45]. Furthermore, using bigger batches increases the speed of convergence on the training set but not necessarily improves performance on the validation set. Using another loss than the very typical mean squared error (MSE) did not turn out to help in increasing performance of the network.

Dataset	Training Procedure	Epochs (+ means continued training)	Batch Size	MSE / MQE Training Set	MSE / MQE Validation Set
Small dataset (90 mio. datapoints)	Shallow Network (≈ 3.5 mio. trainable parameters)	40	512	1.5129	1.7843
”	Shallow Network	+40	512	1.4087	1.6167
”	Shallow Network	+80	512	1.4639	1.9086
”	Deep Network (< 2 mio trainable parameters)	40	512	0.7727	1.0025
”	Deep Network	+40	512	0.6672	0.9649
”	Deep Network	+80	512	0.6585	0.9279
”	Deep Network, bigger layers (≈ 4.7 mio. trainable parameters)	40	512	0.6340	0.9736
”	Deep Network, bigger layers	+40	512	0.5303	0.9025
”	Deep Network, bigger layers	+80	512	0.5333	0.7232
”	Deep Network, bigger layers, MQE loss	40	512	34.55 / 523.0649	34.56 / 532.24
”	Deep Network, bigger layers, regularized	20	512	1.3284	1.6915
”	Deep Network, even bigger layers (≈ 6 mio. trainable parameters)	40	512	0.7321	1.1084
”	Even Deeper Network	14	512	34.5533	34.5676
”	Deep Network (based on Deep Network, bigger layers, after 80 (+40) epochs)	+80	2048	0.4088	0.7467
”	Deep Network (based on Deep Network, bigger layers, after 80 (+40) epochs)	+80	16384	0.3638	0.8157
”	Deep Network (based on Deep Network, bigger layers, after 80 (+40) epochs)	+80	65536	0.3532	1.2388
”	Deep Network (based on Deep Network, bigger layers after 80 (+40) epochs), only updated if validation performance improved	+80	16384	0.3592	1.0641
”	Deep Network (based on Deep Network, bigger layers after 80 (+40) epochs), MQE loss from this point	+80	512	diverged	diverged
Big Dataset (135 mio. datapoints))	Deep Network (based on Deep Network, bigger layers), regularized after 80 (+40) epochs	+80	16384	0.5415	1.0456
”	Deep Network, bigger layers	80	2048	0.3638	0.8157

Chapter 10

Conclusion

10.1 Summary

In this work we present a novel way to design a RMPC as well as an AMPC for the control of a real world robotic platform. We integrate several important results from literature which help us to achieve the desired behavior. We also break down the RMPC scheme from [36] to the for us necessary components. Additionally, we extend the scheme by introducing terminal ingredients for dynamic set point tracking. We also guide the reader through the complex concepts of this approach and show how the derivations and computations are done for a practical example.

We verify the importance of the concept of the AMPC with guarantees introduced by Hertneck et al. [19] and enhance it by using a better validation procedure to be in a position for providing statistical guarantees more easily. We check our framework by simulating the same example as given in the corresponding work [19]. For this we introduce more advanced concepts for sampling and doing the regression, ending up with a huge decrease in offline computation time.

Furthermore, we implement the RMPC scheme by Koehler et al. [36] for the very first time on a complex physical system. We show good performance on Apollo robot while being able to guarantee robust constraint satisfaction, including nonlinear output constraints for obstacle avoidance. The framework is designed in a very modular way, making it easy to integrate and include additional constraints, objectives or concepts. The main drawback of this approach is the speed of the evaluation. Nevertheless, including the full robot control in one optimization problem (i.e. also the motion planning) while guaranteeing robust constraint satisfaction is superior to other concepts in many respects. Usually, multiple different software components are needed and safety can not be guaranteed in the way we are able to do this. The lack in computational simplicity motivates the usage of our AMPC approach.

One drawback of approximating the control policy is the reduction in flexibility. E.g. introducing a second or third obstacle in our RMPC formulation can be achieved by adding additional constraints to the optimization. In contrast, the AMPC controller needs to be provided with new training data and needs to be retrained after every minor modification. This is the same drawback as for general explicit MPC.

We achieve an order-of-magnitude performance improvement by learning an AMPC controller from two formulations, a simplified one describing the states by the joint angles only and a more comprehensive formulation also including the velocities and using the accelerations as input. For the first formulation we are not able to give useful guarantees on full trajectories due to the large model mismatch. The full formulation leads to a lower model mismatch and hence, to a more promising starting point for the AMPC. However, at the time of submitting this thesis we do not provide a sufficiently precise NN approximation, mainly due to the curse of dimensionality. However, we still see big opportunities for future work, by using more tailored learning procedures. The evaluation of the neural network takes less than $1ms$ while solving the RMPC problem takes $200 - 300ms$. For the sampling we are able to highly parallelize this evaluation (i.e. sampling multiple points at a time), however for the practical implementation we do not find a simple way to accelerate this process. Therefore our design easily allows a speed up by a factor of 300 in theory. For our demonstration we choose a sampling time of $10ms$ for the simplified case, and a sampling time of $40ms$ for the more comprehensive one. Especially for well defined problems without too many unknowns, e.g. for flight control of quadrotors, this approach has a lot of potential.

10.2 Future Work

The extensions and implementations of the RMPC scheme of Koehler et al. [36] allow us to do full robot control while guaranteeing stability and robust constraint satisfaction on Apollo Robot. Additionally, this master thesis significantly advances performance and functionality of the underlying AMPC approach compared to the start of the project [19]. At the same time, we identify promising aspects for further improvements and interesting questions for future work.

To make the practical implementation even more meaningful and relevant for the robotics community, an extension to the real world robot dynamics instead of the kinematic description would be worthwhile. Moreover, including exact collision avoidance instead of our approximated description of the obstacles based on differentiable functions, would reduce conservatism and as a result improve the performance. Another potential extension would be to introduce an admissible non-constant model mismatch d_w for the RMPC design, e.g. $d_w(\dot{\Theta})$. We expect the consequent RMPC design to be significantly less conservative. Using parametrized matrices K_δ, P_δ could reduce the conservatism even further.

Also very interesting would be to directly tackle the expensive computational demands of the RMPC optimization problem even further. Potential solutions could be to formulate the problem in a more efficient way or to use real-time iteration approaches (see A.3.2). This could result in a higher practical relevance of the RMPC approach, reducing the need of our presented approximation and hence, to be more flexible.

Furthermore, we see potential in further improving the used learning techniques to even better overcome the problem of the high dimensionality. By further removing outliers in the control signal, the validation would be directly applicable.

Really interesting but challenging would also be to find an approximation which generalizes better. One potential outcome could then be that the network is able to handle different numbers of obstacles without having observed similar situations during training before.

Additionally, it would be interesting to investigate the learning part for the high dimensional robotic use case even more. An example would be to find out whether a classification approach as introduced in 7.2.5 would achieve better performance over the standard regression approach.

10.2.1 Relation to Guided Policy Search

As part of this master thesis we also identified the connection of guided policy search (GPS) [39, 38, 37, 26] to our deployed approach. Especially one paper attracted our attention [73], since it explains an approach of doing MPC guided policy search.

Particularly useful for understanding the main idea of GPS is the work in [51]. During the emergence of this thesis, we talked several times about GPS and tried to understand in more detail the differences of GPS compared to our approach and how we could potentially try to introduce some kind of guarantees to the GPS algorithm. A promising direction for future work is to compare the generalization properties of GPS to the ones from our work. Especially interesting would be to investigate, in which situations the improvement of the reference policy in GPS might be helpful. Additionally, the surrogate cost needs to be adjusted online in GPS to ensure convergence. This is something we don't need in our formulation, since it is already given as a result of our statistical guarantees. For cases such as our real world use case, advantages of GPS are not obvious and are worth exploring in future work.

For future work, combining the advantages of both approaches (for the case of MPC guided policy search [51]) might be really promising.

Appendix A

User Manual

A.1 Introduction

This is the User Manual which comes aside with this Master Thesis. It should help to understand the important steps to reproduce the results presented in this thesis. This includes an overview of the existing code and its functionalities, the installation of the needed frameworks as well as the requirements for deploying the corresponding code on the robot.

In this user manual not all intermediate implementations are described but only those ones which can be useful to the reader. The goal in every single step during the development was to keep the software as modular as possible, i.e. uncoupling the theoretical concepts from the used frameworks, s.t. a change to another framework would be as easy as possible.

A.2 Overview

Most of the code was written in C++ due to real time or at least time-critical demands. However, also Python and MATLAB code is used for training the ML networks, plotting results and performing offline calculations. All programming languages are separated and can be obtained from the name of the corresponding Git repository.

A.2.1 Git Repositories

All repositories are given on the git-amd server and can be accessed through gitlab[1].

The used Github repositories are the following (order depending on the point in time of the core implementation):

- ampc_task.
- cstr_ampc_cpp,
- apollo_ampc_cpp,
- apollo_sampling_cpp,
- ampc_python,
- ampc_matlab.

We will go into more detail about all of them in Section A.4.

[1] `https://git-amd.tuebingen.mpg.de/`

A.3 Frameworks

As described earlier in Chapter 1, the main part of this Master Thesis is to develop and implement an RMPC/AMPC control approach for Apollo robot (see Fig. 1.1) and to deploy it in practice. Due to the time critical demands of the robot control - all hardware related command signals need to be updated at a frequency of $1kHz$ - the whole robotic control framework (Sec. 6.4) is implemented in *real-time C++*. To be compatible with this framework and to fulfill the demanding requirements, we decided in the very beginning to implement the code which will actually run on the robot in *C++*. Some other offline calculations, e.g. for training the network, validating theoretical ideas or designing the RMPC controllers are implemented in *Python* and *MATLAB*.

A.3.1 Robotic Control Framework

As described earlier in Section 6.4, we use the Simulation Laboratory framework [58] for passing the signals to the robot. Information about the functioning of SL can be found in the official user manual [58]. Using SL is not trivial, since it is not written in the most lucid way. However, with the help of my supervisor Vincent Berenz it was manageable. After having implemented the main code base, it runs fast and reliable. Its biggest advantage is that almost no modifications need to be done when moving from simulation to real robot experiments. Therefore, all interfaces and communication issues can already be checked offline in advance.

Important to notice is that the ROS-Apollo version on the git-amd server only works with Ubuntu 14.04 at the time of this thesis. The more general, catkinized version also runs with Ubuntu 16.04.

We included additional ROS communication, real-time safe threading as well as overwriting configurations files when launching the program for reaching our goals.

Creating your own Task

SL works great as long as you adhere closely to the official guidelines SL provides, i.e. writing the code within the frame of a so called SL task. How to create such a task is well described in the AMD wiki.

Examples within our Code Base

The best example for how to write your code within SL is the ampc_task package. For more information on this, refer to A.4.1.

A.3.2 MPC Framework 1 - ACADO

For the control tasks in our chemical stirred-tank reactor simulation example, we used the ACADO Toolkit[2]. The manual is given in [22]. This framework is tailored for solving optimal control problems and its usage seems to very intuitive in the beginning, however, as soon as more special demands appeared in my case I also hit on problems. The user manual is not complete and the official support seems to have been stopped in the meanwhile. Nevertheless it's an incredibly fast problem solver which is absolutely sufficient for most standard model predictive control tasks.

Installation

The usage of ACADO is relatively straightforward. All information can be found on the official installation page[3]. The source code can be cloned from GitHub. The way we installed it, was to download this source code, compile it at a specific location, and then install it, i.e. by moving the header files and shared libraries to the correct locations. This can be done as following:

[2]`https://acado.github.io`
[3]`https://acado.github.io/install_linux.html`

```
$ cd /preferred/location
$ git clone https://github.com/acado/acado.git —b stable ACADOtoolkit
$ cd ACADOtoolkit
$ mkdir build
$ cd build
$ make
$ sudo make install
```

Real-Time Iteration (RTI) Scheme

Especially interesting for real world use of complex MPC schemes is the real-time iteration scheme[23, 14, 68]. It uses the fact, that optimal solutions of an MPC control problem are usually continuous, e.g. the solution doesn't change too much between neighboring points and convergence is a lot faster when using neighboring solutions as warmstart for the new solution attempt. We tried it and it's not especially hard to use, however, since we were aiming for truly converged solutions we abandoned this solution procedure.

Examples within our Code Base

Examples can be found in cstr_ampc_cpp, also how to include the code within a catkin project. The RTI scheme is used within cstr_ampc_cpp/RTI whereas the normal ACADO scheme is used within cstr_ampc_cpp/check_condition, cstr_ampc_cpp/simulation and cstr_ampc_cpp/sample_optimal. The ACADO integrator for simulation purposes can be found in cstr_ampc_cpp/simulation.

A.3.3 CasADi

After we encountered too big problems with ACADO, we started to use CasADi [1] not only in MATLAB but also in C++. CasADi[4] is very well documented for MATLAB and Python, however, really poorly for its C++ version. The example code which comes with the software, only shows very simple use cases. It took quite some effort to find efficient ways for implementing our desires. Since all other APIs are also using the C++ backend we knew that our goals must also be implementable in C++, just needed to find out the exact syntax.

Installation

Since all versions of CasADi come with a C++ backend, each of them also delivers all principally needed header files and libraries. Therefore, the easiest way to use CasADi in C++ is to get one of the official releases and then link against the corresponding libraries. In our case, we always used the Python realease by

```
$ pip install casadi
```

However, this only worked in a straight forward manner for us when using Ubuntu 14.04. Nevertheless, since we didn't put much focus on running it for Ubuntu 16.04, we still think that there must be a way. Another possibility is to build CasADi from source, which definitely would have performance advantages. Since, also third party libraries such as iPOPT need to be included as well, we decided not to do it during this project.

Examples within our Code Base

Certainly the most comprehensive example of how to formulate complex MPC problems in C++ CasADi - including constraint tightening, additional decision variables and matrix algebra - can be found in our MPC predictor, which is for example in ampc_task/predictor/src/mpc_predictor_casadi.cc.

[4]https://web.casadi.org

A.3.4 Machine Learning Framework - Tensorflow

Since this project contains a big learning part, a suitable ML framework is needed. The whole framework should be implemented in C++, therefore, desirably also the ML framework should have a C++ API to avoid unnecessary programming language interfaces. We are using NNs for the approximation of our AMPC controller. One of the most powerful and most common frameworks for the usage of NNs is TensorFlow which also provides a C++ API. We decided to use TensorFlow in the beginning. Alternatives would have been PyTorch or Caffe.

In our case we are using TensorFlow 1.13. There are multiple ways of using TensorFlow. In the following we will try to describe the most important findings. Multiple APIs are provided by TensorFlow. The recommended and most comprehensive one is the Python API. Especially for training and creating custom models this is the way to go. For the training we mainly use the KERAS NN library which is part of TensorFlow's core library in the meanwhile and offers a higher-level set of abstractions, which makes it easier to rapidly develop NN-ML models. Despite the skeptical opinion in the web regarding the C++ API, we decided to deploy it for the inference in our own C++ programming framework.

Details

CUDA If one wants to make use of one or multiple GPUs, CUDA needs to be installed on the system. CUDA 10.0 is only supported by new GPUs with driver versions 410.x or higher and only usable with TensorFlow versions newer than 1.13.0. We always used CUDA 9.0 and it fulfilled all our requirements. The official information on how to set up CUDA can be found on the TensorFlow webpage[5]. However, when running Ubuntu 16.04 there is a nice script prepared by Vincent Berenz which was recently published as open source software. Additionally also CUDNN needs to be installed to use TensorFlow with CUDA. There exist two main ways of using TensorFlow.

Prebuilt Version The usual way of using TensorFlow is to have recourse to the prebuilt version available online. For Ubuntu this is usually done by using pip[6]. If the motivation is to use the Python API this is certainly the easiest solution and usually works. However binary files are then not optimized to the computer and can therefore have worse performance compared to the case of building TensorFlow from source. This version also works with the C-API, however, whose usage we would clearly discourage.

Building TensorFlow from Source Building TensorFlow from source[7] is more tedious and takes longer. However, the resulting framework will offer better performance. Additionally and for us even more importantly, this is necessary to use the C++ API. Unusual is the fact that Bazel[8] is required to build TensorFlow. We recommend to install Bazel in the /home-folder since the installation might block a significant amount of disk space. After having compiled the package it is possible to built a .whl package. This can then be installed on the system by using pip resulting in the same behavior as the prebuilt package but with better performance. To be in a position to use the C++ API in a catkin workspace additional steps are required. Then it's possible to create besides the general shared library libtensorflow_framework.so also a shared library called libtensorflow_cc.so to use the C++ API. This step is described in more detail in the next Sec. because it's not explained in the official installation guide. In the catkin workspace, we can then link against this shared libraray and include all needed header files. Strange is that bazel creates some of the headers during compilation, so you will not find all of them in the TensorFlow software package.

[5]`https://www.tensorflow.org/install/gpu`
[6]`https://www.tensorflow.org/install/`
[7]`https://www.tensorflow.org/install/source`
[8]`https://docs.bazel.build/versions/master/install.html`

Installation

Prebuilt Version To install the pip package:

```
$ # Prerequisite: Python development environment
$ sudo apt update
$ sudo apt install python-dev python-pip
$ sudo pip install -U virtualenv  # system-wide install
$ # Install tensorflow (possibly in virtual environment)
$ pip install --upgrade tensorflow
```

Building TensorFlow from Source After having installed Bazel you can compile the TensorFlow source folder.

The important part here is that we build the shared library libtensorflow_cc.so. For this we can manually build the required shared library by using

```
$ bazel build --config=opt --config=cuda //tensorflow:tensorflow_cc # --config=cuda only for gpu
$ # Sometimes the previous doesn't work, then:
$ bazel build --config=opt --config=cuda //tensorflow:libtensorflow_cc.so
```

Additionally it is necessary to include all required headers. For more information on that, have a look at our coded examples.

Debugging While building in bazel the error: `'int'objectattribute'__doc__'isread-only`. Then we need to uninstall enum and install enum34 (`pipinstallenum34`).

Examples within our Code Base

We use TensorFlow almost within all of our repositories. Examples for the training with the Python API can be found in ampc_python/2_apollo/nn/.

On the other side examples for the inference in C++ can be found in ampc_task/predictor/src/ampc_predictor_tf.cc. It is important to note, that before being able to use models trained in KERAS, they need to be frozen. This is for example done in the end of the Python file ampc_python/2_apollo/nn/neural_network_predict_train_multiple.py.

A.4 Developed Software Packages

A.4.1 ampc_task

This is the the package needed for doing the RMPC and/or AMPC control on Apollo robot. As described earlier, SL requires real-time safe C++ code. There are several possibilities for including non real-time safe code - such as CasADi or TensorFlow in our case - in a real-time framework. We decided to do this by spawning real-time safe threads, i.e. provided by Xenomai in our case. Furthermore, we also include non-real-time-safe communication over ROS in our package, again by using suitable threads.

The package file has a configuration file (in ampc_task/config/ampc_config.yaml) where the mode of operation as well as important parameters (e.g. the sampling time) can be set. The big advantage of handing over details about the configuration in this way is, that no recompilation is needed after doing any changes.

Furthermore, we created two suitable starting scripts called ampc.bash and ampc_real_robot.bash which can be found on the AMD server under start_robot/config/. They allow not only to launch all needed packages (such as SL and Vicon), but also to copy our needed configuration files, e.g. for the robot low-level gains, to the correct position.

Details on Implementation

We decided to create an instance of the so called *ComputeControl* class within our SL task. This class contains several variables as members, which can be used to do the actual robot control. We also use these, i.e. the variable v_{MPC} in particular, to pass the calculated inputs of the RMPC and AMPC respectively. The class spawns two real-time threads, of which one of them creates instances of the non-real-time-safe predictors, i.e. *MpcPredictor* and *AMPCPredictor*. During operation these class instances are used to obtain the computed results and update the corresponding member variables of the *ComputeControl* class instance. Additionally, we also include ros communication, generation of trajectories and others within this repository.

An overview about the most important code snippets can be found in the following. The location of the code is given with respect to the repository ampc_task.

cmake Includes FindCASADI.cmake, a file which is needed to find the corresponding CasADi libraries within our operating system. More information on the inclusion of the other packages can be found in the CMakeLists.txt.

config This folder is really important, since it contains the main config file ampc_config.yaml. Here parameters such as the sampling time, the used TensorFlow model or the mode of operation can be defined. Furthermore, the parameters needed for the operation of SL are defined in the corresponding .cf-files. Those ones are copied to the right locations before runtime, when using our provided .bash scripts (see Section A.4.1).

framework In here, the main framework is defined, from initializing the class instance of ComputeControl over spawning the real time threads to calling the input computations.

predictor In the predictor, the two ways of doing the control are defined, i.e. by using the RMPC as well as the AMPC controller. The header file predictor.h defines all information needed for building the interfaces with the underlying classes, while the actual code is given in ampc_predictor_tf.cc for the AMPC and in mpc_predictor_casadi.cc for the RMPC implementation.

ros Within this folder, the communication to ros is defined, i.e. the visualization of our reference and the obstacles as well as the communication to the vicon_bridge, in order to get information of the pose of the objects within the scene. This pose is currently updated with a frequency of 25 Hz, but can easily be changed within the code.

task/src In here, the actual code for the SL task is defined. Since the structure is mainly predefined by SL there was not much room for changes.

trajectories In this folder, code for the generation of the trajectories is given. The trajectories can be used to either sample the state space as realistically as possible or to validate our underlying AMPC controller.

A.4.2 apollo_ampc_cpp

This package covers all of the standard Apollo related code. It was used to build up the framework, to do the first simulations as well as to validate the AMPC controller. It also shows a standard catkin package which includes ACADO, CasADi as well as TensorFlow in C++.

Details on Implementation

src/calc_disturbance This code snippet is used to check whether the assumptions were violated during the sampling of the trajectory. It takes the .csv file as input which is created by the ampc_task during trajectory sampling operation. It then counts for how many trajectories the conditions are violated and shows how big the corresponding error on the input is.

src/plot This is in principle the python matplotlib library for plotting graphs in C++. However, since it was just wrapped to C++, it doesn't support all functionalities and should therefore only be used for the prototyping.

src/simulate This software package was used to check the correct functioning of both the RMPC as well as the AMPC controller.

A.4.3 apollo_sampling_cpp

We used the apollo_sampling_cpp code for sampling of the data points we then used as groundtruth for the training. The code was particularly designed to run fast in a parallel fashion as well as to be reliable. Once, we've run the code for more than 20 days on two computers with all available threads doing computations.

Details on Implementation

src/mpc_predictor_casadi This is again the CasADi RMPC controller as described earlier. It is used to solve the optimization problems for random points or along trajectories, depending on the mode of operation.

src/rmpc_sampling This executable offers the functionality for sampling points. In the beginning of the code you can define whether you want to do it for the 4-dimensional or 8-dimensional case, whether you want to sample randomly or using trajectories and much more.

A.4.4 cstr_ampc_cpp

This repository contains all C++ code we have for the chemical stirred-tank reactor (CSTR). It is used from simulation over sampling to validation.

Details on Implementation

src/sample_optimal This is the code we used for sampling the solution points which we can then use as a groundtruth for the training. This code offers 3 different ways of doing the sampling: uniformly, recursively and randomly. For each of the 3 implementations an executable is computed.

src/check_condition This collection of code is used to do the validation for the CSTR controller. It also provides functionalities such as measuring the duration of a NN iteration and an integrator implementation for integrating the trajectory.

src/simulate This code is used to simulate the CSTR using both, the RMPC as well as the AMPC controller. In the end of this code, the trajectory for both controllers are directly created.

src/RTI This is an code example where we used the real-time iteration (RTI) scheme of ACADO. It worked, however, since we were interested in the fully converged solutions, we didn't use it for the sampling.

A.4.5 ampc_python

This repository contains all of the Python code written for this Master Thesis. It was used for plotting and training the NNs for the chemical stirred-tankr eactor (CSTR) simulation example as well as for the robot experiment.

Details on Implementation

The repository has two larger sub-directories: 1_cstr and 2_apollo.

1_cstr Here the NN model definitions for the classification as well as for the regression are given. Furthermore, also code for training those models is provided. The latest version for the training is given in neural_net_predict_train_2.py. Furthermore, in plotting/ the code for plotting the results of the regression and the classification is given.

2_apollo In this directory we have several sub-folders. 2_apollo/nn defines all of the learning models and trains the networks. 2_apollo/cluster provides scripts which can be used on the MPI Tuebingen cluster. 2_apollo/utility can be used to create a bigger .npy file out of the many .csv files created by the sampling. Last but not least, 2_apollo/plotting provides scripts for plotting the training progress and for plotting a 3 dimensional trajectory.

A.4.6 ampc_matlab

This repository provides the MATLAB code which was implemented during the project. Two main directories are given: apollo/ and cstr/.

cstr/ In cstr/, the code for the offline calculations of our simulation example is provided. This might be of interest, because also calculations for nonlinear system dynamics are covered.

apollo/ In apollo/, code for writing the optimization problem in CasADi, deriving the end-effector position of Apollo, determining the disturbance level as well as for the RMPC offline calculations is given. The most interesting part are probably the offline calculations which we used for all designs for the 4-dimensional as well as the 8-dimensional cases.

A.5 Deploying the Code on Apollo Robot

For running the code on Apollo robot, not many additional steps compared to running it in simulation with SL are needed.

Check Real-Time Requirements

In the beginning it is necessary to run the SL simulation again on the Xenomai machine, to check whether real-time behavior is given. For this the following command can be run:

```
$ watch -n 1 cat /proc/xenomai/stat
```

Changing numbers indicate, that the real-time behavior can not be fulfilled. If real-time behavior is fulfilled, we can go to the next step.

Setup of Apollo Robot

In the next step Apollo robot needs to be set up. This is well explained in the corresponding Wiki entry[9]. In short what needs to be done in the KUKA console is the following:

[9]//atlas.is.localnet/confluence/display/AMDW/How+to+start+Apollo+and+control+it+from+SL

1. Tell the robot arm that it is equipped with a Barrett hand.
2. Perform the gravity compensation by "massaging" the robot arm.
3. Go to position control and select the suitable script.
4. Start SL by using our ampc_real_robot.bash script.

During the experiments it is important to always keep the emergency stop in your hand and to always be aware to press it.

A.6 Direct Re-usability of the Code

We tried to make it as easy as possible to reuse our code afterwards. On the one hand we created a treep project - Treep is the MPI open source package manager - in an early stage of the project. On the other hand, we are currently working on a docker image of our C++ software, to make it possible to run the code despite complex dependencies.

A.6.1 Treep

Treep is an open-source package manager provided by the Max Planck Institute for Intelligent Systems[10]. By providing suitable project files, it helps to install full projects consisting of several repositories. It also directly places the source code at the right position. For the AMD repositories, this file is given on the AMD server in treep_amd_clmc. For our project for the Apollo robot - i.e. consisting of SL, our ampc_task and many more - we also created a corresponding project called AMPC. It includes all necessities for using the Vicon system, SL, as well as our own code. Nice about treep is that it also allows to include full projects within other projects, e.g. in our AMPC project we include the full ROS-Apollo project. The full project can be installed as following:

```
$ pip install treep
$ mkdir apollo_ws
$ cd apollo_ws
$ git clone git@git-amd.tuebingen.mpg.de:amd-clmc/treep_amd_clmc.git
$ treep --clone AMPC
```

Then you are ready to use the provided catkin workspace within ./worksapce.

A.6.2 Docker

Since we are using several different software packages which are not fully straightforward to install, we are currently working on a docker image of our code. This image will contain not only ampc_task but all C++ code which requires packages such as ACADO, CasADi or TensorFlow. The big advantage of docker is, that it allows to build containers which can even emulate whole operation systems with almost no loss in computational speed. The docker image will enable usage of our code in almost every unix-environment. More information on docker can be found online[11].

[10] https://pypi.org/project/treep/
[11] https://www.docker.com

Appendix B

Extrapolation over the Potential for Tackling Climate Change

B.1 Introduction

Temperatures are increasing, melting ice leads to rising sea levels and solutions need to be found to satisfy the growing demand of food and fresh water due to a ever larger world population [57].

These are just a few examples which show the fragility of the situation we are currently living in. I am an engineering student interested in math, machine learning, control theory and robotics. Hence, I also decided to write my master thesis in this sector, trying to contribute to the so called field of *learning control*. However, of course this does not imply that I do not feel responsible to act with respect to the environmental problems we are facing.

This is also the reason why I decided to join the Climate-KIC community as a master label student for the Climate-KIC master label programme back in 2018. Climate-KIC[1] is part of the European Institute of Innovation and Technology (EIT) and was established and funded in 2010. The master label I am pursuing besides my actual studies in *Robotics, Systems and Control* is an opportunity for students to develop skills needed for commercializing their clean-tech driven business ideas. For me, one of the most remarkable parts of this programme was the participation in the 5-weeks summer school in which a business idea was found, developed and pitched in front of a professional and experienced jury.

Since this master thesis is very technical, there is also no direct interconnection to climate change. Nonetheless I would like to use the following sections to present some ideas how the progress in engineering can help us to tackle climate change, food support and other challenges. Furthermore, I would like to put emphasize on the fact that the approaches elaborated in this thesis enable increase in efficiency and lower power consumption compared to previous approaches.

B.2 Gain in Efficiency

Often, one core motivation for introducing new technologies is gain in efficiency. By neglecting the rebound effects [63], this directly leads to lower power consumption and hence, to lower emissions. Estimates for the rebound effect range from 0 to 30%, and among other reasons it is brought about by the following [4]: i) the substitution effect (due to cheaper energy), ii) the income effect (due to more spending) and iii) a macroeconomic rebound effect. The awareness of the rebound effect can strongly influence its impact, and potentially even result in a negative rebound effect [12] - if saved money is invested in ultra low carbon technology. As a result, it is important that people and policy makers are aware of the rebound effect and that it is clearly taken into account. In particular, 'green' investments are viable strategies for mitigating the rebound effect according to [12]. In any case, an increase in efficiency is an effective tool to reduce carbon emissions.

[1]`https://www.climate-kic.org/`

Large progress in the area of machine learning within the last decade enabled its practical employment in many areas. It clearly offers great opportunities in the evaluation of large amounts of data, and a more efficient operation. Concerning this matter, a recent study by leading researchers from different areas provides an overview of the field and proposes potential applications [56]. Among others, climate modeling, solar forecasts, supply chain optimization for reducing waste and intelligent transportation systems are discussed.

In the following I will focus on our approach and give some examples within which areas our approach can be helpful.

B.2.1 Lower Power Consumption through Direct Efficiency Enhancement

For complex control tasks, linear or nonlinear approaches with explicit control laws might not suffice. Especially in situations where performance over a future horizon is of interest (e.g. for an heating system), model predictive control (MPC) approaches are often desirable. Solutions for these approaches are obtained by solving an optimization problem in each time step. This is computationally expensive and hence, contributes to the power consumption of the device. In this work, we introduce an approximation of this controller by fitting a neural network to samples of the optimization problem. In our specific case, we can decrease the evaluation time from 200 ms for the MPC to 1 ms for the neural network. As a result, also the power consumption can be decreased by a large amount, leading to a more efficient operation.

B.2.2 Lower Power Consumption through More Efficient Operation

Besides the direct reduced power consumption through introducing the approximation as introduced in the last subsection, our proposed robust model predictive control approach (RMPC) is a technical contribution in the area of control of complex, uncertain and constrained systems. Therefore, our approach contributes to a more advanced operation of physical systems. In this work, we demonstrated this for the use case of controlling a robotic manipulator in presence of obstacles. MPC approaches find the optimal solution with respect to a given objective. Since the objective can be adapted arbitrary, it is also able to find more efficient solutions for the control input.

In the following I will provide some further examples, where model predictive control approaches can be used to obtain a more efficient operation.

Heating and Cooling System

One tangible example is the control of heating or cooling systems in private homes or office buildings. It is intuitive, that the heating input should not only consider the current state but also the predicted evolution. Further, external influences such as changes in weather or direct solar radiation can be taken into account.

Another idea, which some colleagues and I investigated more during the Climate-KIC summer journey, is to even take the energy market prices into account and to heat when prices are low. This not only saves money for the user, but also significantly helps to consume power when it is available. By doing so, this helps to smooth out peaks and lows in the energy production.

Mobility and Delivery of Goods

The control approach we introduce in this work could in principle be applied to various physical systems. Hence, it could also be deployed for autonomous cars and trucks. This enables more efficient individual transport, the need for fewer cars and automated, highly efficient delivery of goods. To elaborate the latter, imagine the following numeric example: in a middle-sized city, 300 households are living at the main road. To avoid that each of the households separately drives to the supermarket to buy goods twice a week, a few automated trucks drive along the road and deliver ordered goods to the households one after another. By doing so, multiple rides by many different people can be combined into one, and hence, much less overall distance needs to be covered. In terms of personal mobility, individual rides could be combined by picking up several people in an optimal way with autonomous cars/buses.

Power Production/Consumption

The power market is already highly complex, dynamic and uncertain. This will become even more extreme with the enhanced expansion of renewable energies. Complex systems require advanced control techniques. For the electricity net reliable control is of particular interest, in order to avoid blackouts, to be more efficient and to use resources in an optimal way.

B.3 A Tool to Tackle Upcoming Challenges

As seen in the previous section, advanced control and machine learning provide a powerful tool to achieve a gain in efficiency and as a result to reduce carbon emissions. Since temperatures are rising, in any case we are facing additional challenges. In my opinion, advanced technologies can help to better deal with those.

B.3.1 Adaptation

Besides pushing hard to limit the further evolution of climate change as much as we can, also adapting to climate change is an increasingly important topic. In particular elderly people, children and people living in poverty will suffer from increasing temperatures and water scarcity.

Again, better and more efficient cooling systems powered by advanced control can help to facilitate adaptation. Another example is using machine learning to better predict extreme weather events and hence, to help people to better protect oneself.

B.3.2 Agriculture

In the year 2050, 9.7 billion people will live on earth according to predictions of the *United Nations*[2]. Together with increasing temperatures and changing conditions all over the planet, this will contribute to big challenges in terms of food supply. Autonomous farming robots, weather (event) predictions and a better monitoring can help to make better use of the area of arable land and to prevent crop failures. In many of the challenges, advanced control can help to better deal with these incoming challenges.

B.4 Conclusion

In this Appendix B I tried to emphasize my opinion on the significance and potential of novel technologies, in particular advanced control, for tackling and mitigating climate change and for adaptation to climate change. In my opinion, it is important that people start to realize what their developments and creativity could be used for. I tried to underline the potential of the work proposed in this master thesis in this regard. Even though the proposed work seems to have nothing to do with climate change and sustainability at first glance, connections and potential use cases can be discovered.

If we want to bound the negative effects arising from climate change, we should not solely rely on politicians and policy makers. Instead, in order to solve this great human challenge, we need everyone. In particular, we need experts from many different fields, dedicating their life to this challenge.

[2]United Nations World Population Prospects 2019

Bibliography

[1] Joel A E Andersson, Joris Gillis, Greg Horn, James B Rawlings, and Moritz Diehl. CasADi – A software framework for nonlinear optimization and optimal control. *Mathematical Programming Computation*, 11, 2019.

[2] M. H. Arbo, E. I. Grøtli, and J. T. Gravdahl. On model predictive path following and trajectory tracking for industrial robots. In *Proceedings 13th IEEE Conference on Automation Science and Engineering (CASE)*, pages 100–105, Aug 2017.

[3] V. Bargsten, P. Zometa, and R. Findeisen. Modeling, parameter identification and model-based control of a lightweight robotic manipulator. In *Proceedings IEEE International Conference on Control Applications (CCA)*, pages 134–139, Aug 2013.

[4] Peter H.G. Berkhout, Jos C. Muskens, and Jan W. Velthuijsen. Defining the rebound effect. *Energy Policy*, 28(6):425 – 432, 2000.

[5] D. Bertram, J. Kuffner, R. Dillmann, and T. Asfour. An integrated approach to inverse kinematics and path planning for redundant manipulators. In *Proceedings IEEE International Conference on Robotics and Automation.*, 2006.

[6] F. Blanchini. Set invariance in control. *Automatica*, 35(11):1747 – 1767, 1999.

[7] S. Boyd, L. El Ghaoui, E. Feron, and V. Balakrishnan. *Linear Matrix Inequalities in System and Control Theory.* Society for Industrial and Applied Mathematics, 1994.

[8] M. Canale, L. Fagiano, and M. Milanese. Fast nonlinear model predictive control using set membership approximation. *IFAC Proceedings Volumes*, 41(2):12165 – 12170, 2008. 17th IFAC World Congress.

[9] H. Chen and F. Allgoewer. A quasi-infinite horizon nonlinear model predictive control scheme with guaranteed stability. *Automatica*, 34(10):1205 – 1217, 1998.

[10] S. Chen, K. Saulnier, N. Atanasov, D. D. Lee, V. Kumar, G. J. Pappas, and M. Morari. Approximating explicit model predictive control using constrained neural networks. In *Proceedings Annual American Control Conference (ACC)*, pages 1520–1527, June 2018.

[11] L. Chisci, J.A. Rossiter, and G. Zappa. Systems with persistent disturbances: predictive control with restricted constraints. *Automatica*, 37(7):1019 – 1028, 2001.

[12] Angela Druckman, Mona Chitnis, Steve Sorrell, and Tim Jackson. Missing carbon reductions? exploring rebound and backfire effects in uk households. *Energy Policy*, 39(6):3572 – 3581, 2011.

[13] T. Faulwasser, T. Weber, P. Zometa, and R. Findeisen. Implementation of nonlinear model predictive path-following control for an industrial robot. *IEEE Transactions on Control Systems Technology*, 25(4):1505–1511, July 2017.

[14] J. V. Frasch, A. Gray, M. Zanon, H. J. Ferreau, S. Sager, F. Borrelli, and M. Diehl. An auto-generated nonlinear mpc algorithm for real-time obstacle avoidance of ground vehicles. In *Proceedings European Control Conference (ECC)*, pages 4136–4141, July 2013.

[15] C. Gaz, F. Flacco, and A. De Luca. Identifying the dynamic model used by the kuka lwr: A reverse engineering approach. In *Proceedings IEEE International Conference on Robotics and Automation (ICRA)*, pages 1386–1392, May 2014.

[16] Markus Giftthaler, Michael Neunert, Markus Stäuble, and Jonas Buchli. The Control Toolbox - an open-source C++ library for robotics, optimal and model predictive control. In *Proceedings IEEE International Conference on Simulation, Modeling, and Programming for Autonomous Robots (SIMPAR)*, pages 123–129, May 2018.

[17] Ian Goodfellow, Yoshua Bengio, and Aaron Courville. *Deep Learning*. MIT Press, 2016. `http://www.deeplearningbook.org`.

[18] Trevor Hastie, Robert Tibshirani, and Jerome H. Friedman. *The elements of statistical learning: data mining, inference, and prediction, 2nd Edition*. Springer series in statistics. Springer, 2009.

[19] M. Hertneck, J. Koehler, S. Trimpe, and F. Allgoewer. Learning an approximate model predictive controller with guarantees. *IEEE Control Systems Letters*, 2(3):543–548, July 2018.

[20] Wassily Hoeffding. Probability inequalities for sums of bounded random variables. *Journal of the American Statistical Association*, 58(301):13–30, 1963.

[21] B. Houska, H.J. Ferreau, and M. Diehl. ACADO Toolkit – An Open Source Framework for Automatic Control and Dynamic Optimization. *Optimal Control Applications and Methods*, 32(3):298–312, 2011.

[22] B. Houska, H.J. Ferreau, M. Vukov, and R. Quirynen. ACADO Toolkit User's Manual. http://www.acadotoolkit.org, 2009–2013.

[23] Boris Houska, Hans Joachim Ferreau, and Moritz Diehl. An auto-generated real-time iteration algorithm for nonlinear mpc in the microsecond range. *Automatica*, 47:2279–2285, 2011.

[24] Radoslav Ivanov, James Weimer, Rajeev Alur, George J. Pappas, and Insup Lee. Verisig: Verifying safety properties of hybrid systems with neural network controllers. In *Proceedings of the 22nd ACM International Conference on Hybrid Systems: Computation and Control*, HSCC '19, pages 169–178, New York, NY, USA, 2019. ACM.

[25] A. Jubien, M. Gautier, and A. Janot. Dynamic identification of the kuka lwr robot using motor torques and joint torque sensors data. *Proceedings 19th IFAC World Congress*, 2014.

[26] G. Kahn, T. Zhang, S. Levine, and P. Abbeel. Plato: Policy learning using adaptive trajectory optimization. In *IEEE International Conference on Robotics and Automation (ICRA)*, 2017.

[27] R.E. Kalman. Contributions to the theory of optimal control, 1960.

[28] Benjamin Karg and Sergio Lucia. Efficient representation and approximation of model predictive control laws via deep learning, 2018.

[29] Diederik P. Kingma and Jimmy Ba. Adam: A method for stochastic optimization. *CoRR*, abs/1412.6980, 2014.

[30] J. Koehler, E. Andina, R. Soloperto, M. A. Mueller, and F. Allgoewer. Linear robust adaptive model predictive control: Computational complexity and conservatism. In *Proceedings Conference on Decision and Control (CDC)*, 2019.

[31] J. Koehler, M. A. Mueller, and F. Allgoewer. Distributed economic model predictive control under inexact minimization with application to power systems. Master's thesis, University of Stuttgart, 2017.

[32] J. Koehler, M. A. Mueller, and F. Allgoewer. A nonlinear model predictive control framework using reference generic terminal ingredients. Technical report, Institute for Systems Theory and Automatic Control, University of Stuttgart, 2018.

[33] J. Koehler, M. A. Mueller, and F. Allgoewer. A novel constraint tightening approach for nonlinear robust model predictive control. *Proceedings Annual American Control Conference (ACC)*, pages 728–734, 2018.

[34] J. Koehler, M. A. Mueller, and F. Allgoewer. Nonlinear reference tracking: An economic model predictive control perspective. *IEEE Transactions on Automatic Control*, 64(1):254–269, Jan 2019.

[35] J. Koehler, M. A. Mueller, and F. Allgoewer. A nonlinear tracking model predictive control scheme for dynamic target signals. Technical report, Institute for Systems Theory and Automatic Control, University of Stuttgart, 2019.

[36] J. Koehler, R. Soloperto, M. A. Mueller, and F. Allgoewer. A computationally efficient robust model predictive control framework for uncertain nonlinear systems. *submitted to Transaction of Automatic Control*, 2018.

[37] Sergey Levine and Pieter Abbeel. Learning neural network policies with guided policy search under unknown dynamics. In Z. Ghahramani, M. Welling, C. Cortes, N. D. Lawrence, and K. Q. Weinberger, editors, *Advances in Neural Information Processing Systems 27*, pages 1071–1079. Curran Associates, Inc., 2014.

[38] Sergey Levine, Chelsea Finn, Trevor Darrell, and Pieter Abbeel. End-to-end training of deep visuomotor policies. *J. Mach. Learn. Res.*, 17(1):1334–1373, January 2016.

[39] Sergey Levine and Vladlen Koltun. Guided policy search. In *Proceedings of the 30th International Conference on Machine Learning*, ICML'13, pages III–1–III–9. JMLR.org, 2013.

[40] D. Limon, I. Alvarado, T. Alamo, and E.F. Camacho. MPC for tracking piecewise constant references for constrained linear systems. *Automatica*, 44(9):2382 – 2387, 2008.

[41] D. Limon, I. Alvarado, T. Alamo, and E.F. Camacho. Robust tube-based MPC for tracking of constrained linear systems with additive disturbances. *Journal of Process Control*, 20(3):248 – 260, 2010.

[42] D. Limon, J. M. Bravo, T. Alamo, and E. F. Camacho. Robust mpc of constrained nonlinear systems based on interval arithmetic. *IEE Proceedings - Control Theory and Applications*, 152(3):325–332, May 2005.

[43] D. Limon, A. Ferramosca, I. Alvarado, and T. Alamo. Nonlinear MPC for tracking piece-wise constant reference signals. *IEEE Transactions on Automatic Control*, 63(11):3735–3750, Nov 2018.

[44] Robert Lovelett, Felix Dietrich, Seungjoon Lee, and Yannis Kevrekidis. Some manifold learning considerations towards explicit model predictive control. *arXiv preprint arXiv:1812.01173*, 2018.

[45] Sergio Lucia and Benjamin Karg. A deep learning-based approach to robust nonlinear model predictive control. *Proceedings 6th IFAC Conference on Nonlinear Model Predictive Control*, 51(20):511 – 516, 2018.

[46] D. L. Marruedo, T. Alamo, and E. F. Camacho. Input-to-state stable mpc for constrained discrete-time nonlinear systems with bounded additive uncertainties. In *Proceedings of the 41st IEEE Conference on Decision and Control, 2002.*, volume 4, pages 4619–4624 vol.4, Dec 2002.

[47] D. Q. Mayne, E. C. Kerrigan, E. J. van Wyk, and P. Falugi. Tube-based robust nonlinear model predictive control. *International Journal of Robust and Nonlinear Control*, 21(11):1341–1353, 2011.

[48] D. Q. Mayne and W. Langson. Robustifying model predictive control of constrained linear systems. *Electronics Letters*, 37(23):1422–1423, Nov 2001.

[49] D. Q. Mayne and H. Michalska. Receding horizon control of nonlinear systems. *IEEE Transactions on Automatic Control*, 35(7):814–824, July 1990.

[50] David Q Mayne, María M Seron, and SV Raković. Robust model predictive control of constrained linear systems with bounded disturbances. *Automatica*, 41(2):219–224, 2005.

[51] William H Montgomery and Sergey Levine. Guided policy search via approximate mirror descent. In *Advances in Neural Information Processing Systems 29*, pages 4008–4016. Curran Associates, Inc., 2016.

[52] J. Nubert, J. Koehler, V. Berenz, F. Allgoewer, and S. Trimpe. Safe and fast tracking control on a robot manipulator: Robust mpc and neural network control. 2020.

[53] Julian Nubert, Johannes Köhler, Vincent Berenz, Frank Allgöwer, and Sebastian Trimpe. Safe and fast tracking on a robot manipulator: Robust mpc and neural network control. *IEEE Robotics and Automation Letters*, pages 3050 – 3057, 2020.

[54] Davide Martino Raimondo, Daniel Limon, Mircea Lazar, Lalo Magni, and Eduardo Fernandez Camacho. Min-max model predictive control of nonlinear systems: A unifying overview on stability. *European Journal of Control*, 15(1):5 – 21, 2009.

[55] J Rawlings, D.Q. Mayne, and Moritz Diehl. *Model Predictive Control: Theory, Computation, and Design.* 01 2017.

[56] David Rolnick, Priya Donti, Lynn Kaack, Kelly Kochanski, Alexandre Lacoste, Kris Sankaran, Andrew Ross, Nikola Milojevic-Dupont, Natasha Jaques, Anna Waldman-Brown, Alexandra Luccioni, Tegan Maharaj, Evan Sherwin, s. Karthik Mukkavilli, Konrad Kording, Carla Gomes, Andrew Ng, Demis Hassabis, John Platt, and Y. Bengio. Tackling climate change with machine learning. 06 2019.

[57] J. Romm. *Climate Change: What Everyone Needs to Know.* What Everyone Needs to Know Series. Oxford University Press, 2016.

[58] S. Schaal. The sl simulation and real-time control software package. Technical report, Los Angeles, CA, 2009. clmc.

[59] Johan Schoukens and Lennart Ljung. Nonlinear system identification: A user-oriented roadmap. *ArXiv*, abs/1902.00683, 2019.

[60] Bruno Siciliano. Kinematic control of redundant robot manipulators: A tutorial. *Journal of Intelligent and Robotic Systems*, 3(3):201–212, Sep 1990.

[61] Bruno Siciliano, Lorenzo Sciavicco, Luigi Villani, and Giuseppe Oriolo. *Robotics: Modelling, Planning and Control.* Springer Publishing Company, Incorporated, 1st edition, 2008.

[62] R. Soloperto, J. Koehler, M. A. Mueller, and F. Allgoewer. Collision avoidance for uncertain nonlinear systems with moving obstacles using robust model predictive control. In *Proceedings European Control Conference (ECC)*, 2019.

[63] Steve Sorrell and John Dimitropoulos. The rebound effect: Microeconomic definitions, limitations and extensions. *Ecological Economics*, 65(3):636 – 649, 2008.

[64] Y. R. Stuerz, L. M. Affolter, and R. S. Smith. Parameter identification of the kuka lbr iiwa robot including constraints on physical feasibility. *Proceedings 20th IFAC World Congress*, 2017.

[65] N. Vahrenkamp, D. Berenson, T. Asfour, J. Kuffner, and R. Dillmann. Humanoid motion planning for dual-arm manipulation and re-grasping tasks. In *2009 IEEE/RSJ International Conference on Intelligent Robots and Systems*, pages 2464–2470, Oct 2009.

[66] Ulrike von Luxburg and Bernhard Sch˙ Statistical learning theory: Models, concepts, and results. In Dov M. Gabbay, Stephan Hartmann, and John Woods, editors, *Inductive Logic*, volume 10 of *Handbook of the History of Logic*, pages 651 – 706. North-Holland, 2011.

[67] M. Vukov, A. Domahidi, H. J. Ferreau, M. Morari, and M. Diehl. Auto-generated algorithms for nonlinear model predictive control on long and on short horizons. In *Proceedings 52nd IEEE Conference on Decision and Control*, pages 5113–5118, Dec 2013.

[68] M. Vukov, S. Gros, G. Horn, G. Frison, K. Geebelen, J.B. Jørgensen, J. Swevers, and M. Diehl. Real-time nonlinear mpc and mhe for a large-scale mechatronic application. *Control Engineering Practice*, 45:64 – 78, 2015.

[69] Z. Wan and M. V. Kothare. An efficient off-line formulation of robust model predictive control using linear matrix inequalities. *Automatica*, 39, 2003.

[70] Z. Wan and M. V. Kothare. Efficient scheduled stabilizing model predictive control for constrained nonlinear systems. *International Journal of Robust and Nonlinear Control*, 13, 2003.

[71] Y. Wang and S. Boyd. Fast model predictive control using online optimization. *IEEE Transactions on Control Systems Technology*, 18(2):267–278, March 2010.

[72] M. Zeilinger. Mpc lecture, eth zürich, lecture slides. 2018.

[73] Tianhao Zhang, Gregory Kahn, Sergey Levine, and Pieter Abbeel. Learning deep control policies for autonomous aerial vehicles with mpc-guided policy search. *2016 IEEE International Conference on Robotics and Automation (ICRA)*, pages 528–535, 2015.

[74] Xiaojing Zhang, Monimoy Bujarbaruah, and Francesco Borrelli. Safe and near-optimal policy learning for model predictive control using primal-dual neural networks. *CoRR*, abs/1906.08257, 2019.

[75] Xiaojing Zhang, Alexander Liniger, and Francesco Borrelli. Optimization-based collision avoidance. *CoRR*, abs/1711.03449, 2017.

[76] Kemin Zhou, John C. Doyle, and Keith Glover. *Robust and Optimal Control*. Prentice-Hall, Inc., Upper Saddle River, NJ, USA, 1996.